Université Catholique de Louvain
Institut de Recherche Expérimentale et Cliniques
Pôle de Recherche Cardiovasculaire

Noninvasive detection of the vulnerable plaque: The quest of the Grail

Fabian DEMEURE, MD

Thesis submitted in fulfillment of the requirements
for a PhD degree in Medical Science

Promoters:

David VANCRAEYNEST, MD, PhD

Jean-Louis VANOVERSCHELDE, MD, PhD

Octobre 2018

Committee of thesis

Promoter:	Prof. David Vancraeynest Université catholique de Louvain
Co-promoter:	Prof. Jean-Louis Vanoverschelde Université catholique de Louvain
President of the Jury:	Prof. Alexandre Persu Université catholique de Louvain
Jury members:	Prof. Anne Bol Prof. Christophe Beauloye Université catholique de Louvain
	Prof. William Wijns The Lambe Institute for translational Medicine and Curam, Saolta University Healthcare Group, Galway
	Prof. Fabien Hyafil CHU Bichat, Université Paris 7 René Diderot

Remerciements

Durant ma formation médicale j'ai rapidement eu l'envie de faire de la recherche, je savais que cette voie permettait d'apprendre énormément tant sur le plan scientifique que sur le plan humain. C'est lorsque s'est présenté le choix de ma spécialisation en cardiologie que j'ai contacté le Prof. Vanoverschelde pour lui parler de mon souhait de réaliser de la recherche et qu'il m'a proposé de réaliser une thèse avec le Prof. Vancraeynest sur le domaine de la plaque vulnérable. Je suis heureux que ces années de recherche et de collaboration aient pu aboutir à cette thèse.

Je remercie donc particulièrement mon promoteur de thèse le Professeur Vancraeynest pour m'avoir initié et conduit dans les arcanes de la recherche.

Je remercie mon co-promoteur, le Professeur Vanoverschelde, pour la formation tant médicale que scientifique qu'il m'a apportée durant ces années.

Je remercie le Professeur Persu, président du Jury, d'avoir accepté de coordonner et superviser mon travail ainsi que de m'avoir guidé et encouragé.

Je remercie très chaleureusement le Professeur Anne Bol pour tout ce qu'elle m'a appris dans le domaine de la médecine nucléaire et de la physique ainsi que pour tous les échanges et l'aide qu'elle m'a apportée durant ces années.

Je remercie le Professeur Beauloye pour ses conseils et encouragements.

Je remercie les Professeurs Wijns et Hyafil d'avoir accepté de participer à mon jury ainsi que pour leurs précieux conseils et encouragements.

Ma gratitude va aux Professeurs Pasquet, Pouleur et Gerber pour leur enseignement et de m'avoir emmené dans les méandres de la recherche.

Egalement aux Professeurs Roelants et Hanin du service de médecine nucléaire pour m'avoir guidé et enseigné énormément de choses dans le domaine du PET-scanner et de la scintigraphie. Mais également pour leur aide précieuse dans l'analyse des images et dans la relecture des articles.

Je remercie Caroline Bouzin pour son aide dans la préparation et l'analyse des prélèvements histologiques, également les Professeurs Astarci et Verhelst du service de chirurgie cardiaque pour leur participation à notre travail dans la collecte des échantillons histologiques.

Je remercie chaleureusement tous les membres du département cardiovasculaire (cardiologie, chirurgie cardiaque et soins intensifs) et du service de médecine nucléaire pour leur aide durant ces années.

Ma gratitude va aussi à mes collègues et amis avec qui j'ai partagé ces années de recherche : Julie, Christophe, Fred, Djamila, Siham, Laurianne, Alisson, Clotilde, Mihaela et bien d'autres.

Je remercie mes collègues du service de cardiologie du CHU UCL Namur pour leur aide à la relecture et à la finalisation de ce manuscrit.

Pour terminer, je remercie les membres de ma famille et tout particulièrement mon mari pour leur soutien au cours de ces années.

Table of content

LIST OF ABBREVIATIONS AND ACCRONYMS

ACC	Acetyl Coa carboxylase
ACS	Acute coronary syndrome
AMP	Adenosine monophosphate
AMPK	Adenosine monophosphate protein kinase
ATP	Adenosine triphosphate
AUC	Area under the curve
CCB	Calcium channel blocker
CE	Contrast enhancement
CEA	Carotid endarterectomy
CEUS	Contrast-enhanced ultrasound
CPT	Carnitinepalmitoyltransferase
CT	Computed tomography
CTA	Computed tomography angiography
CVD	Cardiovascular disease
DCE-MRI	Dynamic contrast-enhanced magnetic resonance imaging
DNA	Deoxyribonucleic acid
EC	Endothelial cell
ECM	Extracellular matrix
FDG	Fluorodeoxyglucose
FFA	Free fatty acid
Gd	Gadolinium
GLUT	Glucose transporter
HFLC	High-fat low carbohydrate
HIF1-α	Hypoxia inducible factor 1-α
HK	Hexokinase
IFN	Interferon
IL	Interleukine

IPH	Intraplaque hemorrhage
IVUS	Intravascular ultrasound
LCBI	Lipid core burden index
LCP	Lipid core plaque
LDL	Low density lipoprotein
MDCT	Multidetector-row computed tomography
MI	Mechanical index
MMP	Matrix metalloproteinase
MRI	Magnetic resonance imaging
NF-κB	Nuclear factor κB
NIRS	Near-infrared spectroscopy
OCT	Optical coherence tomography
PET	Positron emission tomography
PI3K	Phosphoinositide 3-kinase
PKB	Serine/threonine kinase protein kinase B
PPAR	Peroxisome proliferator-activated receptor
QVS	Qualitative visual scale
RBC	Red blood cell
ROC curve	Receiver operating characteristics curve
ROI	Region of interest
SGLT	Sodium-dependent glucose transporter
SMC	Smooth muscle cell
SPECT	Single photon emission computed tomography
SUV	Standardized uptake value
TBR	Target to background ratio
TCFA	Thin-cap fibroatheroma
TNF α	Tumor necrosis factor α
VCAM-1	Vascular cell adhesion molecule-1
VEGF	Vascular endothelial growth factor
VH-IVUS	Virtual histology intravascular ultrasound

I. Introduction

Cardiovascular disease (CVD) still represents an important burden for the medical and economic world. Despite considerable therapeutic advances over the past decade and the decline in deaths attributable to CVD, acute cardiovascular events remain the leading cause of death in the Western world (1 in every 3 deaths) [1]. Most of these deaths are due to atherosclerotic plaque rupture.

It is well-established that the majority of acute ischemic events are caused by the rupture or erosion of an atherosclerotic plaque [2, 3]. The plaques likely to cause an acute event are called "vulnerable". Currently, identification of patients at risk of developing an acute event is based on an estimate of the 10-year probability of presenting with or dying from an acute event derived either from the Framingham Risk Evaluation equation [4] or the Systemic Coronary Risk Evaluation system [5]. Unfortunately, despite their usefulness in epidemiological surveys of populations, the predictive accuracy of these models remains insufficient at the individual patient level [6].

The development of new imaging and functional techniques has led to considerable interest in predicting the individual risk of plaque destabilization that could result in an acute ischemic event. Classical noninvasive tests such as stress single-photon emission computed tomography (SPECT), and stress echocardiography, and invasive angiography provide information on the most obstructive plaques that are flowlimiting, but do not provide precise information on the risk of future

acute events. Over the last few years, several invasive and non-invasive imaging modalities have been developed to more accurately study the morphology, biology, and physiology of vulnerable plaques. Recently developed techniques, including coronary calcium scoring and identification of biomarkers of plaque inflammation or collagen breakdown, represent possible additional tools to refine an individual's risk score. Considerable interest is focused on the potential role of these techniques in predicting and hopefully influencing the risk of acute ischemic events.

II. Atherosclerosis

II.A. Introduction

Atherosclerosis (from the Greek *athere* – gruel, and *sclerosis* – hardening) is a systematic pathological process that can manifest with acute clinical events, such as myocardial infarction or stroke. More than thirty years ago, the scientific community understood atherosclerosis as a lipid storage disease; i.e., lipids are deposited on the surface of arteries and grow until they decrease and block the blood supply to the tissues. We now have a better understanding of the mechanisms responsible for the initiation and development of atherosclerosis [7]. The arteries are recognized as an organized organ compound of living cells where inflammation plays a key role. Atherosclerotic plaques develop within, rather than on, the arterial walls.

II.B. Atherosclerotic plaque. Initiation and development of atherosclerosis

Human artery walls consist of three distinct regions called the *tunica intima*, *tunica media*, and *tunica adventitia*. The innermost layer, the *tunica intima*, consists of a basement membrane underlying the innermost surface composed of a continuous layer of endothelial cells (ECs) facing the lumen of the vessel. The *tunica media,* in elastic arteries (the aorta and its branches), consists of resident smooth muscle cells (SMCs) important for contractility. The outermost layer, the *tunica adventitia,* consists of SMCs,

fibroblasts, connective tissue, and blood vessels. The blood vessels present in the adventitia are called the vasa vasorum.

Atherosclerosis is characterized by the progressive accumulation of lipids and fibrous elements in the large arteries, but the exact "spark" that initiates this process is not known in detail. Most of what is known about the process is derived from pathological studies.

Atherosclerotic plaque development is a slow process that takes several decades. Inflammation participates in atherosclerosis from its inception and development to its ultimate endpoint, thrombotic complications [8-11].

Well-known triggers of atherosclerosis, such as the consumption of a high-saturated-fat diet, smoking, hypertension, diabetes, and obesity, can initiate the expression of adhesion molecules by ECs, thus allowing the attachment of leukocytes to the arterial wall. Vascular cell adhesion molecule-1 (VCAM-1) is responsible for the interaction between the endothelium and leukocytes. VCAM-1 binds monocytes and T lymphocytes, the types of leukocytes found in early atherosclerotic plaques. The accumulation of modified lipoprotein particles in the arterial intima is the initiating event that induces VCAM-1 expression through a pathway mediated by nuclear factor-κB (NF-κB), interleukin-1β (IL-1β), and tumor necrosis factor-α (TNF-α) [8].

Laminar blood flow produces shear stress, which elicits several atheroprotective mechanisms, such as increased nitric oxide synthase expression. The resulting increase in production of the vasodilator nitric oxide can limit VCAM-1 gene expression by inhibiting NF-κB activation.

Monocytes adhere to the endothelium surface, and penetrate and enter the intima by diapedesis between ECs. This process depends in large part on the

expression of chemoattractant cytokines [12]. Within the intima, the monocytes mature into macrophages that express scavenger receptors and engulf modified lipoproteins.

The early stage of atherosclerosis consists of subendothelial accumulation of macrophages with a high cholesterol content, especially oxidized low density lipoprotein (LDL) – the so-called "foam cells" [7]. This stage, termed "fatty streaks", can be observed in the aorta in the first decade of life, the coronary arteries in the second decade, and the cerebral arteries in the third or fourth decades[13]. This early stage is reversible. There are preferred sites of lesion formation within the arteries, which is the consequence of differences in blood flow dynamics and shear stress. Fatty streaks are the precursors of more advanced lesions characterized by lipids and SMCs accumulation. Such "fibrous lesions" typically have a "fibrous cap", consisting of SMCs and extracellular matrix (ECM) that encloses a lipid-rich "necrotic core". The accumulation of lipids is tightly correlated with endothelial dysfunction, infiltration of monocytes, and immigration of other inflammatory cells. These processes, together with activation of vascular SMCs and their excessive production of ECM in the arterial wall, result in vessel wall thickening and a usually asymmetrical narrowing of the vessel. Early atherosclerotic lesions mainly consist of an excess of lipids, cholesterol, and ECM components, especially collagen I and III, elastin, and proteoglycans. These lesions initially involve a thickening of the vessel wall without any vessel narrowing, extensive vessel wall remodeling, and a proteolytic degradation of ECM. At later stages, lumen narrowing occurs. Inflammatory processes within the plaque, together with infiltrated leukocytes and activated macrophages, are involved in lesion progression and contribute to plaque vulnerability [14, 15]. Atherosclerotic plaque is

characterized by a heterogeneous population of macrophages, reflecting the complexity and diversity of the microenvironment to which cells are exposed after entry into the arterial wall [16]. After monocyte differentiation into macrophages, the latter become polarized and their phenotype and function change under the influence of several cytokines and growth factors. Several of the phenotypes present in atherosclerotic lesions have been described [17]. Coexistence of the two main macrophage phenotypes (M1 and M2) has been described in carotid atherosclerotic lesions [18]. Histological analysis of human atherosclerotic plaques revealed a distinct spatial distribution of macrophage phenotypes in human plaques [19]. The M1 (so-called "classical") macrophages are found mainly in the shoulder areas of the plaque, which is considered to be one of the most fragile zones of the plaque and is also near the lipid core [20]. M1 macrophages, activated by the lipids, promote the formation of the necrotic core and the destabilization of the plaque leading to thrombotic events [17].
In contrast, M2 (so-called "alternative") macrophages are located in the adventitia, in stable areas close to the fibrous cap and in areas of neovascularization that also contain iron deposits [21, 22]. M2 macrophages modulate the progression of atherosclerosis by attenuating the inflammatory response via secretion of anti-inflammatory factors [23] and contribute to the resolution of inflammation by phagocytizing M1 macrophages in apoptosis [24].

In later stages of atherosclerosis, plaques can become increasingly complex, with calcifications, ulcerations at the luminal surface, and hemorrhages from small vessels (vasa vasorum) that grow into the plaque from the media [25-27].

Figure 1: Atherosclerosis lesion progression and potential targets for molecular imaging.

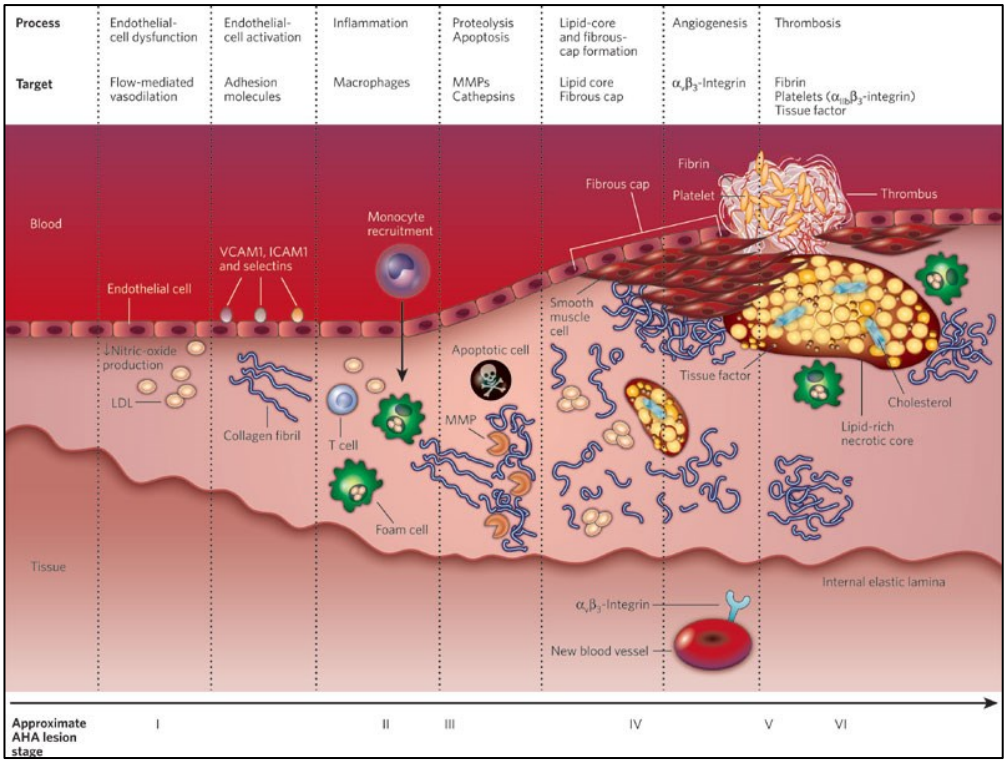

The progression of an atherosclerotic lesion is shown in a simplified form, developing from a normal blood vessel (far left) to a vessel with an atherosclerotic plaque and superimposed thrombus (far right). Potential targets for molecular imaging at each stage are also listed. AHA, American Heart Association; ICAM1, intercellular adhesion molecule 1; LDL, low-density lipoprotein; MMP, matrix metalloproteinase; VCAM1, vascular cell-adhesion molecule 1.

JavierSanz&Zahi A. Fayad
Nature 2008; **451**, 953-957

II.C. Vulnerable plaque

Histopathological investigations have revealed that in two-thirds of patients with acute coronary syndrome (ACS), luminal thrombosis is caused most frequently by atherosclerotic plaque rupture, followed by plaque erosion. The least frequent cause is calcified nodules, where disruptive nodular calcifications protrude into the lumen [28-31]. The mechanisms are similar in carotid arteries [32, 33].

In plaque rupture, a structural defect in the fibrous cap exposes the lipid core and other constituents of the plaque to the blood constituents and promotes thrombosis. Plaque material is sometimes found in the thrombus, indicating that rupture and thrombosis are simultaneous.
Plaque erosion is described as a thrombus without rupture, where the surface endothelium is absent but there are no visible distinct morphological features of the underlying plaque [34].

In the literature, the terms ‘‘vulnerable plaque’’ [35-37] or ‘‘rupture-prone plaque’’ are frequently used to define plaques at high risk of causing local thrombosis.

The most common cause of ACS is hypoperfusion subsequent to plaque rupture and local thrombosis [38]. Even though plaque rupture with luminal thrombosis is similarly considered to be the major etiology of carotid atherosclerosis, artery-to-artery embolism appears to be the dominant vascular mechanism causing brain ischemia. The large vessel caliber and increased flow velocity may explain the more embolic nature of carotid

plaque rupture. Several studies have shown the presence of micro-emboli distally to a carotid severe stenosis [39], supporting the view of embolization as the etiology of most strokes. However, in a substantial proportion of cryptogenic strokes, embolization resulting from non-stenotic plaques with vulnerable characteristics is suspected [40, 41].

Anatomicopathological studies in sudden coronary deaths [42] established characteristics of rupture-prone plaque in coronary arteries. These lesions, usually called thin-cap fibroatheromas (TCFA), showed typical characteristics including a thin fibrous cap (<65 μm) [43] and a large lipid necrotic core [28] infiltrated by numerous inflammatory cells such as macrophages and lymphocytes [42], diffuse spotty calcifications, and neovessels coming from vasa vasorum that are responsible for intraplaque hemorrhage (IPH) (see **Figure 2**). This type of plaque presents a substantial outward remodeling described as a "compensatory enlargement" of the artery in response to an increase in plaque area, also called "the Glagov phenomenon"[44]. These hallmarks of vulnerable plaque have also been found in carotid plaque and are supported by histopathology studies [45, 46].

Figure 2: Thin-cap fibroatheroma

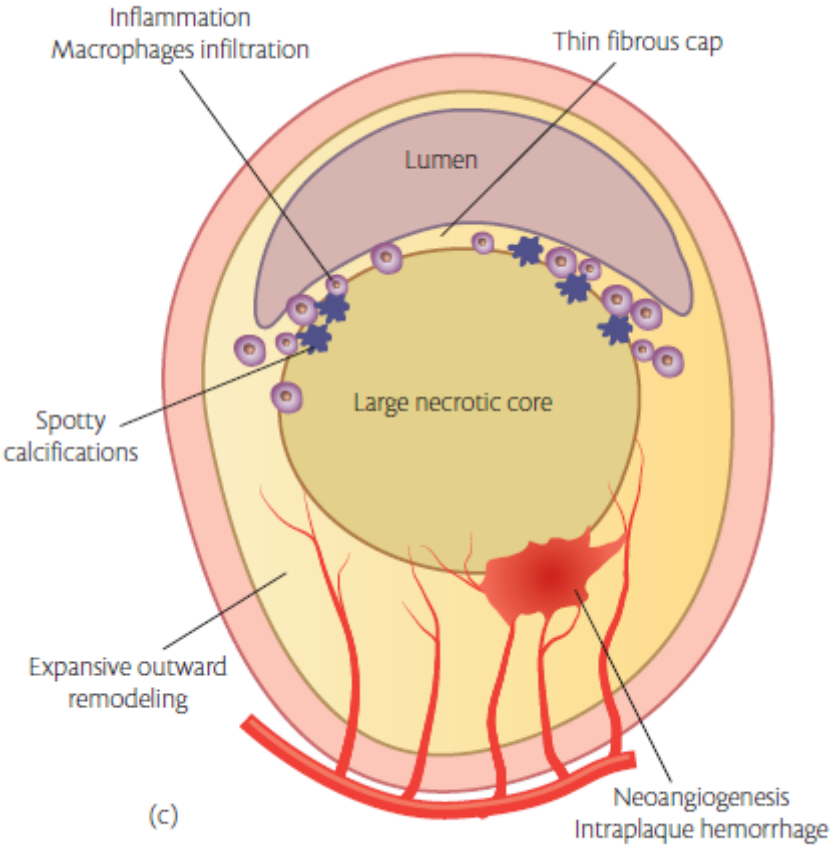

ESC Textbook of Cardiovascular Imaging, 2d edition

The **fibrous cap** covering the lipid core consists of proteoglycans, collagen, and elastin. In the thin cap of the vulnerable plaque, few or no SMCs are present. The cap thickness is a balance between matrix synthesis by SMCs and matrix degradation by matrix metalloproteinases (MMPs) produced by inflammatory cells such as macrophages [47].

Results derived from analyses of coronary arteries cannot necessarily be extrapolated to other atherosclerotic vessels, such as the carotid artery. Indeed, *Redgrave et al.* [48] performed detailed histological analysis of 526 carotid plaques of symptomatic patients undergoing carotid endarterectomy (CEA) and determined the thickness of the fibrous cap associated with plaque rupture. In the ruptured plaques, mean cap thickness was observed to be 300 μm, with a minimum cap thickness of 150 μm. For non-ruptured plaques, mean and minimum cap thickness averaged 500 μm and 250 μm, respectively. Consequently, the optimum cut-offs to discriminate between ruptured and non-ruptured plaques were set at <200 μm for minimum cap thickness and <500 μm for mean cap thickness. Interestingly, these values were much greater than those reported for coronary plaques. Based on the pioneering work of *Virmani et al.* [49, 50] and *Redgrave et al.* [45], it has been proposed that a vulnerable carotid atherosclerotic plaque is one with a thin fibrous cap of <200 μm overlying a large necrotic/lipid core [49-51].

The **lipid core** is composed mainly of lipids and cholesterol from dead foam cells [52] and is typically larger in ruptured plaques compare to non-ruptured plaques [42]. This lipid core is avascular, hypocellular, devoid of collagen matrix, and extremely thrombogenic due to the presence of tissue factors produced by macrophages [53, 54].

The **inflammatory cell** population is predominantly represented by macrophages; the remainder is composed of a mix of T lymphocytes, neutrophils, and mast cells.

Extracellular matrix protein synthesis by vascular SMCs may be inhibited by interferon-γ (IFN-γ) secreted by activated T cells, thereby disrupting collagen synthesis, which may interfere with the maintenance and repair of the collagen framework supporting the fibrous cap. CD40 ligand expression on T cells may promote tissue proteolysis through the release and activation of matrix-degrading enzymes produced by vascular SMCs and inflammatory macrophages. Activated macrophages within the fibrous cap (the M1 macrophage phenotype) can secrete tissue proteases that support the destruction of collagen and elastin. This process can thin and weaken the fibrous cap. Additional factors involved in the activation of macrophages include TNF-α, macrophage colony-stimulating factor (M-CSF), and macrophage chemoattractant protein-1 (MCP-1), among others [55].

Microvessels, called "vasa vasorum", are present in the adventitia of normal vessels. They supply oxygen and nutrients to the other components of the vessel wall [56]. Proliferation of the adventitial vasa vasorum, i.e. **neovascularization**, is inherently linked with early atherosclerotic plaque development due to impairment of oxygen diffusion [57]. These early stages, fatty streaks and preatheromas, show neovascularization, with apolipoproteins deposits around neovessels suggesting local lipid deposition leading to plaque progression [58]. More extensive intraplaque neovascularization is associated with vulnerable plaque and advanced lesions in coronary [59, 60] and carotid plaques [61]. This neovascularization appears in a disorganized network with excessively enlarged and irregular vessels.

Neovascularization is stimulated by hypoxia mediated through hypoxia-inducible factor-1α (HIF-1α) secreted by hypoxic macrophages located in

the necrotic core. HIF-1α is a subunit of a heterodimeric transcription factor, HIF-1. Under normoxic conditions, HIF-1α is hydroxylated by an oxygen-dependent pathway. Under hypoxic conditions, HIF-1α is stabilized, which allows dimerization with the other subunit, HIF-1β. This active complex binds to DNA, initiating the transcription of downstream genes involved in angiogenesis and inflammation (such as vascular endothelial growth factor (VEGF)) [62-64].

The leaky nature of neovascularization, regulated by VEGF and NF-κB, is responsible for extravasation of red blood cells (RBCs), leading to IPH. RBC deposits attract macrophages, participate in enlargement of the necrotic core, and represent a critical event in the induction of plaque instability [65].

Expansion of the neovascularization is linked to neointima formation and growth of the atherosclerotic plaque, whereas regression is accompanied by a reduction in neointima and plaque size [66].

Moreno et al. [67] hypothesized that neovascularization may contribute to removal of intimal fat when the concentration of LDL is lower in the neovessel circulation than in the intima. This efflux of LDL is followed by regression of neovessels, which may be a marker of plaque stabilization [68, 69].

II.D. Vulnerable patient

In 2003, a review published in *Circulation* proposed the term "cardiovascular vulnerable patient". The aim of this paper was to define subjects susceptible to an ACS or sudden cardiac death. Criteria were based on plaque characteristics, but also on blood sample analysis, which was undertaken to identify conditions that were prone to thrombosis using a set

of serum markers (markers of inflammation, immune activation, lipid peroxidation or metabolic syndrome, and coagulation/anticoagulation balance), and on myocardial vulnerability (favoring fatal arrhythmias) [36, 37].

Several studies have noted the presence of more than one vulnerable plaque in patients at risk of or presenting with a cardiovascular event [43, 70-72]. The PROSPECT trial demonstrated that only 1% of the patients in whom intravascular ultrasound (IVUS) had identified a large number of non-culprit (meaning not related to the acute event) vulnerable plaques experienced a myocardial infarction related to the non-culprit lesion during the three-year follow-up [71]. In addition to the aforementioned observations, there is some evidence in favor of temporal changes in plaque morphology. Indeed, an IVUS-based study by *Kubo et al.* revealed that a large proportion (75%) of TCFA had changed into stable plaque after one year and, conversely, that new TCFA had developed [73]. These data suggest that a plaque can appear vulnerable at a given time and less vulnerable at another time, and that coronary artery disease is an active process that is constantly changing.

Vulnerable plaques frequently rupture without any clinical symptoms [74, 75] and healing of asymptomatic ruptured plaques leads to progressive lumen obstruction [70, 76]. This mechanism likely explains the results of *Kubo et al.* [73].

Because most plaque ruptures do not lead to symptomatic events (e.g. thrombosis), other factors must be present. Numerous factors other than plaque characteristics may be involved, including plaque location, endothelial dysfunction but also coronary flow dynamics, intrinsic hemostatic/fibrinolytic dysfunction, neurohormonal dysregulation, and environmental factors/triggers. These different conditions may explain why

vulnerable plaques with similar characteristics have different clinical presentations and evolution [77].

This suggests that detection of a vulnerable state in a patient ("vulnerable patient") is more important than identification of individual vulnerable plaque characteristics.

III. Imaging modalities

III.A. Introduction

The diagnostic approach to atherosclerotic diseases often consists of evaluating luminal patency either directly, by angiography, computed tomography (CT), magnetic resonance imaging (MRI), or ultrasonography (for some specific arteries such as the carotid artery), or indirectly, by tissue perfusion imaging (Positron emission tomography (PET), SPECT, perfusion MRI, or perfusion CT). These tools offer information about the severity and location of luminal stenosis (or its consequences on distal blood flow).Nevertheless, they provide little information regarding features that determine a plaque's propensity for rupture or erosion. Information on plaque composition can, however, be partially obtained by CT or MRI.

Studies have shown that the majority of plaques responsible for acute coronary events are not associated with severe stenosis in angiographic exams [78, 79]. However, angiography is a luminography technique; as such it is influenced by remodeling and underestimates the plaque volume. Conversely, histological and intravascular imaging studies have demonstrated the importance of positive remodeling [36, 80, 81].
In contrast, the stroke risk in patients with symptomatic stenosis (>50%) is directly related to the extent of stenosis for the first two years after symptoms develop [82-84].

Ischemia-based revascularization of coronary stenosis allows symptom relief but is unlikely to reduce the incidence of acute coronary events

(sudden death or myocardial infarction),as demonstrated in the COURAGE and BARI 2D trials [85-87].The focus on treating the few isolated angina-producing stenosis does not take into account the many non-obstructive potentially vulnerable plaques.

CEA has been shown to prevent stroke in patients with high-grade carotid artery stenosis ("benefit of carotid endarterectomy in patients with symptomatic moderate or severe stenosis" study) [88]. However, it is becoming increasingly clear that the degree of luminal stenosis alone is not the optimal clinical decision parameter. Patients with an almost occluded carotid artery may remain completely asymptomatic throughout their lifetime, whereas strokes may occur in the absence of severe carotid stenosis because of outward arterial remodeling of a vulnerable plaque [89].

As discussed earlier, atherosclerosis is a systemic and diffuse disease involving the entire arterial tree. Studies have reported the presence of additional vulnerable plaque to the culprit lesion in symptomatic patients [43, 90, 91]. The usefulness of locating vulnerable plaques remains to be demonstrated and seems not to be able to predict the occurrence of all coronary events, though it may provide additional prognostic information. Therefore, it is questionable whether there is any benefit in detecting an isolated vulnerable plaque. Indeed, the treatment is based primarily on the use of well-known systemic medications (aspirin, P2Y12 inhibitors, statins, etc.). The benefit of individual treatment of a vulnerable plaque (e.g. by stenting) is currently being investigated in large randomized trials (PROSPECT-ABSORB trial [NCT02171065], PECTUS trial [NTR5590] and PREVENT study [NCT02316886]) to assess its therapeutic potential for

reducing acute events [3]. Nowadays, it might be better to assess the global extent of the atherosclerotic disease, which may lead to a life-saving change in diet and lifestyle, and influence the number/dose of medications and patient's adherence to the treatment. This global burden can be established using non-invasive imaging of larger arteries more accessible than coronary arteries.

This chapter describes the current methods of diagnosing atherosclerotic plaques. Both non-invasive and invasive imaging as well as their advantages and limitations are discussed.

III.B. Non-invasive imaging

Various anatomical components of TCFA, as well as metabolic processes, have been targeted as candidates for non-invasive imaging. Positron emission tomography (PET), contrast-enhanced ultrasound (CEUS), computed tomography angiography (CTA), and magnetic resonance imaging (MRI) have emerged as possible non-invasive modalities to visualize the vulnerable plaque. The characteristics of these imaging modalities are summarized in **Table 1** and will be discussed in this section.

Table 1: Non-invasive imaging modalities: technical characteristics and targeted vulnerable plaque features.

	FDG-PET	CEUS	CTA	MRI
Technical characteristics				
Contrast agent	-	microbubbles	iodine	gadolinium
Ionizing radiation	yes	no	yes	no
Spatial resolution (mm)	4-5	0.1	0.4	0.5-1(0.35)*
Vulnerable plaque features				
Remodeling	-	-	+	+
Lipid core	-	-	+	+
Plaque rupture	-	+	-	
Thin fibrous cap	-	-	+	+
Inflammation	+	-	-	(+)
Neovascularization	-	+	-	+
Intraplaquehemorrhage	-	-	-	+
Spotty calcification	-	-	+	-

*with 3T MRI

Despite the ability of these techniques to detect some features of a vulnerable plaque, novel targets for non-invasive imaging of vulnerable plaques are still required for reliable patient risk stratification. There have been many advancements in molecular imaging, which visualizes specific molecular biomarkers or molecular processes in vivo. In particular, various molecular imaging methods have been developed in cancer imaging to identify molecular characteristics of tumors. These methods can also be applied to a vulnerable plaque, which has similar targets (e.g. macrophages, neovascularization, etc.).At this stage of development, these modalities are not well-suited for imaging of coronary arteries, mainly due to their small size and continuous movement. By contrast, they can be used successfully for carotid imaging. Further developments are needed for coronary imaging.

1. Nuclear imaging : PET-CT

Nuclear imaging methods are not used for anatomical structures imaging due to their low resolution, but rather provide information about metabolic activity.

1.a. General principle

PET is based on the detection of the 511 keV annihilation photons that are released in opposite directions when radionuclides, such as fluorin-18, carbon-11, and oxygen-15, emit positrons (positively charged electrons) (β+) that undergo annihilation with electrons in tissues (Fig 3). These radionuclides are used to synthesize radiopharmaceuticals that are part of

biochemical pathways in the human body, such as fluoro-deoxy-glucose (FDG) in glucose metabolism. After radiopharmaceutical injection, patients are placed in the PET scanner where they are surrounded by a ring of detectors, and the coincident detection of two photons in opposite detectors determines a line of response along which the annihilation occurred. By detecting all the possible lines of response, the system can reconstruct an image of the activity distribution of the radiopharmaceutical inside the patient. This "coincidence" detection makes PET much more efficient than other nuclear medicine procedures. The spatial resolution of the final image is mainly limited by the size of the detectors: typical spatial resolution of current PET systems is in the order of 5 mm.

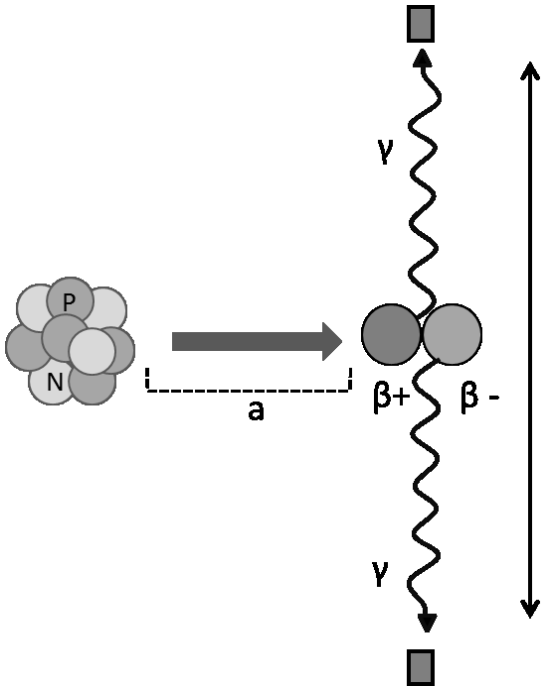

Figure 3: Annihilation reaction.

Positrons (β+) released from the nucleus of F-18 annihilate with electrons (β-), releasing two coincidence 511-keV photons (γ), which are detected by scintillation crystals (rectangles).
Positrons (β+) travel a small distance (a) before annihilating with electrons (β-). This difference in position between the origin of the positron and its site of annihilation results in a small deterioration of the spatial resolution that can be achieved with PET.
N = neutron, P = proton.

^{18}F-fluoro-2-deoxy-D-glucose (^{18}F-FDG)

Fluorine-18 (^{18}F) radionuclide is produced in a cyclotron and used for ^{18}F-FDG synthesis.

FDG is a radiopharmaceutical glucose analog that concentrates in metabolically active cells in proportion to cellular demand in glucose.

Like glucose, the FDG is transported into cells by glucose transporters (GLUTs) and phosphorylated by hexokinase (HK). As FDG-6-phosphate is not a suitable substrate for glucose-6-phosphate isomerase, it accumulates within the cells (**Figure 4**).

The major advantage of PET is its high sensitivity, allowing the detection of a picomolar concentration of tracer, which can be used to quantify a biological process of interest. PET with the tracer ^{18}F-FDG allows measurement of metabolic activity. In atherosclerosis evaluation, ^{18}F-FDG reflects the metabolic activity of macrophages and therefore plaque inflammation[92].

Figure 4: Comparison between ^{18}F-FDG and glucose metabolization.

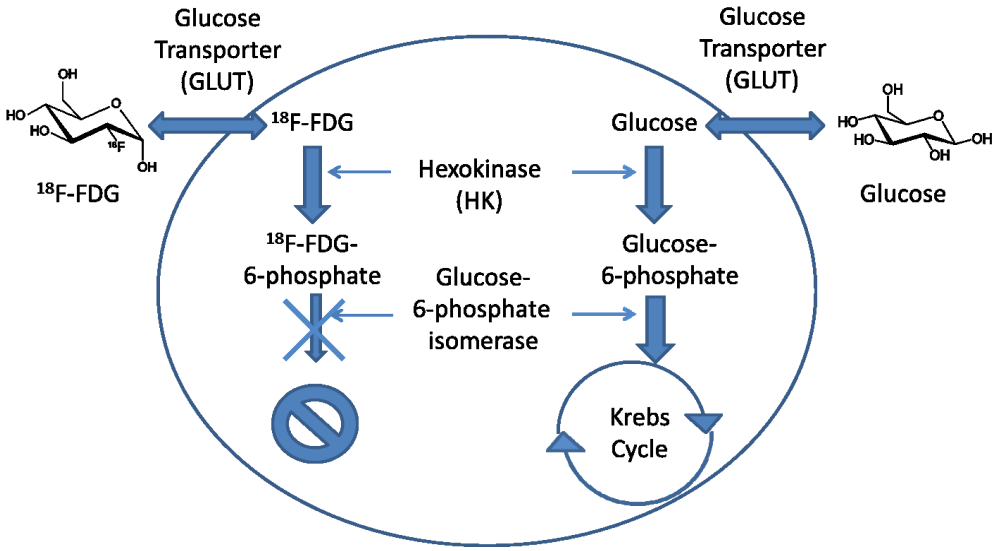

PET-CT Fusion

PET is limited by poor anatomic detail, and correlation with some other form of imaging, such as CT, is desirable. PET-CT is a technique which combines, in a single gantry, a PET scanner and an x-ray CT scanner, to acquire sequential images from both devices in the same session. These images are combined into a single superimposed (coregistered) image. Thus, functional imaging obtained by PET, which depicts the spatial distribution of metabolic activity, can be more precisely aligned or correlated with anatomic imaging obtained by CT scanning. Common software and control systems can subsequently produce two- and three-dimensional image reconstructions.

Interpretation of Images

PET provides images of quantitative uptake of the radionuclide injected that can give the concentration of radiotracer activity in kilo becquerels per milliliter. However, for accurate results, the images must be corrected for effects of attenuation of the 511-keV photons as they pass through the patient. PET-CT uses CT transmission data to correct for attenuation differences.

The conventional methods of measuring radiotracer activity are the standardized uptake value (SUV) and tissue to background ratio (TBR). The SUV is a semiquantitative assessment of the radiotracer uptake from a static (single point in time) PET image. The SUV of a given tissue is calculated with the following formula: tracer concentration in tissue normalized to injected radiotracer dose/patient weight. It is important to standardize the time interval between injection of the radiotracer and the PET study, as the SUV variability with time has been well documented.

In contrast, TBR was devised to correct for blood uptake of radiotracer, the blood pooling effect. TBR is calculated as the ratio of the SUV of a region of interest (ROI) to the SUV in the mid-lumen of a large vein with no evident spill-over effect from neighboring tissues.

Limitations and Artefacts of PET-CT

Patient motion in PET-CT imaging can produce significant artefacts on the fused images and may cause confusion as to the correct position of the origin of the detected photon. Patients are carefully instructed not to move for the entire study (during CT, between CT and PET, and during PET) and placed in a comfortable position before the start of the study. This is extremely important for proper coregistration of the CT and PET studies, on

which both accurate spatial localization of tracer activity and valid attenuation correction depends. Patient motion between the CT and PET studies appears as a mismatch between the two sets of images. Finally, normal muscles may take up the radiotracer and show increased activity on the PET images. This can be the case for myocardial muscle in some basal situations or for peripheral muscles after strenuous activity preceding or following injection of FDG. The uptake of FDG in normal muscles is diffuse and frequently symmetric.

1.b. Imaging of the carotid and coronary plaques

Preclinical studies of vascular injury in the iliac arteries of atherosclerotic rabbits showed enhanced ^{18}F-FDG uptake in the vessel wall and an associated increase in macrophage activity at the site of injury [93].

Due to the infiltration and retention of oxidized lipids in the arterial wall, vulnerable plaques contain a higher density of macrophages compared with asymptomatic plaques [28]. Activated macrophages have a significantly increased metabolic rate compared to their non-activated counterparts, and therefore an increased ^{18}F-FDG uptake. The rate of glucose utilization of macrophages is high at baseline and can increase 50-fold further when activated [94].

Rudd et al. found increased^{18}F-FDG in macrophage-rich regions of carotid plaques removed at endarterectomy in eight symptomatic patients compared with contralateral asymptomatic plaques in the same patients [95]. *Tawakol et al.* demonstrated that in vivo ^{18}F-FDGuptake correlated with the degree of

plaque inflammation in 17 patients when macrophage staining was assessed histologically [96].

A more recent and larger study of 21 patients confirmed these findings, demonstrating that ^{18}F-FDG uptake in carotid plaque, expressed as the maximal standardized uptake value (SUV_{max}), was strongly associated with macrophage density and enhanced tissue expression of VEGF [97].

In addition to its application for detection of carotid atherosclerosis, ^{18}F-FDG has been used in coronary imaging but studies have reported conflicting results (see **Table 2**). These different studies emphasize the technical limitations of the method with problems related to myocardial tracer uptake, respiratory motion, and partial volume artifacts [98].

Table 2: Studies evaluating ^{18}F-FDG for coronary imaging.

Study	Type of Study	Study Subjects	Results	p value
Rogers et al. [99]	Feasibility study	ACS post angioplasty vs stable CAD	FDG uptake is higher in ACS patients	p = 0.02
Cheng et al.[100]	Exploratory study	ACS vs stable CAD	FDG uptake is higher in ACS patients	p = 0.04
Joshi et al.[101]	Prospective clinical trial (FDG and NaF)	ACS vs stable CAD	No difference between FDG uptake by culprit and non-culprit plaque	p = 0.34

ACS : Acute Coronary Syndrome ; CAD : Coronary Artery Disease ; FDG : Fluorodeoxyglucose ; NaF : Natrium Fluoride

1.c. Technical limitations

In addition to the spatial resolution (4–5 mm), the difficulties in suppressing endogenous myocardial glucose uptake and the combined respiratory and motion artifacts that are associated with cardiac imaging are also obstacles in terms of coronary plaque imaging (as illustrated in **Figure 5**).

It would be advantageous to have a method that decreases physiological myocardial FDG uptake. Indeed, suppressing or minimizing the myocardial FDG uptake improves the detection of FDG uptake in adjacent structures and decreases the risk of false-positive studies. It has been demonstrated that a high-fat low-carbohydrate (HFLC) diet significantly reduces myocardial FDG uptake [102-104].

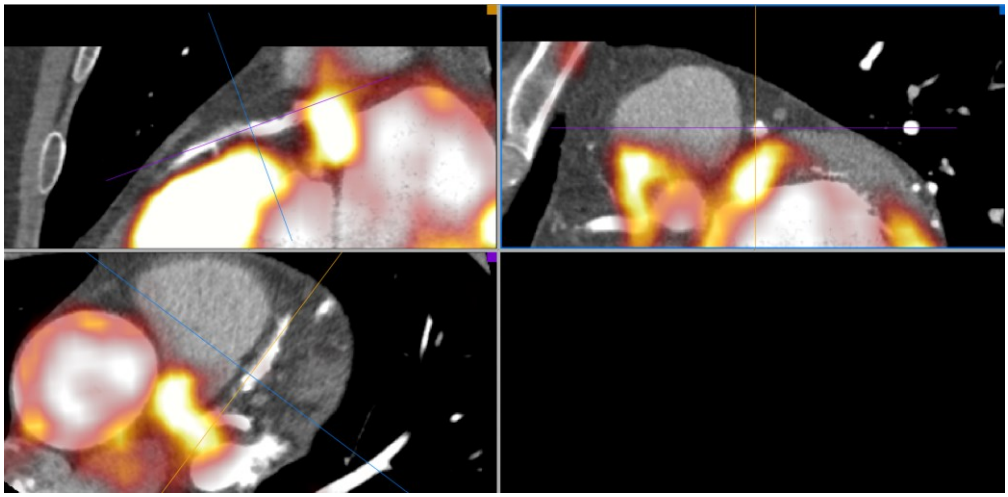

Figure 5: Endogenous myocardial FDG uptake makes it difficult to visualize FDG uptake in coronary arteries.

1.d. Myocardial metabolism

Glucose and fatty acids are the major oxidative fuels for mammals. The utilization of free fatty acids (FFAs) and glucose in the mitochondria accounts for the vast majority of adenosine triphosphate (ATP) production in the healthy adult heart [105].The adult heart has the ability to switch energy sources as dictated by substrate availability, hormonal status, and physiological conditions [106, 107]. Under normal circumstances at rest, 60–90% of the acetyl-CoA that enters the tricarboxylic acid cycle comes from the β-oxidation of FFAs (diacylglycerol and non-esterified fatty acids), and 10–40% from the oxidation of pyruvate that is derived in almost equal amounts from glycolysis and lactate oxidation [108]. However, during conditions of increased metabolic demands, such as increased heart rate or blood pressure, in a postprandial state with an increase in plasma glucose and insulin level, or in hypoxic conditions, there is a shift towards a greater utilization of glucose to maintain ATP production. During prolonged starvation, ketone bodies and lactate serve as the fuel for cardiac energy production.

Cardiac carbohydrate metabolism [109]

Glucose, glycogen, and lactate are the carbohydrates used by the heart to produce energy. Glucose has a hydrophilic nature and the lipid bilayer of plasma membrane is impermeable to it. Glucose transport across the plasma membrane in the cardiomyocyte therefore occurs via glucose transporters. There are two major classes of glucose transporters: GLUT family (the facilitative glucose transporters) and the sodium-dependent glucose

transporters (SGLTs), which are located in the sarcolemma. GLUT proteins mediate the majority of glucose transport.

In the human heart, the major isoforms of the GLUT family are GLUT4 (up to 70% of the GLUT found in the cardiomyocyte membrane) and GLUT1. In basal conditions, GLUT4 is located mainly in intracellular membrane compartments. In response to stimuli such as insulin or increased heart work, GLUT4is translocated to the cell surface.

Physiological stimuli initiate distinct signaling mechanisms leading to enhanced GLUT4 translocation and glucose uptake. Phosphoinositide 3-kinase (PI3K) is a crucial intermediate in the insulin signaling process; it activates the serine/threonine kinase protein kinase B (PKB) involved in the hormonal regulation of the glucose transport that is primarily attributable to an increase in the plasma membrane recruitment of GLUT4 [110]. The ability to induce GLUT4 translocation is not restricted to insulin, but can also be achieved by an increase in the mechanical activity of the heart. This pathway has been shown to include adenosine monophosphate-activated protein kinase (AMPK), which appears to function as a “sensor” of the energy status of cells, and becomes phosphorylated and activated by a stress-induced rise in intracellular adenosine monophosphate (AMP) and a concomitant drop in ATP [111].

After uptake, glucose is metabolized via glycolysis and glucose oxidation. This process produces 30–32 ATP molecules per glucose molecule. The heart uses glycogen and lactate when the supply of other fuels is inadequate to meet its requirements.

Cardiac fatty acid metabolism[112]

Under normal physiological conditions, the heart takes up fatty acids and converts them to long-chain fatty acyl-CoA esters via the action of fatty acyl-CoA synthase and exports most of these esters into the mitochondria for β-oxidation. FFAs enter cardiac myocytes either by via protein carriers (fatty acid translocase (FAT)/CD36, plasma membrane isoform of fatty acid binding protein (FABPpm), and fatty acid transport protein (FATP)). Mitochondrial transport is carried out by the carnitine system, which contains carnitine palmitoyl transferase 1 and 2 (CPT1 and 2). The activity of CPT1 is regulated by the cytosolic concentration of malonyl-CoA. Two enzymes control the cytosolic levels of malonyl-CoA; acetyl-CoA carboxylase (ACC) and malonyl-CoA decarboxylase. Phosphorylation of ACC by AMPK induces an inhibition of ACC and therefore a decrease in malonyl-CoA, thereby stimulating fatty acid oxidation. Several enzymes whose expression is controlled by peroxisome proliferator activated receptors (PPARs) act to regulate mitochondrial fatty acid oxidation, including the retinoid X receptor α (RXRα; a nuclear receptor transcription factor that complexes with PPAR and coordinates the control of energy utilization and storage) and the PPAR γ co-activator (PGC) 1α (an essential regulator of mitochondrial biogenesis and energy metabolism). Increased fatty acid oxidation occurs in cardiomyocytes during exercise.

1.e. Non-coronary cardiac FDG PET/CT

The clinical applications of FDG-PET/CT are extending beyond the area of oncology. As previously discussed, FDG also accumulates at the sites of inflammation, such as in atherosclerotic disease but also sarcoidosis, at sites of infection, for example in endocarditis [113] and during myocardial ischemia [114]. As discussed previously in the section on technical limitations (see Section 1.c), a proper myocardial preparation is crucial to obtain valuable exams.

Sarcoidosis is a multisystemic inflammatory disorder characterized by non-caseating granuloma in many organs. It most commonly affects the lungs and the lymph nodes. Clinically, 5% of patient with sarcoidosis have cardiac involvement. Myocardial FDG uptake in patients with suspected or confirmed sarcoidosis has prognostic value and is useful in patient stratification. Among patients with FDG uptake in the heart that is within a normal range, patients with no uptake at all have significantly lower event rates than those with a diffuse myocardial uptake pattern.

Infective endocarditis is a severe disease with an increasing incidence rate globally, especially in the elderly. The current diagnostic gold standard for endocarditis is the modified Duke criteria, which is based on clinical, echocardiographic, microbiological and histological findings. Due to the lack of sensitivity of the Duke criteria (80%), there is a growing interest in molecular imaging with FDG-PET, which demonstrates increased metabolic activity at the site of infection before morphologic changes occur. Combined PET/CT imaging provides complementary morphologic and metabolic information at the site of infection; this requires a good

myocardial suppression. FDG-PET/CT has the unique attribute of imaging the whole body. This is useful in identifying sites of metastatic infections. Determining the extent of infection is important in deciding the treatment modality in prosthetic valve infectious endocarditis. When infection extends into the perivalvular area, early surgical intervention is necessary. In this early phase, echocardiography may still be negative, since an abscess is not yet formed. ^{18}F-FDG-PET/CT, however, is able to show abnormal accumulation in the prosthetic valve with extensions into the perivalvular area, consistent with perivalvular spread. Electronic device infections can also be imaged in the same way.

The complete deregulation of glycolytic energy metabolism in hypoxic myocardium is the main reason behind using ^{18}F-FDG-PET/CT to directly image the hypoxic or ischemic myocardium. Myocytes without available oxygen are turned towards glycolysis. The conversion occurs rapidly in several minutes (even when induced by stress testing). When ischemia occurs, glycolysis remains and lasts for several hours/daysafter the hypoxic/ischemic period ends, even if the blood supply is restored. The upregulation of glycolysis by the myocytes is one cause of the increased FDG accumulation within the postischemic myocardium. However, stress-induced hypoxic myocardium imaging is not yet clinically established and the enhanced FDG uptake induced by myocardial ischemia is controversial [114, 115], since non-ischemic myocardium can also exhibit varying extents of FDG uptake even under a fasting state.

Finally, abnormal patterns of cardiac FDG activity can be noted in a variety of other conditions, including lipomatous hypertrophy of the interatrial

septum, epicardial and pericardial fat, increased atrial activity associated with atrial fibrillation or a prominent crista terminalis, myocarditis, and pericarditis.

2. Nuclear imaging : SPECT and other PET tracers

Other tracers, using PET or SPECT radionuclides, have been created to target metabolic and signaling pathways associated with the characteristics of plaque vulnerability.

Table 3: PET (other than FDG) and SPECT radionuclides used to evaluate plaque vulnerability

Target Process	Imaging Target	Imaging Probe	Study Subjects	Target Artery	TRR	LNR	Ref
PET							
Endothelium	P-selectin	^{64}Cu-anti P-selectinAb	AM	Aorta	1.3	5.9	[116]
		^{68}Ga-fucoidan	AM	Aorta	5.1	1.7-2.4	[117]
Inflammatorycell	Chemokinerecep tor	^{64}Cu-DOTA-vMIP-II	AM	Femoral		3.4-3.7	[118]
		^{64}Cu-DOTA-DAPTA	AM	Femoral		2.9-4.4	[119]
	Mannose receptor	^{18}F-fluoro-D-mannose	AM/Hu-T	Carotid		2.3-4.8	[120]
	SST receptor	^{68}Ga-DOTATATE	Hu-I	Aorta/coronary	1.4-3.7	1.2-1.5	[121-123]
	TSPO	^{11}C-PK11195	Hu-I	Aorta/carotid	1.1-2.4	1.2-2.5	[124, 125]
	Choline metabolism	^{18}F/^{11}C-choline	Hu-I			1.9	[126, 127]
	Phagocytosis	^{64}Cu-nanoparticle	AM	Aorta			[128]
Neoangiogenesis	Integrin	^{68}Ga-NOTA-RGD	AM/Hu-I	Aorta/carotid			[129]
		^{18}F-flotegatide	AM	Aorta	1.5-4.7	2.8-5.2	[130]
		^{18}F-galactoRGD	Hu-I	Carotid	2.0	1.7	[131]
	VEGF receptor	^{89}Zr-bevacizumab	Hu-T	Carotid	2.1		[132]
Hypoxia	Redox	^{18}F-FMISO	AM	Aorta		2.5	[133]
Calcification	Chemisorption	^{18}F-fluoride	Hu-I	Coronary	1.3-1.7	1.1	[101, 134]
SPECT							
Endothelium	VCAM-1	^{99m}Tc-cAbVCAM1-5	AM	Aorta		1.3	[135]
Inflammatorycell	IL-2 receptor	^{99m}Tc-HYNIC-IL-2	Hu-T	Carotid	1.1-1.6	1.2-1.4	[136]
	Folatereceptor	^{111}In-EC0800	AM	Carotid			[137]
		^{99m}Tc-folate	Hu-T	Carotid			[138]
	LOX-1	^{111}In-liposome-LOX-1 Ab	AM	Aorta			[139]
Proteolysis	MMP	^{99m}Tc-RP805	AM	Aorta/carotid		1.3-1.7	[140, 141]
Neoangiogenesis	Integrin	^{99m}Tc-NC100692	AM	Carotid		6.5	[142]
		^{99m}Tc-maraciclatide	AM	Aorta		1.6	[143]

Ab = antibody, AM = animal model, Hu-I = human imaging, Hu-T = human tissue specimen, IL = interleukin, LDL = low-density lipoprotein, LNR = lesion-to-normal ratio, LOX = lectin-like oxidized LDL receptor, MMP = matrix metalloproteinase, SST = somatostatin, TRR = target-to-reference tissue ratio, TSPO = translocator protein, VCAM = vascular cell adhesion molecule, VEGF = vascular endothelial

Many tracers target activated macrophages. The use of surfaces receptors, such as the IL-2 receptor [144] and scavenger receptors [145, 146], labeled with ^{99m}Technetium was tested over 10 years ago. More recently, chemokine receptors have been investigated. Proteins or peptides that have an affinity for chemokine receptors were labeled with ^{64}Cu and used for PET imaging [118, 119]. Other surface receptors have been studied, such as

the folate receptor β [137], mannose receptor [120], lectin-like oxidized LDL receptor [139], and somatostatin receptors [123]. Choline is used for cell membrane synthesis, and choline metabolism is enhanced in activated macrophages. Radiolabeled choline (^{11}C-choline and ^{18}F-choline) is also available for application in humans [126, 127].

Other inflammation-related processes can be targeted. MMP and cathepsin are the most important proteases in inflammatory proteolysis; some radiolabeled imaging tracers have been developed. MMP inhibitors labeled with ^{123}I or ^{99m}Tc have been used in scintigraphy scans or SPECT [147, 148]. Neoangiogenesis is another hallmark of vulnerable plaque and can be targeted by the integrin αvβ3 [130, 131, 143] or other targeting VEGF receptors [132].

^{18}F-fluoromisonidazole (FMISO), first used for tumor visualization, allows visualization of hypoxic vulnerable plaques [133]. Apoptosis of macrophages can be visualized by radiolabeled ^{99m}Tc-annexin V [149].

Calcification is the final process in inflammation and can be easily seen on CT scans. However, visualizing the ongoing calcifying activity in the plaque is more challenging; imaging can be undertaken using ^{18}F-fluoride PET [134, 150]. This tracer allows discrimination of symptomatic plaques [151].

Contrast-enhanced ultrasound (CEUS)

This method can only be applied to large vessels with an ultrasound window (meaning a segment of the vessel accessible to the ultrasound beam), typically the carotid artery, and is not applicable to coronary arteries. The method improves the quality of traditional B-mode ultrasound images, with a better delineation of structures where the contrast can reach (producing angiography-like images).

3.a. General principle

CEUS is the application of ultrasound contrast medium to traditional sonography. Ultrasound contrast agents consist of microbubbles of a low molecular weight inert gas (e.g. sulfur hexafluoride, octafluoropropane) surrounded by a stabilizing shell (e.g. phospholipids, albumin) to improve circulation time. Microbubble size is fairly uniform; they lie within a range of 1–4 micrometers in diameter. They are thus smaller than RBCs, which allows them to flow easily through the circulation, as well as the microcirculation. These microbubbles stay in the vascular system for a few minutes and then are eliminated by the respiratory tract. Ultrasound contrast is not nephrotoxic, does not require radiation, and complications such as severe anaphylactic reactions are rare (<1 in 100,000). The more common side effects are minor and include headache, injection site pain, burning, or paresthesias.

Ultrasound pulses are applied with a frequency near the resonance frequency of the gas bubbles and the microbubbles expand and contract (increase and decrease in diameter) with each cycle of pressure pulses,

producing strong echoes of the imaged region. Trains of ultrasound pulses with varied frequency, phase, and amplitude are designed to separate microbubbles and tissue echoes.

Contrast-specific ultrasound modes are required and are based on the cancellation and/or separation of linear ultrasound signals from tissue and utilization of the non-linear response from microbubbles. Power-modulation imaging is a pulse subtraction technique that transmits multiple pulses per image line, alternating full-amplitude pulses with half-amplitude pulses (as illustrated in **Figure 6**). Subtracting twice the return signal of the half-amplitude pulse from the return signal of the full-amplitude pulse cancels the linear response from the tissue, but not the non-linear response from bubbles.

Non-linear harmonic ultrasound signals also arise in tissues themselves from distortion of the sound wave during its propagation through the tissue. The extent of this tissue harmonic response increases with the acoustic pressure, which is proportional to the mechanical index (MI). The precise unit of measurement for acoustic pressure is the Pascal, but the most common reference unit is the MI. Minimization of bubble disruption is the main reason for using low MIs for real-time imaging, but it also reduces tissue harmonics and artifacts, thus facilitating the separation of signals from vessels from those of tissue. Low MI is typically below 0.3 [152]. In cases where the MI is more than 0.5, microbubbles oscillate strongly and expand beyond their limit, resulting in a disruption of the bubble (as illustrated in **Figure 7**).

Carotid CEUS imaging uses a linear array transducer that transmits frequencies between 3 and 10 MHz and uses a low-level mechanical index between 0.06 and 0.2. It requires the use of dedicated contrast imaging software with a pulse inversion or a harmonic imaging technique. We used the following protocol: after injection of the ultrasound contrast agent, the lumen of the carotid artery was enhanced within 10 to 25 seconds. To assess replenishment kinetics, microbubble destruction was achieved using five on-demand consecutive high-power frames (mechanical index (MI) 1.0). Imaging then returned automatically to low-power, real-time scanning (MI 0.13) [153] (as illustrated in **Figure 8**).

Figure 6: **Pulse subtraction principle.** The transmitted pulses are drawn on the left. The received echoes are in the middle. Combination of the received echoes is on the right. **A:** With a linear acoustic response (e.g. tissues), the received echoes are similar to the transmitted ones. The sum of the two signals is close to zero. **B:** When the acoustic response is non-linear (e.g. microbubbles), the shapes of the received echoes are different and their sum differs from zero. In this way, identification of the non-linear part of the acoustic signal is possible.

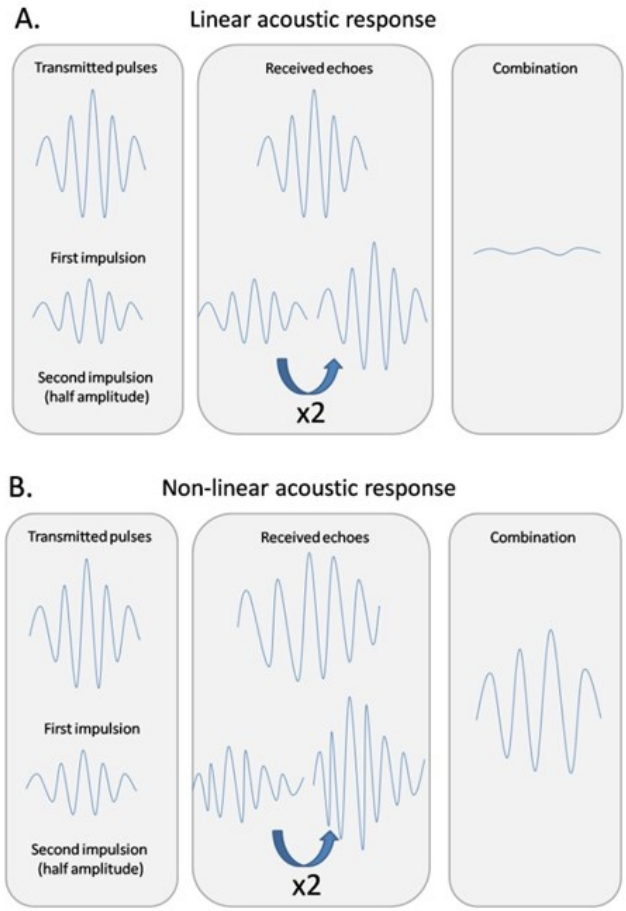

Figure 7: Schematic changes of microbubbles by interaction with acoustic field of various acoustic intensities: using very low MI (< 0.1), resonance is observed, between 0.1 and 0.5 asymmetrical vibrations with emission of harmonics, and with MI > 0.5, bubbles burst.

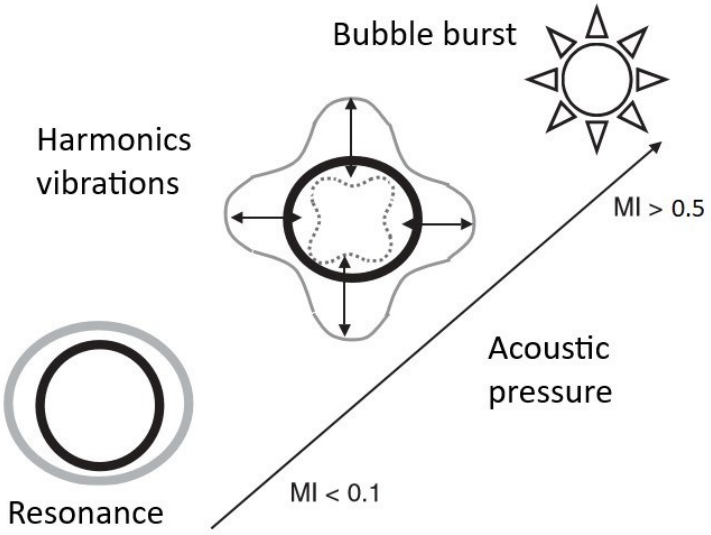

Figure 8: Microbubbles replenishment in carotid plaque in seconds after microbubble destruction.

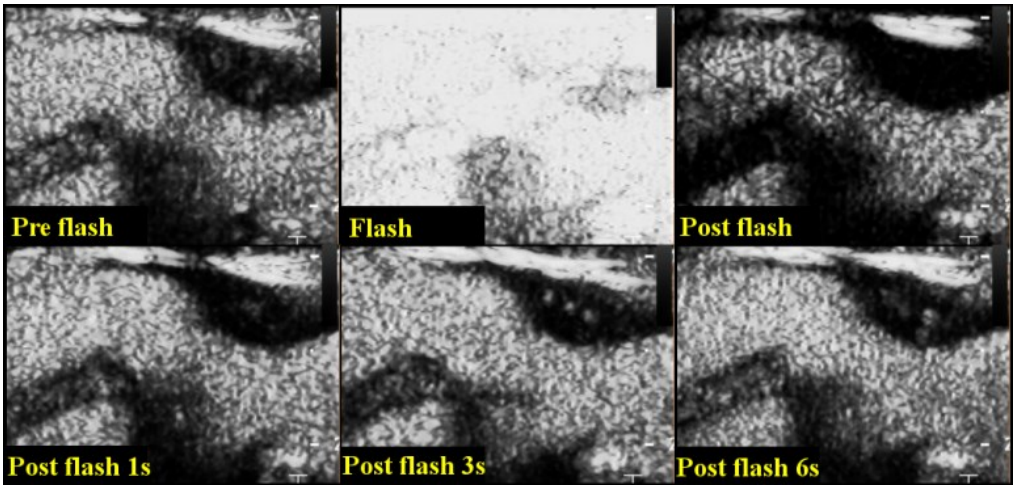

3.b. Imaging of the carotid plaque

Doppler and B-mode ultrasound of the carotid artery are the most common methods used in clinical practice to find carotid atherosclerotic plaques and to evaluate stenosis. The carotid artery is easily accessible for assessing patient atherosclerosis. *Feinstein et al.*[154]first reported the feasibility and clinical application of CEUS imaging in the carotid artery. Carotid plaque imaging has largely improved with the introduction of CEUS, for two main reasons. First, CEUS imaging enhances the carotid lumen, which results in improved visualization of luminal irregularities including soft plaques, dissections, and ulcerations [155, 156]. Second, it can detect intraplaque neovascularization and adventitial vasa vasorum. The microbubbles of contrast serve as ideal intravascular tracers and allow assessment of carotid plaque neovascularization [157-159].

A number of studies report histological validation of CEUS; higher contrast enhancement (visual semiquantitative analysis) correlated with an increase in vessel density in endarterectomy specimens [158, 160]. *Coli et al.* [158]used a double staining of microvessels with a cocktail of CD31/CD34 antibodies. In another study, *Shah et al*. [157] used a composite of CD31, CD34, von Willebrand factor, and hemosiderin. The presence of neovascularization within atherosclerotic plaques is a marker of plaque vulnerability and has been associated with symptoms(transient ischemic attack or stroke) [161] independently of the plaque thickness [162]. In an observational study of 147 subjects, the past history of cardiovascular events (myocardial infarction and transient ischemic attacks or stroke) correlated with plaque neovascularization detected by CEUS [159]. These studies support the role of CEUS imaging in cardiovascular risk stratification.

Quantification of the vasa vasorum remains a major issue. Currently, studies use 2D ultrasound imaging and semiquantitative evaluation based on visual gradation of the contrast effect within the plaque [157-160]. *Xiang et al.* evaluated a quantitative analysis of plaque contrast enhancement and examined the correlation with semiquantitative assessment and symptoms. Quantitative analysis was performed using software. A ROI was determined manually to include the entire plaque. Motion compensation was used to isolate the region from movement of the surrounding tissues. The software automatically generated signal time-intensity curves of contrast enhancement for the carotid plaque, which were fitted to an exponential function. Baseline intensity and peak intensity values were derived from the time-intensity curves. Enhanced intensity (in decibel, dB) values of the plaque were calculated by subtracting the baseline intensity values for each area.

3.c. Technical limitations

The use of ultrasound contrast agents is contraindicated in patients known to have right-to-left shunts, severe pulmonary hypertension (pulmonary artery pressure >90 mmHg), or uncontrolled systemic hypertension, and in patients with adult respiratory distress syndrome [163].

During ultrasound, heavily calcified plaques that produce acoustic shadows hinder the examination of the lumen and plaques. The topography of the evaluated plaques may well also act as a confounding factor. In particular, when plaques located in the posterior arterial wall are evaluated, microbubbles may produce acoustic shadowing that alters grayscale

intensity and therefore image interpretation. This phenomenon as known as far-wall pseudo-enhancement [164].

3. Computed tomography angiography (CTA)

Multidetector-row CT (MDCT) is a widely available non-invasive imaging tool. MDCT allows for multiplanar reconstructions in the axial, sagittal, and coronal planes as well as high spatial (submillimeter) and contrast resolution [165]. MDCT uses the voxel Hounsfield units (HUs) to characterizeplaques (calcification, cap thickness, IPH, and lipid core) [166, 167].

Coronary plaques are imaged using a bolus-tracking CTA technique. Regarding the coronary arteries, most clinical CTA investigations have classified atherosclerotic plaques into three categories based on the presence and amount of calcified plaque components[168]:calcified plaques with higher attenuation, partially-calcified plaques, and non-calcified plaques with lower attenuation. However, classifying non-calcified coronary plaques as lipid-rich or fibrous lesions is challenging[169].Positive remodeling can be derived with CTA and was well correlated with autopsy and IVUS study [170]. Positive remodeling and low attenuation plaque in CTA was associated with optical coherence tomography (OCT)-derived TCFA [171]. These two features were independent predictors for the occurrence of ACS in short- and mid-term follow-up [172]. The napkin-ring sign is an additional suspected CT feature of vulnerability and represents a necrotic core with low attenuation surrounded by a ring-like area of higher attenuation. This CT feature has been confirmed by autopsy studies [173].

CTA is a traditional method of imaging the carotid artery. MDCT angiography of the carotid artery is able to identify plaque ulceration, calcification, and lipid cores with a good agreement with histology [174, 175]. Macroscopic changes in the carotid plaque, such as large hemorrhage or low-density lipid cores, can easily be recognized. IPH is associated with very low attenuation [176] and MDCT angiography is able to detect plaques complicated with hemorrhage [177]. In general, the lower the density of the plaque, the more likely it is to be vulnerable. Furthermore, MDCT angiography is able to measure fibrous cap thickness with a good correlation to histology [174]. Finally, MDCT angiography can quantify calcification; a lower level of calcification is associated with a greater prevalence of neurological symptoms [178].

Studies using MDCT with specific contrast agent for molecular imaging have reported promising results. Activated macrophages have been imaged using targeted nanoparticle contrast agents [179, 180] or gold-labeled high-density lipoprotein nanoparticles [181]. MMPs have been imaged using the contrast agent P947 (DOTA-Gd-peptide) [182].

The main limitations of MDCT include artefacts from calcified lesions, the need for iodinated contrast, and radiation exposure.

4. Magnetic resonance imaging (MRI)

MRI is the most well-established imaging modality for carotid plaque characterization. This non-invasive and non-radiation imaging modality is capable of assessing both the lumen and the vessel wall. Nevertheless, the visualization of coronary atherosclerotic plaques by MRI is still challenging

[183]. The resolution of MRI scanners of 1.5 Tesla is about 460–750 μm [184] and is 350 μm for a 3 Tesla MRI scanner [185].

There is a wide variety of sequences available for plaque characterization. Certain sequences, like fast spin echo sequences, allow for a very high spatial resolution, but suffer from prolonged scanning time. Other sequences are available to reduce scan time, such as gradient echo imaging. The black-blood techniques result in high contrast between the dark lumen and the vessel wall with a high signal-to-noise ratio.

The use of contrast-enhanced images is essential to differentiate the various plaque components. Gadolinium (Gd)-based contrast agents can be used to evaluate neovascularization, as well as differentiate the necrotic core from fibrous tissue. Increased enhancement with Gd is also associated with the detection of neovascularization and plaque inflammation [186-188].

Studies comparing MRI with histopathology have demonstrated that MRI can distinguish between plaque calcification, the fibrous cap, intraplaque hemorrhage, and the lipid-rich necrotic core [189]. Other studies have used dynamic contrast-enhanced (DCE) MRI to quantify plaque enhancement and thus neovascularization and inflammation using adventitial K^{trans} (volume transfer coefficient)[190-192]. The presence of symptoms (ipsilateral ischemic events) has been associated with increased Gd enhancement [191, 193].

Molecular imaging using specific contrast is feasible. Activated macrophages have been imaged using ultra-small super-magnetic particles of iron oxide (USPIO) [194]; paramagnetic gadolinium-based nanoparticles

targeted to the αvβ3-integrin have been used for imaging of angiogenesis [195].

The main advantage of cardiac MRI is the absence of ionization. Limitations include the contraindications for this technique (non-compatible cardiac implanted device, metallic foreign body in eye or cerebral clip aneurysm, severe claustrophobia), the use of Gd-based contrast agent, and the limited access to the technique.

III.C. Invasive imaging

Intravascular imaging modalities display plaques at a high spatial resolution and allow the precise visualization of the vessel and lumen dimensions, as well as the distribution and severity of atherosclerotic disease. Some of them can characterize atherosclerotic plaque composition. The characteristics of the three main imaging modalities are summarized in **Table 4** and will be discussed in this section.

Table 4: Invasive imaging modalities: technical characteristics and targeted vulnerable plaque features.

	VH-IVUS	OCT	NIRS
Technical characteristics			
Energy source	Ultrasound	Infrared light	Near-infrared light
Pullback speed, mm/s	0.5	10–40	0.5
Depth penetration, mm	7–10	0.1–2.0	1–2
Spatial resolution, µm	150–250	10	NA
Vulnerable plaque features			
Remodeling	++	-	-
Lipid core	+	+	++
Plaque rupture	+	++	-
Thin fibrous cap	-	++	-
Macrophage infiltration	-	++	-
Neovascularization	-	+	-
Intraplaque hemorrhage	-	-	-
Spotty calcification	++	+	-

NIRS: near-infrared spectroscopy; OCT:optical coherence tomography; VH-IVUS:virtual histology intravascular ultrasound

There are some limitations to be considered, and these restrict the use of intravascular imaging. These limitations include the fact that it can be used only in symptomatic patients undergoing coronary angiography for clinical purposes, that it does not enable complete assessment of the coronary tree, and the time required for processing of data acquisition.

1. Intravascular ultrasound (IVUS)

IVUS is performed using a miniaturized piezoelectric crystal placed at the distal tip of a catheter attached to a computerized ultrasound station. The IVUS technique is based on the reflection of emitted ultrasound waves, according to the acoustic properties of the tissue. The transducer is advanced through the coronary artery, guided by x-ray (fluoroscopy). An automatic pullback of the catheter is then performed at constant speed and usually acquiring images every 1 mm [196]. Rotational scanning of the vessel can be achieved by mechanical rotation of the transducer. Gray-scale IVUS images are based only on the amplitude of sound waves backscattered from tissue. The spatial resolution is relatively low, with an axial resolution around 100 μm and a lateral resolution around 300 μm. IVUS has been extensively validated against histology. Lumen and vessel dimensions, plaque distribution, lesion length, and remodeling can be accurately determined in vivo [197, 198].Unfortunately, the resolution hampers detailed plaque characterization (poor differentiation between fibrous and lipid-rich plaques) and determination of the thickness of a thin fibrous cap.

More recently, use of radiofrequency (RF) analysis IVUS has been proposed. Virtual histology (VH-IVUS) is the most widely available and uses frequency spectral analysis. VH-IVUS can distinguish between four types of plaque components (fibrous or fibro-fatty plaque, necrotic core, and calcification) [199-201]. Using this data, the techniques provide color-coded maps of plaque composition for each cross-sectional image, which are superimposed on the grayscale IVUS images [200, 202].

TCFA can be evaluated by VH-IVUS, which has demonstrated a fairly good correlation with histology, despite the low axial resolution that limits the visualization of a thin cap (≤ 65 μm); this was first demonstrated by *Rodriguez-Granillo et al.* [203] and confirmed by *Pundziuteet al.* [204]. A comparison with optical coherence tomography (OCT) confirmed that VH-IVUS can accurately detect vulnerable plaque [205]. VH-derived TCFA (VH-TCFA) is defined as a lesion with a confluent necrotic core (≥10%) in direct contact with the lumen for ≥ 3 image slices and a plaque burden > 40% [199, 203].

Three relevant studies have shown the prognostic value of VH-TCFA; the PROSPECT study (Providing Regional Observations to Study Predictors of Events in the Coronary Tree) [71], the VIVA study (Virtual Histology in Vulnerable Atherosclerosis) [206], and the ATHEROREMO-IVUS study (European Collaborative Project on Inflammation and Vascular Wall Remodeling in Atherosclerosis – Intravascular Ultrasound) [207].

The disadvantages of the IVUS technique are the requirement for radiation exposure (a fluoroscopy is required to guide the catheter) and the invasive nature of the procedure [208].

2. Optical coherence tomography (OCT)

OCT is based on the use of a low-coherence interferometry to generate images. A low-coherence infrared light beam is directed at the vessel wall and using the backscattered light produces an image of the tissue. The OCT catheter has an inner imaging core that rotates to provide cross-sectional images from distal to proximal using an automated pullback system [209].

OCT has a high spatial resolution of 10–20 μm (versus 100 μm for IVUS) at the cost of a limited depth penetration of 0.1 to 2.0 mm (versus 7 to 10 mm for IVUS). Due to the high scattering of blood, saline, or contrast media, flushing is mandated during measurement [210].

OCT can detect all physiological characteristics that are detectable with IVUS [211]. Due to the high spatial resolution, OCT enables more detailed assessment of vulnerable plaque characteristics that cannot be detect by IVUS, such as the presence of macrophages [212], neovascularization [213], and microcalcifications [214], and allows more accurate estimation of fibrous cap thickness in TCFA [215]. In an in vivo comparison of OCT and VH-IVUS, both reliably identified advanced coronary plaques [205].

Nevertheless, OCT has significant limitations in assessing plaque morphology. These include a low penetration depth that restricts the analysis to the internal elastic lamina, its limited accuracy in detecting macrophages [216], and its limited efficacy in differentiating deep lipid-rich cores from calcified nodules [217].TCFA are defined as having a fibrous cap of less than 70 μm, and certain trials also require the arc of the lipid pool to subtend an angle superior to 90 degrees. However, there is no strict definition of OCT TCFA [214].

OCT has been extensively used to assess plaque composition, including in a small study investigating its efficacy in identifying lesions that are likely to progress [218].

The disadvantages of the OCT technique are the requirement for radiation exposure (a fluoroscopy is required to guide the catheter), the invasive nature of the procedure, and the necessity of using contrast media.

Figure 6: OCT illustration of TCFA (☆)

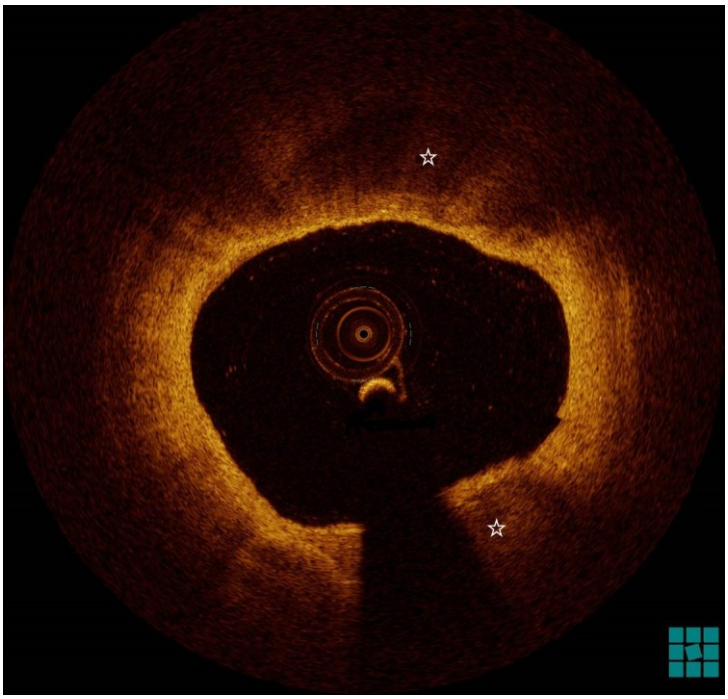

3. Near infrared spectroscopy (NIRS)

NIRS uses a scanning laser to deliver a near-infrared light to the tissue of interest. The proportion of light reflected back is analysis by a detector. Lipid has a specific signature in the wavelength region of NIRS, allowing distinct imaging of a lipid-core plaque (LCP) [219]. The data are displayed as a chemogram (2D dimensional distribution of the probability of the presence of an LCP per millimeter). Using NIRS data, a lipid core burden

index (LCBI) can be calculated, which is the amount of lipid in a scanned artery length (usually 4 mm – $LCBI_{4mm}$).

The first validation study in human histological data showed that NIRS is able to detect lipid-rich lesions with high accuracy (AUC of 0.86) [220]. More recent studies, showing that NIRS is the best invasive modality for detection of fibroatheromas, confirm these data [221, 222].

Nevertheless, NIRS alone is limited by its inability to provide lumen and wall structure information. Therefore, NIRS is commonly combined with IVUS in a combined NIRS-IVUS catheter. The combined data are superior to NIRS or IVUS data alone [221, 223]. In vivo studies showed that a $LCBI_{4mm}$ with a cut-off of more than 400 was able to identify culprit lesions in ACS patients [224].

IV. AIMS OF THIS WORK

As previously mentioned, atherosclerotic disease is still the leading cause of death in the Western world. Identifying patients at an increased risk of suffering an acute event within a population in which the majority exhibit no prior symptoms is a major challenge.

Recent advancements in invasive and non-invasive imaging have improved the potential to identify vulnerable plaques.

-Invasive imaging is the ideal approach to study atherosclerotic disease progression and detect vulnerable plaques. Several studies have been published on the natural history of suspected vulnerable plaques. However, invasive imaging techniques have some limitations making their use difficult for large population screening.

-Non-invasive imaging is the ideal tool to screen an asymptomatic population and identify patients at high risk.

This thesis evaluates the role of two widely accessible techniques of non-invasive imaging, FDG-PET/CT and CEUS, in the assessment and characterization of atherosclerosis and vulnerable plaque.

In the first part of this work, we compare CEUS, a method used to evaluate neovascularization, and FDG-PET/CT, a method used to evaluate inflammation, in carotid plaque with histological validation. The link between the presence of neovascularization and inflammatory plaque

components is frequently debated in the literature. *Hoogi et al.*[225] found a correlation between the quantity of neovessels and the number of inflammatory cells determined by CD3 and CD68 stains, whereas *Li et al.* did not [226]. There are conflicting results in literature regarding the association of intraplaque neovascularization and the degree of stenosis. *Coli et al.* [158] report no correlation, but *Staub et al.*[227] found a significantly higher grade of neovascularization in lesions with a higher degree of stenosis. In addition, we evaluate the temporal associations between inflammation and neovascularization.

FDG-PET/CT is the most validated nuclear technique for imaging vulnerable plaque, mainly for larger arteries (aorta, carotid, or iliac arteries). As previously mentioned, the main limitations of applying this technique to coronary imaging are the image resolution and the physiological endogenous myocardial glucose uptake.

In the second part of this work, we try to optimize the coronary FDG-PET/CT technique for the visualization of coronary plaque inflammation. We conduct an evaluation of various patient preparations in the goal to suppress the physiological myocardial uptake of FDG.

.

V. Head to head comparison of inflammation and neovascularization in human carotid plaques: implications for the imaging of vulnerable plaques.

Fabian Demeure, MD [1], Caroline Bouzin, PhD [2], VéroniqueRoelants, MD, PhD [3], Anne Bol, PhD [3], Robert Verhelst MD, PhD [1], ParlaAstarci, MD, PhD [1], Bernhard L. Gerber MD, PhD [1], Anne-Catherine Pouleur MD, PhD [1], AgnèsPasquet MD, PhD [1], Christophe de Meester, PhD [1], Jean-Louis J. Vanoverschelde, MD, PhD [1], David Vancraeynest, MD, PhD [1]

1. From the Pôle de Recherche Cardiovasculaire (CARD), Institut de Recherche Expérimentale et Clinique (IREC), Université Catholique de Louvain, Brussels, Belgium and the CardiovascularDepartment, Institut Cardiovasculaire, Cliniques Universitaires Saint-Luc, Brussels, Belgium.
2. From the IREC Imaging Platform, Institut de Recherche Expérimentale et Clinique (IREC), Université Catholique de Louvain, Brussels, Belgium.
3. From the Pôle d'imagerie médicale, radiothérapie et oncologie (MIRO), Institut de Recherche Expérimentale et Clinique (IREC), Université Catholique de Louvain, Brussels, Belgium and the division of Nuclearmedicine, InternalMedicineDepartment, Cliniques Universitaires Saint-Luc, Brussels, Belgium.

Circulation Cardiovascular Imaging 2017; 10(5)

ABSTRACT

Background:Inflammation and intra-plaque neovascularization (IPN) are acknowledged to be two features of plaque vulnerability although their temporal expression and their respective value in predicting clinical events are poorly understood. To determine their respective temporal associations, we conducted a comprehensive assessment of inflammation and IPN in the carotid plaque of symptomatic and asymptomatic patients.

Methods and Results: Thirty patients with severe carotid stenosis underwent ^{18}F-fluorodeoxyglucose (FDG)-PET/CT imaging. Plaque FDG-uptake, indicative of inflammation, was measured by calculating the target-to-background ratio (TBR). The presence of IPN during contrast-enhanced ultrasound was judged semi-quantitatively; low-grade contrast enhancement (CE) suggested its absence and high-grade-CE, the presence of neovascularization. Carotid surgery was performed 1.6±1.8 days after completing both imaging modalities in all patients, and the presence of macrophages and neo-vessels were quantified by immuno-histochemistry. We identified a significant correlation between the TBR and macrophage quantification ($R=0.78$, $p<0.001$). The number of vessels was also significantly higher in carotid plaque with high-CE ($p<0.001$). Surprisingly, immunohistochemistry showed that high-CE and vessel number were neither associated with an elevated TBR ($p=0.28$ and $p=0.60$ respectively) nor macrophage infiltration ($p=0.59$ and $p=0.40$ respectively). Finally, macrophage infiltration and TBR were higher in the carotid plaque of symptomatic patients ($p=0.021$ and $p=0.05$ respectively), whereas CE-grade and the presence of neo-vessels were not.

Conclusions: Inflammation and IPN are not systematically associated in carotid plaques, suggesting a temporal separation between the 2 processes. Inflammation seems more pronounced when symptoms are present. These data highlight the challenges that face any imaging strategy designed to assess plaque vulnerability.

Key Words: ^{18}F-FDG-PET/CT; Contrast-Enhanced Ultrasound; Plaque Inflammation; Plaque Neovascularization; Carotid Plaque.

INTRODUCTION

In the majority of cases, acute vascular events such as myocardial infarction or stroke are caused by the disruption of a vulnerable atherosclerotic plaque. Compared to stable lesions, "rupture-prone" or "vulnerable" plaques typically exhibit inflammation and intra-plaque neovascularization (IPN) [28]. The ability to identify which atherosclerotic plaques are at risk of rupture would constitute a major advance in the management of atherosclerotic disease. Accordingly, both invasive and non-invasive imaging techniques are being developed to achieve this, and to ensure the timely treatment of patients [228, 229].Unfortunately, despite these objectives, robust predictors of plaque rupture remain to be determined.

Atherosclerotic plaques develop in response to local inflammatory processes. Cardiovascular risk factors cause endothelial cell dysfunction and a proinflammatory state that promotes the expression of cellular adhesion molecules and consequently the recruitment of inflammatory cells, mainly monocytes and lymphocytes. Monocytes differentiate into macrophages, the principal inflammatory cell constituent of the atherosclerotic plaque [11]. Macrophages may themselves contribute to the destabilization of the plaque by their secretion of metalloproteinases that degrade the fibrous cap separating the lipid-rich core from the arterial lumen. A strong correlation exists between macrophage plaque infiltration and ischemic symptoms, with this association persisting for several months after becoming symptomatic [45].

Numerous validation studies have proven ^{18}F-Fluorodeoxyglucose (FDG), a glucose analog that accumulates in cells with a high glycolytic rate, to be the most robust PET tracer with which to image plaque

inflammation [92]. FDG-PET/CT imaging is therefore a reliable and reproducible measure of vascular inflammation and provides valuable prognostic data [121, 230]. As the plaque size increases, oxygen levels deep within the plaque diminish, local hypoxia ensues, and micro-vessel formation from adventitia is triggered. Abnormal vascular development, characterized by leaky immature endothelial vessels, can lead to intra-plaque hemorrhage, which promotes the transition from a stable to vulnerable plaque. This process may therefore predict future clinical outcomes [27, 231]. Novel noninvasive imaging modalities capable of detecting neovascularization include carotid contrast-enhanced ultrasound (CEUS). This promising imaging tool detects IPN with a good histologic correlation [158, 159]. One advantage of this technique is that the ultrasound contrast media is "purely intravascular" and its tissue uptake therefore reflects the total number of micro-vessels, rather than permeability of the activated endothelium. Furthermore, IPN as assessed by CEUS has been associated with past ischemic neurological events [159].

While a pathophysiologic link exists between the presence of inflamed cells and the triggering of neo-angiogenesis, the temporal association between inflammation and neovascularization within the plaque has yet to be firmly established. Therefore the aim of this study was to systematically assess the presence of inflammation and neovascularization using FDG-PET/CT and CEUS respectively in a population of consecutive asymptomatic and symptomatic patients scheduled for carotid surgery. Imaging findings were then systematically compared with histology.

MATERIALS AND METHODS

PATIENT RECRUITMENT AND STUDY PROTOCOL

Patients referred for carotid endarterectomy were prospectively recruited for this study. After obtaining written informed consent and completing a baseline questionnaire, patients were invited to attend a same-day combined assessment of carotid plaque inflammation by ^{18}F-FDG PET/CT, and carotid IPN by CEUS. Imaging was performed by a physician blinded to the patient's history and with a maximal delay of 72 hours from the carotid surgery. The inclusion criteria were as follows: age >18 years, >70% carotid stenosis as determined by duplex ultrasound and/or CTA. The indication for surgery was based on the referring physician's decision. The exclusion criteria were pregnancy, inability to provide informed consent, and a known allergy to sulfur-containing drugs. Both asymptomatic and symptomatic patients were recruited. Symptoms were defined as a carotid-territory related transient ischemic attack or stroke within 6 months of imaging. The study protocol was approved by the ethical committee of our institution and was conducted in the Cliniques Universitaires Saint-Luc, which obtained full AAHRPP accreditation for clinical research in 2015.

^{18}F-FDG-PET/CT IMAGING PROTOCOLANDANALYSES

After a fasting period of >6 hours, patients received an intravenous injection of 300±20 MBq of ^{18}F-FDG. Imaging was performed after a circulation time of 150±22 minutes. The patient's head was secured in a head-holder, with arms placed to either side. Images were acquired using a Gemini PET/CT system (Philips Healthcare, The Netherlands). The patients breathed normally while CT imaging was performed with a 16-slice multidetector

scanner (adaptive dose in Z-DOM mode; voltage, 120 kV; rotation, 500 ms; pitch, 0.813). One 15-minute bed position PET image (voxel size 2x2x2 mm^3) of the neck was obtained with the 3D mode and iterative reconstruction (3D line of response time-of-flight algorithm, Philips) using CT-based attenuation correction, random, and scatter corrections. Patients were kept in a quiet environment before and after injection.

On the basis of anatomic boundaries defined by CT, carotid FDG uptake was measured at 2-mm intervals along the long axis of the carotid artery within a region of 6 mm above and below the bifurcation point. At each axial cross section, a single region of interest (ROI) was drawn around the wall of the common or the internal carotid artery, and the maximum standardized uptake value (SUVmax) measured. SUV is the decay-corrected tissue concentration of FDG (kBq/mL) divided by the injected dose per body weight (kBq/g). Background FDG-uptake was measured within the internal jugular vein on 4 consecutive cross sections. Target-to-background ratio (TBR) was calculated by dividing the carotid plaque SUVmax by the venous blood SUVmax.

Plaque calcium score was evaluated by the Agatston method on an independent workstation (Osirix v5.7, Geneva, Switzerland). A calcified plaque was defined as a radiation-attenuating structure above an attenuation threshold of 130 Hounsfield units (HU). The same ROIs that we used for PET analysis were used for the calcium score.

CAROTID ULTRASONOGRAPHY, CONTRAST IMAGING PROTOCOL, AND ANALYSES

Carotid ultrasonography and CEUS were performed using a high-resolution ultrasound system (iU22; Philips Healthcare, The Netherlands) equipped with a 9-3 MHZ linear transducer designed for contrast applications. The examination consisted initially of B-mode imaging, color Doppler ultrasound, and pulsed Doppler ultrasound of the common and internal carotid artery to determine topography and plaque severity. The operator then switched to a contrast-specific real-time low mechanical-index (0.13) imaging modality (power modulation). SonoVuecontrast agent (Bracco Diagnostics, Milan, Italy) was then injected via the antecubital vein as a bolus of 2 mL followed by a saline bolus of 5 mL. During this time, the carotid artery was re-imaged longitudinally with a focus on stenosis. After the injection of ultrasound contrast agent, the lumen of the carotid artery was enhanced within 10 to 25 seconds. Power-modulation imaging is a pulse cancellation technique that transmits multiple pulses per image line, alternating full-amplitude pulses with half-amplitude pulses. Subtracting twice the return signal of the half-amplitude pulse from the return signal of the full-amplitude pulse cancels the linear response from the tissue, but not the nonlinear response from bubbles. To assess replenishment kinetics, microbubble destruction was achieved using five on-demand consecutive high-power frames (mechanical index (MI) 1.0). Imaging then returned automatically to low-power, real-time scanning (MI 0.13). This switch to low MI preserves the microbubbles that are destroyed by imaging at high MI, and therefore allows microbubble replenishment to be imaged in real-time [153]. A cineloop including images obtained at least 2 seconds before and 15 seconds after the appearance of the contrast agent in the lumen was

acquired and digitally stored for subsequent analysis. If necessary, the bolus injection and the imaging sequences were repeated. IPN was graded semi-quantitatively as absent (low-grade CE: grade 0) or present in the plaque body (high-grade CE: grade 1). Images were graded by 2 independent investigators who were blinded to the patient's symptoms in order to evaluate inter-observer consistency.

IMMUNOHISTOCHEMICAL ANALYSES

At the time of carotid endarterectomy, the atherosclerotic plaques were immediately fixed in 10% buffered formalin and decalcified in the standard fashion. Specimens were transversally sectioned at 2-mm intervals. Each interval section was embedded in paraffin block, from which 5-µm sections were collected. Sections were then mounted on gelatin-coated slides and stained with the macrophage and endothelial cell markers, anti-CD68 (monoclonal antibody diluted 1/100, Dako), and anti-CD34 (monoclonal antibody diluted 1/500, Biocare Medical), respectively. A total of 8±2 slices covering the entire length of the plaque burden were analyzed per patient and per staining. All slices were scanned using Digital Image Hub 4.0 (Leica) for signal quantification. To evaluate CD68-staining intensity, computer-assisted planimetry (Tissue Image Analysis 2.0, Leica) was used. For each slice, the software identified the immunohistochemical staining to be quantified by minimizing background-staining artifacts using image filters **(Figure 1).** The same filter was used for every patient. Macrophage staining was reported as a percentage of the plaque area (macrophage area/total plaque area, %CD68), and was averaged for all slices. Vasa-vasora were identified by CD34-positive immunostaining and were counted at a magnification of 20X **(Figure 2)**. Each section was examined using a

grid to manually measure the number of neo-vessels and ensure coverage of the entire area of the section. Neovascularization was then expressed as micro-vessel density (number of micro-vessels per mm^2), and averaged for all slices. Furthermore, to enhance the confidence in the validity of our observations, we performed a double CD34/CD31-staining in 10 randomly selected patients participating in our study (see supplemental data). Intra-observer and inter-observer agreement was assessed for the quantification of micro-vessels. Finally, intraplaque haemorrhage was semi-quantitatively assessed on histological samples.

Figure 1.

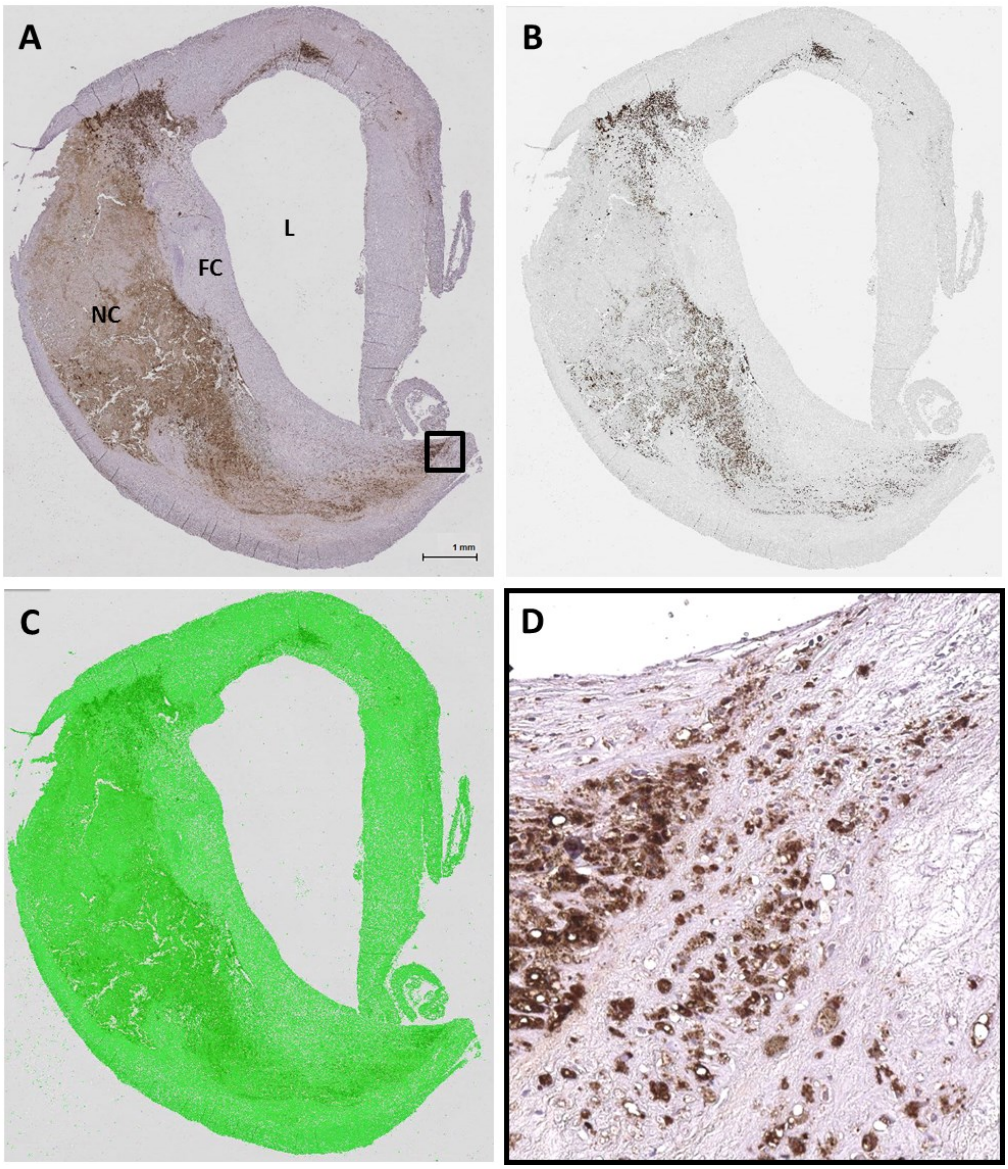

Quantification of the area percentage of CD68 staining on digitized immunohistochemically stained slides by using a computer-assisted planimetry. For each slice (A), the software identified the immunohistochemical staining to be quantified by minimizing background-staining artifacts using image filters (B). Macrophage staining was reported as a percentage (in this example: 7.16%) of the total plaque area (C). The boxindicates the region corresponding to the high-powered CD68 stain (D). L indicates lumen, FC indicates fibrous cap and NC indicates necrotic core.

Figure 2.

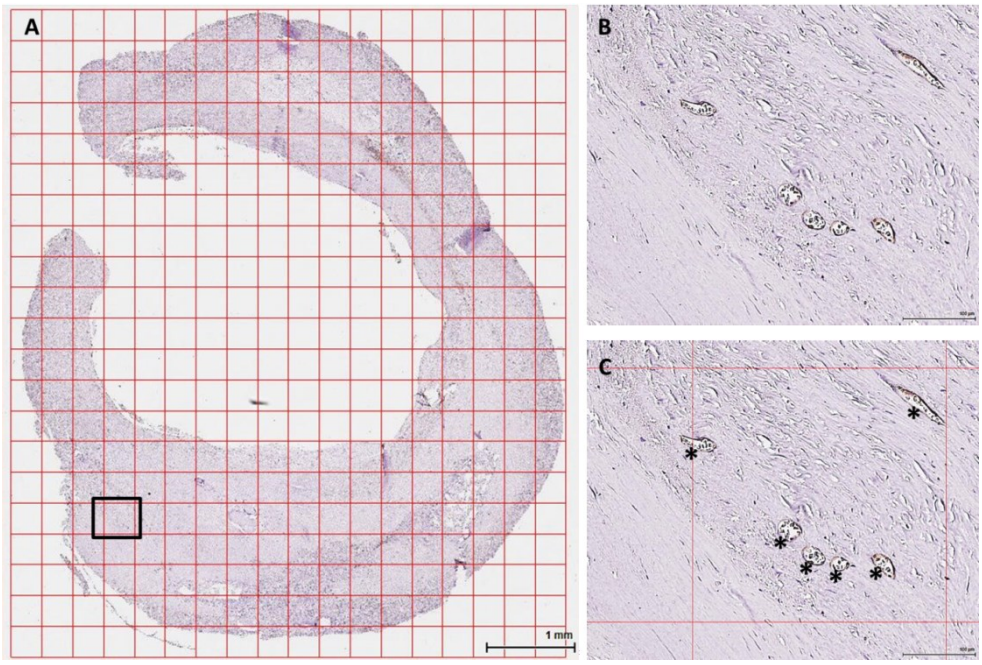

CD34 quantification. Each section was examined using a grid (A) to ensure coverage of the entire area of the section. Vasa-vasora were identified by CD34-positive immunostaining (*) and were counted at a magnification of 20X (the boxindicates the region corresponding to the high-powered CD34 stain, B and C).

STATISTICAL ANALYSES

Continuous variables are presented as mean ± SD or as median with interquartile range. Continuous variables were compared between two groups using the Mann-Whitney U-test. The Spearman method was used to assess correlations between TBR and the histopathologic assessment of inflammation (CD68-staining) and the number of neo-vessels, and between CD68-staining and the number of neo-vessels. To determine intra- and inter-observer variability, CD34-stained images were re-analyzed separately by 2 observers. The interval between the initial analyses and those made for variability assessment were >3 months. Intra- and inter-observer variability

in quantitative parameters were assessed by computing intra-class correlation coefficients (ICC) and by calculating the limits of agreement between measurements using Bland-Altman analysis. Kappa statistics were used to determine the levels of agreement between the visual grading scores of the CEUS readers. Kendall's tau coefficient was used to measure the association between TBR and the CE-grade and between CE-grade and symptoms. A two-sided value of $P< 0.05$ was considered significant. All statistical analyses were performed using SPSS version 21.0 statistical software (Chicago, IL).

RESULTS

PATIENT VARIABLES

A total of 30 patients were included in this study; their characteristics are displayed in **Table 1**. The mean age was 72 ± 9 years, 22 patients were male, with 11 patients symptomatic. Symptoms consisted of transient ischemic attack for 4 patients and stroke for 7 patients. The mean delay between symptoms and surgery was 25 (10-36) days.

Table 1 Patient's characteristics.

Patient Characteristics	All Patients (n=30)	AsymptomaticPatients(n=19)	SymptomaticPatients(n=11)	p value
Age, y	72±9	71.5±9	73±10	0.6
Male sex	22/8 (73%)	14/5 (74%)	8/3 (73%)	0.97
Body mass index, kg/m²	27.7±4.5	27.5±4.1	28.3±5.3	0.8
Diabetes	7 (23%)	5 (26%)	2 (18%)	0.73
Smoking	5 (17%)	4 (21%)	1 (9%)	0.6
Hypertension	28 (93%)	17 (90%)	11 (100%)	0.64
Hyperlipidemia	24 (80%)	15 (79%)	9 (82%)	0.9
Statin use	24 (80%)	15 (79%)	9 (82%)	0.9
Coronary artery disease	16 (53%)	10 (53%)	6 (54.5%)	0.93
Carotidstenosis (%)	84%±9	85%±9	82%±10	0.46
Glucose pre FDG-PET/CT (mg/dL)	106±25	100±16	114±34	0.32
Delay between FDG-PET/CT and CEUS (hours)	3 (2-17)	3 (2-4)	5 (3-20)	0.97
Delay between imaging and surgery (days)	1 (1-1.2)	1 (1-1)	1(0-2)	0.52
Delay between symptoms and surgery (days)	NA	NA	25 (10-36)	NA

Values are presented as mean±SD or n (%) or as median with interquartile range.

IMAGING DATA VALIDATED BY HISTOLOGY

As expected, we found a good correlation between the plaque ^{18}F-FDG-uptake and the number of macrophages (**Figure 3A**, r =0.78, p < 0.001). ^{18}F-FDG-uptake as well as macrophage number were inversely associated with calcium score (r= -0.43, p=0.017 and r=-0.37, p= 0.041, respectively). Plaques with more intense CE showed a significantly higher amount of neo-vessels as assessed by histology (mean vessel density: 4.84±2.41/mm² in plaques with grade 0 contrast enhancement versus 9.92±3.53/mm² in plaques with grade 1 contrast enhancement (**Figure 3B**, p < 0.001)). We could find no correlation between vessel number and the calcium score (r=-0.24, p=0.21).

Figure 3.

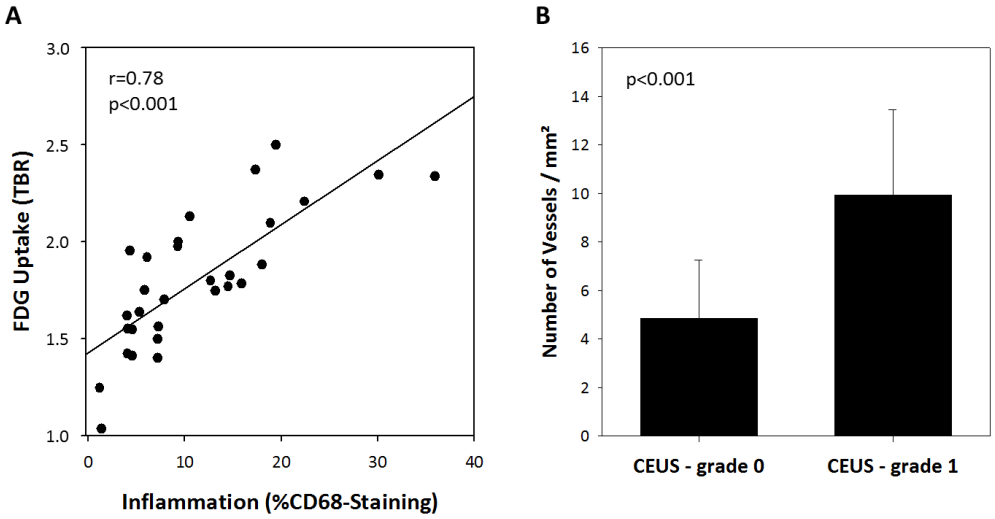

(A) PET measurement of ^{18}F-FDG uptake versus macrophage staining. The PET measurement of carotid plaque FDG uptake (TBR) was compared with an immunohistochemical assessment of inflammation. We identified a significant correlation between TBR and macrophage density. (B) A quantitative evaluation of CEUS versus vessel number within the plaque. The density of micro-vessels is greater in plaques with CEUS - grade 1 compared with CEUS – grade 2. The bar graph shows mean values, with standard deviations.

INFLAMMATION AND NEOVASCULARIZATION ARE NOT SYSTEMATICALLY ASSOCIATED WITHIN THE PLAQUE

As illustrated in **Figures 4and 5** respectively, grade-1 CEUS did not correlate with a high ^{18}F-FDG-uptake, and inflammation could be observed in carotid plaques with a grade-0 CEUS. When patients were categorized according to their inflammatory status based on median TBR, no agreement was found between inflammation and IPN (**Table 2**, Kendall coefficient Ţ: 0.0, p>0.99). The mean TBR observed for grade-0 and -1 CEUS plaques were comparable (1.69±0.39 vs. 1.87±0.31 respectively, p= 0.28, **Figure 6A**). Similarly, macrophage infiltration as determined by immunohistochemistry was comparable for grade-0 versus grade-1 CEUS plaques (CD68% 9.77±6.47 vs. 12.38±9.5 respectively, p= 0.59, **Figure 6B**). Finally, neither 18F-FDG uptake nor CD68% were found to correlate with the degree of intra-plaque neo-vascularization (**Figures 7A and 7B**) or the presence of haemorrhage (p= 0.4 and p= 0.23 respectively).

Figure 4.

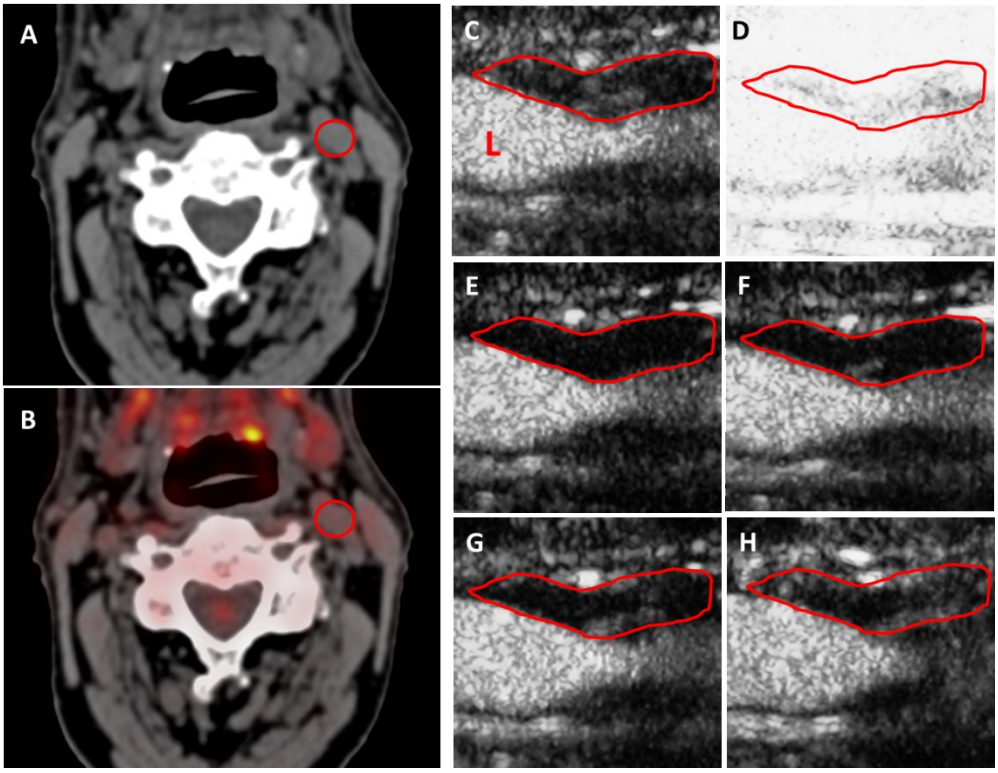

Examples of ^{18}F-FDG PET/CT and CEUS in an asymptomatic male patient (76-years-old) with severe non-calcified carotid stenosis. A low ^{18}F-FDG uptake (TBR: 1.47) was demonstrated by ^{18}F-FDG PET/CT at the level of the left proximal internal carotid artery (red circle, panel A (CT image, axial plane) and B (^{18}F-FDG PET/CT image, axial plane). In this patient, the presence of extensive IPN (panels C to H) was evidenced by CEUS. On the pre-flash image (panel C), contrast microbubbles are visualized in the plaque (red contour). These microbubbles are destroyed by a high-energy (MI: 1.0) ultrasound burst (panel D). The imaging frame immediately after the burst shows the complete disappearance of the microbubbles from the plaque (panel E) and their progressive replenishment after 1 second (panel F), 3 seconds (panel G), and 6 seconds (panel H). Histologic analyses confirmed the imaging findings, with a low percentage of CD68 staining (4.1%) and a high micro-vessel density (10.6 vessels per mm²). L indicates the lumen of the ICA.

Figure 5.

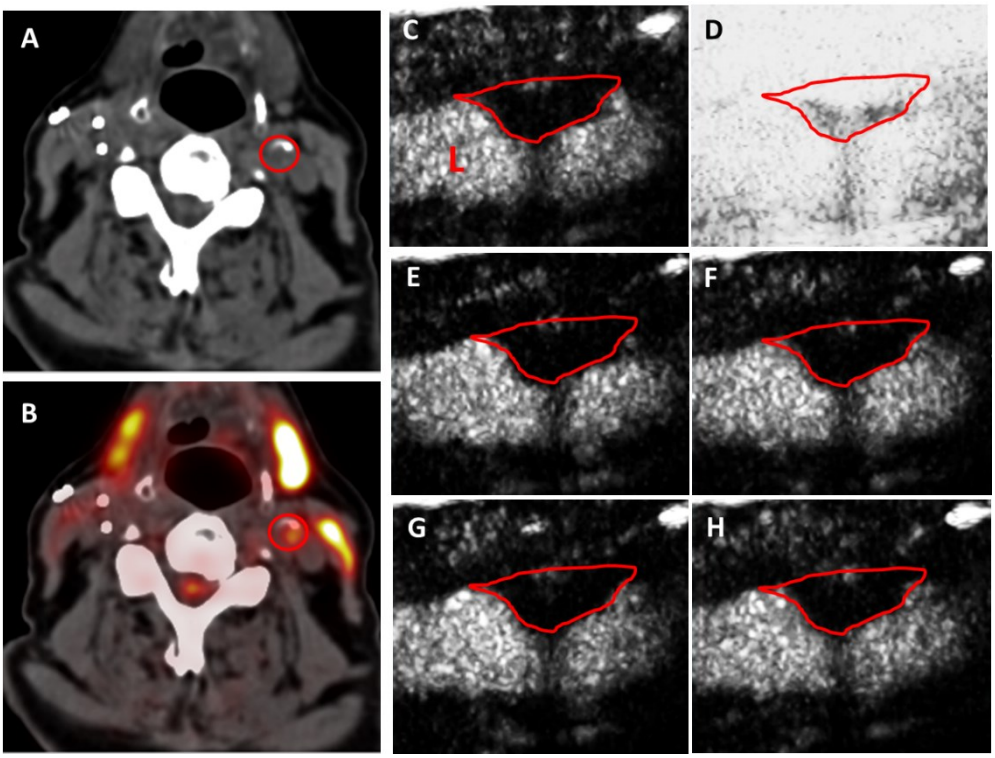

Examples of ^{18}F-FDG PET/CT and CEUS in a symptomatic male patient (68-years-old) with severe, lightly calcified carotid stenosis. A high ^{18}F-FDG uptake (TBR: 2.14) was demonstrated by ^{18}F-FDG PET/CT at the level of the left proximal internal carotid artery (red circle, panel A (CT image, axial plane, calcified area on the top of the red circle) and B (^{18}F-FDG PET/CT image, axial plane). In this patient, CEUS revealed no IPN (panel C to H). On the pre-flash image (panel C), contrast microbubbles are not visualized in the plaque (red contour). After a high-energy (MI: 1.0) ultrasound burst (panel D), the subsequent images (E-H) fail to show microbubble replenishment, either immediately after the high-MI US burst (E), or 1 second (F), 3 seconds (G), or 6 seconds after the high-MI US burst (H). Histologic analyses confirmed the imaging findings with a high percentage of CD68 staining (22.4%) and a low micro-vessel density (5.5 vessels per mm²). L indicates the lumen of the ICA.

Table 2. Association between FDG-PET/CT based inflammation and CEUS based IPN.

	CE grade O	CE grade 1
TBR -	6	9
TBR +	6	9

Patients were categorized according to their inflammatory status based on the median TBR value (1.81). No association was found between inflammation and IPN (Kendall coefficient Ţ: 0.0, p>0.99).

Figure 6.

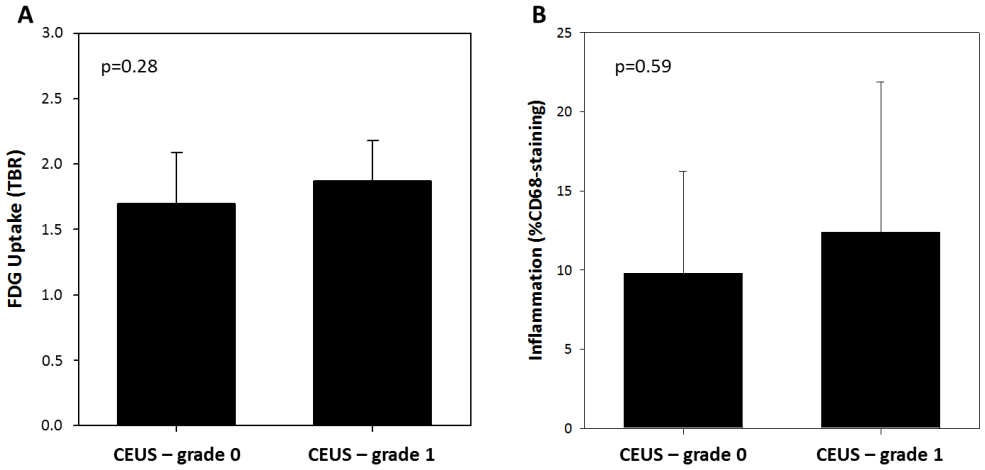

Inflammation and imaging-derived IPN. (A) The mean TBR that we observed in grade-0 CEUS plaques was no different to that observed in grade-1 CEUS plaques. (B) Macrophage infiltration by histology did not differ between grade-0 or grade-1 CEUS plaques. Bar graphs show mean values with standard deviations.

Figure 7.

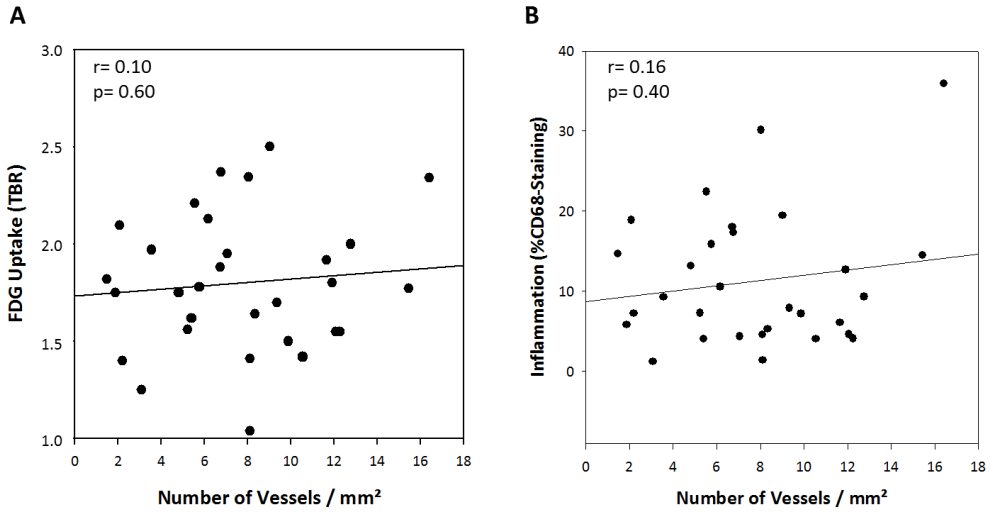

Inflammation versus histology-derived IPN. Neither 18F-FDG uptake (A), nor CD68% (B), correlated with the degree of neo-vascularization within the plaque.

FEATURES ASSOCIATED WITH SYMPTOMS

TBR was higher in symptomatic patients compared to asymptomatic patients (1.97±0.28 vs. 1.68±0.35, **Figure 8A**, p= 0.05). Similarly, macrophage infiltration was significantly higher in the carotid plaque of symptomatic patients compared to asymptomatic patients (14.16±6.2 *vs.* 8.1±6.6 %CD68 respectively, **Figure 8B**, p= 0.021). In contrast, the degree of neovascularization was comparable for asymptomatic and symptomatic patients (8.24±4 vs. 6.82±4 vessels/mm² respectively, **Figure 8C**, p= 0.35). When patients were categorized according to their symptomatic status, no agreement was found between symptoms and IPN based on CEUS-grade (Kendall coefficient Ƭ: 0.085, p=0.65, **Table 3**). Finally, we could identify no difference in the grading of carotid calcification (calcium score) according to symptomatic status (p= 0.98).

Figure 8.

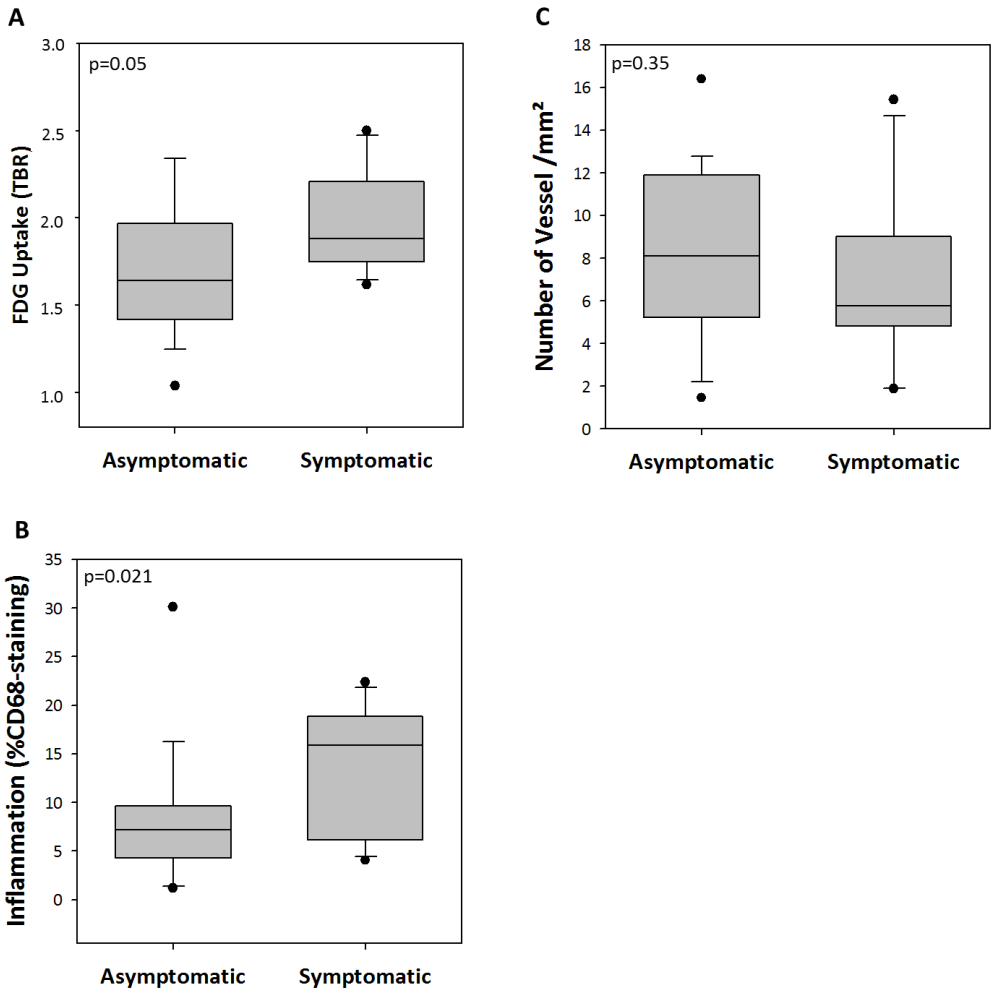

Box whisker plots showing inflammation versus symptoms. (A) TBR is higher in symptomatic patients compared with asymptomatic patients. (B) Macrophage infiltration is higher in the carotid plaques of symptomatic patients compared with asymptomatic patients. (C) The degree of neo-vascularization within the plaques does not differ according to symptomatic status. Horizontal lines within boxes represent medians, with the top and bottom of the box representing the upper and lower quartiles. The extensions above and below these indicate maximum and minimum values, together with outliers denoted by dots. The vertical line shows the full range of data values.

Table 3. Association between symptomatic status and CEUS based IPN.

	CEUS-grade 0	CEUS-grade 1
symptomatic	5	6
asymptomatic	7	12

Patients were categorized according to their symptomatic status. No association was found between symptoms and IPN based on CEUS-grade (Kendall coefficient: Ţ: 0.085, p=0.65)

INTRA- AND INTER-OBSERVER AGREEMENT

We found an intra-observer reproducibility (ICC) of 0.77 with a bias of 80 ± 74, and an inter-observer reproducibility (ICC) of 0.83 with a bias of 93 ± 81 for micro-vessel measurements. The concordance for the qualitative assessment of CEUS was determined by grading intra-plaque neovascularization by 2 different readers and by 1 reader at an interval of more than 3 months using CEUS cine-loops. The intra-observer agreement was 91% (kappa = 0.82), with an inter-observer agreement for the same parameter of 77% (kappa = 0.51).

DISCUSSION

Plaque inflammation and neovascularization are 2 recognized features of plaque vulnerability [49]. Here, we demonstrate that inflammation is not systematically associated with the degree of neovascularization within the plaque, suggesting a temporal separation of these processes. Further, intra-plaque inflammation was found to be associated with clinical symptoms whereas IPN was not.

Atherosclerosis is a chronic inflammatory disease characterized by lipid-containing lesions of large- and medium-sized arteries. Vasa vasora participate in the pathogenesis of the disease and proliferate to meet the nutritional needs of the artery's outer medial layer when metabolic demands exceed oxygen delivery from the luminal blood. Hypoxia is the most potent stimulus for angiogenesis, predominantly by its activation of the hypoxia-inducible factor/vascular endothelial growth factor pathway [232]. A molecular link exists between the expansion of adventitial vasa vasora, neointima formation, and atherosclerotic plaque development. Notably, their regression is accompanied by reduced plaque growth [66]. Neo-vessels may serve as a pathway for the recruitment of leucocytes to high-risk areas of plaque. Micro-vessel density has been shown to increase in inflamed lesions and correlates with plaque rupture [233]. Newly formed micro-vessels may promote intra-plaque bleeding, which increases the levels of free cholesterol, and leads to rapid necrotic core expansion. This mechanism contributes to the vulnerability of the plaque. Fortunately, not all plaques will progress to destabilization and a substantial number will heal spontaneously. Some of the relevant mechanisms have been elucidated and promising strategies to stabilize atherosclerotic plaques are under development [234]. Atherosclerotic lesions evolve in successive phases during which inflammation and neovascularization are intertwined [235, 236]. However, it must be acknowledged that our ability to predict which plaques will progress to destabilization and cause an unstable syndrome such as TIA, stroke, or acute coronary syndrome is currently very limited. Identifying vulnerable plaques before their rupture is the Holy Grail for clinicians. In this work, we identify patients with plaque inflammation without evidence of neovascularization, as well as the opposite. Our

imaging findings have been validated by a systematic immunohistochemical evaluation covering the entire length of the surgical specimen.

Conflicting data for the temporal association of intra-plaque inflammation and neovascularization currently exists in the literature. Some authors have found a weak correlation between the two processes [237], which is contradicted by others [238]. We could find no correlation between either of these major determinants of plaque vulnerability, highlighting the practical challenges in defining imaging strategies with which to assess plaque vulnerability. Furthermore, plaque characteristics also seem to be dependent on general factors such as sex and age [239]. Several outstanding questions have yet to be satisfactorily addressed. For example, which plaque feature is the best predictor of a clinical event? When should we image, and should imaging be repeated? Can we base our imaging strategy on one plaque feature alone, and will we be in a position to predict the natural history of an atherosclerotic plaque? Ultimately, it is likely that imaging based on multiple structural and/or molecular targets will be required to identify atherosclerotic plaques at risk of rupture. Shear stress imaging, active calcification imaging (^{18}F-NaF) or other imaging tracers could also be helpful in achieving this goal [143, 240].

In previous studies to image vulnerable plaques, multimodality imaging has been investigated. In particular, the combined assessment of inflammation by ^{18}F-FDG PET-CT and neovascularization by dynamic contrast-enhanced magnetic resonance imaging (DCE-MRI) has been evaluated in patients with carotid plaques [188, 192, 237], with divergent results reported (inverse, weak, or a moderate correlation between inflammation and neovascularization). However, systematic histologic validation was either lacking in those studies, or was limited to a comparatively small number of

patients [192]. Furthermore, the same parameter for assessing neovascularization, K^{trans}, was used, which reflects microvascular flow and permeability rather than the total number of neo-vessels. The contrast agent used for CEUS evaluation in our study is purely intravascular and does not bridge the endothelial barrier. Consequently, this approach reveals the total number of neo-vessels in the plaque and not endothelial permeability, which is linked to inflammation. This approach therefore constitutes the major difference with DCE-MRI, with either technique evaluating different tissue criteria (i.e. the number of neo-vessels *vs.* endothelial permeability). This may explain the discrepancies reported between results obtained using the two techniques, and the absence of any correlation between inflammation and the total intra-plaque number of vessels that we found in our study. The systematic immuno-histologic evaluation of the entire length of the surgical specimens of our patients confirmed our imaging findings, and constitutes, to date, the largest series in which the two imaging techniques have been correlated with histology.

In our series and others [95, 239], a history of neurological symptoms is associated with increased plaque inflammation, whereas neovascularization is not. It is noteworthy that inflammation also seems to be associated with a higher risk of subsequent stroke, unlike neovascularization [121, 241, 242]. Collectively, an assessment of these data leads us to hypothesize that inflammation is probably the more useful parameter (than the presence of neovascularization) in discriminating patients at a high *vs.* low risk for presenting acute syndromes. This hypothesis now warrants prospective validation. Interestingly, Staub et al. [159] found an association with plaque enhancement, as assessed by CEUS, and a past history of cardiovascular events; a finding that we failed to repeat here. One explanation could be that

our patients manifested more advanced disease. Like FDG-PET/CT, the value of CEUS for predicting clinical events should also now be evaluated in prospective trials. We found an inverse correlation between CT calcium score and plaque inflammation while no correlation was found between vessel number and the calcium score. It confirms that FDG is providing a measure of disease activity beyond measurement of plaque burden. Secondly it is consistent with the hypothesis that extensive macroscopic calcification observed on CT are associated more with burnt-out stable disease than acute inflammation. Hence, this might have potential clinical utility. Finally, recent data suggest that emotional stressors could lead to cardiovascular disease by increasing arterial inflammation [243]. Whether stroke might induce a similar stress response and up-regulation of plaque inflammation is unknown. Future studies are needed to confirm this hypothesis.

The possible limitations of this study are as follows. First, although the results of the present study are limited by its modest sample size, its strength lies in the simultaneous assessment of PET activity, IPN by CEUS, and histologic validation. Nonetheless, subgroup analyses of asymptomatic versus symptomatic patients must be interpreted with caution. Second, we did not co-register imaging with histologic datasets. Given the poor spatial resolution of FDG-PET, and the impossibility of co-registering CEUS with histology, we deliberately chose not to perform co-registration. We attempted to overcome this limitation by analyzing the total length of the surgical specimen to collect the entirety of the information contained within the plaque. Furthermore, inherent to the surgical technique, we could not quantify inflammation and neovascularization present in the adventitia by histology. Third, since histological analyses were mandatory for this study,

we did not include patients with less advanced disease. Fourth, atherosclerotic plaques were not imaged by a high resolution imaging modality like MRI. Thus, components including fibrous cap thickness, lipid-rich necrotic core, or intra-plaque hemorrhage which could be the physiopathological link between neoangiogenesis and inflammation were not evaluated. Finally, no scan-rescan reproducibility was performed.

CONCLUSIONS

Inflammation and neovascularization are not systematically associated in the carotid plaques of patients suggesting a temporal separation of these processes. Inflammation seems also more pronounced when symptoms are present, whereas neovascularization seems not. This study highlights the practical challenges in defining imaging strategies with which to assess plaque vulnerability.

SUPPLEMENTAL MATERIAL

Supplemental Methods.

Assessment of microvessel density by using a cocktail of endothelial cell markers CD34/CD31. Comparison with the single CD34-staining.Double CD34/CD31-staining was performed in 10 randomly selected patients participating in our study. Sections were mounted on gelatin-coated slides and stained with the endothelialcell markers anti-CD34 (monoclonal antibody diluted 1/500, Biocare Medical). The signal was quantified as described in the methods section: vasa-vasorawere identified by CD34-positiveimmunostaining and were counted at a magnification of 20X. Afterwards, the same sectionswere stained with the endothelial cell markers anti-CD31 (monoclonal antibody diluted 1/50,DAKO). The vasa vasora were identified by CD34/CD31-positive immunostaining and were recounted. The signal was compared to the single CD34 staining. As shown in this figure, we did not observe any visual difference between the single CD34-staining and the doubleCD34/CD31-signal. The correlation between the 2 different staining was excellent (r= 0.9).

Supplemental figure

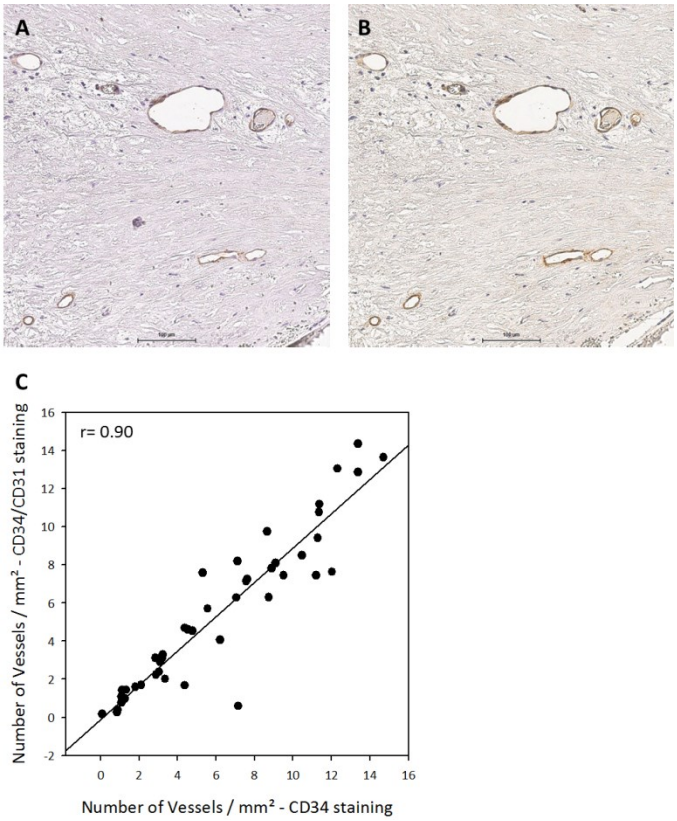

As shown in this typical example, no visual difference was observed between the single CD34 staining (A) and the double CD34/CD31 staining (B). The correlation between the 2 different staining was excellent (C).

DATA NOT PUBLISHED

Assessment of microvessel density by using other markers

Some others markers have been try without good vessel visualization.

a. vWF : van Willebrand Factor. b. eNOS : endothelial Nitric Oxide Synthase. c. Isolectine B4

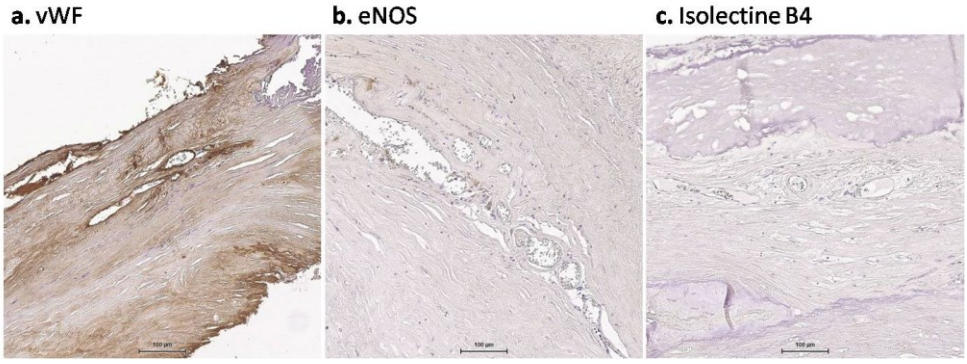

VI. A Randomized Trial on the Optimization of ^{18}F-FDG Myocardial Uptake Suppression: Implications for Vulnerable Coronary Plaque Imaging

Fabian Demeure [1]; François-Xavier Hanin [2]; Anne Bol [2]; Marie-Françoise Vincent [3]; Anne-Catherine Pouleur [1]; Bernhard Gerber [1]; Agnès Pasquet [1]; François Jamar [2]; Jean-Louis J. Vanoverschelde [1]; David Vancraeynest [1].

4. From the Pôle de Recherche Cardiovasculaire (CARD), Institut de Recherche Expérimentale et Clinique (IREC), Université Catholique de Louvain, Brussels, Belgium.
5. From the Pôle d'imagerie médicale, radiothérapie et oncologie (MIRO), Institut de Recherche Expérimentale et Clinique (IREC), Université Catholique de Louvain, Brussels, Belgium.
6. From the Laboratoire des Maladies Métaboliques et Centre de Dépistage Néonatal, Cliniques Universitaires St-Luc, Université Catholique de Louvain, Brussels, Belgium.

Journal of Nuclear Medicine2014 Oct;55(10):1629-35

ABSTRACT:

^{18}F-FDG-PET/CT can be used to detect arterial atherosclerotic plaque inflammation. However, avid myocardial glucose uptake may preclude its use for visualizing coronary plaques. Fatty acid loading or calcium channel blockers (CCB) could decrease myocardial ^{18}F-FDG uptake, thus assisting coronary plaque inflammation identification. The present prospective randomized trial compared the efficacies of different interventions for suppressing myocardial ^{18}F-FDG uptake. We also investigated whether circulating free fatty acid (cFFA) levels predicted the magnitude of myocardial ^{18}F-FDG uptake. **Methods:** Thirty-six volunteers ate a high-fat low-carbohydrate (HFLC) meal, followed by a 12-hour fasting period. They were then randomized to one of four intervention groups. Group 1 received no additional preparation and served as reference. Groups 2 and 3, respectively, received a solution containing 43.8 g lipids (KetoCal®) or 50 mL olive oil one hour before ^{18}F-FDG injection to evaluate the impact of fatty acid loading on myocardial ^{18}F-FDG uptake. Group 4 received verapamil to evaluate the effect of CCB. Cardiac PET/CT was performed after administration of 370 MBq^{18}F-FDG. Myocardial uptake suppression was assessed using a qualitative visual scale (QVS) and by measuring the myocardial SUV_{max}. Insulin, glucose, and cFFA were serially measured. **Results:** QVS showed good myocardial ^{18}F-FDG uptake suppression in 8/9, 5/9, 4/9, and 8/9 subjects of group 1, 2, 3, and 4, respectively (P = 0.09). SUV_{max} did not significantly differ between groups (P = 0.17). Interestingly, cFFA levels were higher in volunteers with good **suppression** (0.80 ± 0.31 mmol/L) versus those with poor suppression (0.53 ± 0.15 mmol/L; P = 0.011). We found an inverse correlation between cFFA level (measured at ^{18}F-FDG injection) and the SUV_{max} (R = 0.61). ROC-curve analysis

identified 0.65 mmol/L cFFA as the best cut-off value to predict adequate ^{18}F-FDG uptake suppression (PPV: 89%). **Conclusion:** A HFLC meal followed by a 12-hour fasting period effectively suppressed myocardial ^{18}F-FDG uptake in a majority of subjects. Neither complementary fatty acid loading nor verapamil administered 1 hour before ^{18}F-FDG injection conferred any additional benefit. Myocardial ^{18}F-FDG uptake was inversely correlated with cFFA level, representing an interesting way to predict myocardial ^{18}F-FDG uptake suppression.

Key Words: free fatty acids; ^{18}F-FDG-PET/CT; calcium channel blocker; inflammation; vulnerable coronary plaque

INTRODUCTION

Cardiovascular diseases are still a leading cause of mortality in western countries [244]. The high mortality rate of cardiovascular diseases results from arterial thrombosis, which is often triggered by a ruptured plaque. Rupture-prone plaques—also called vulnerable plaques—exhibit typical features, among which inflammation is a key factor [10, 11, 229]. Metabolically active cells, such as activated macrophages, take in and progressively accumulate ^{18}F-FDG which can then be imaged and quantified with PET. ^{18}F-FDG is a well-validated tracer for imaging plaque inflammation in large arteries and aorta [96, 245]. However, coronary artery imaging is more challenging, mainly due to intense tracer uptake in adjacent myocardium.

The quantity and quality of substrate supply to the heart are determined by the dietary state. Long-chain fatty acids (FFA) are the major substrates for the heart. Under fasting conditions, FFA are released from the adipose tissue, enter the circulation, and are taken up by cardiac cells. FFA inhibit glycolysis, rerouting glucose toward glycogen synthesis. On the other hand, glycogen phosphorylase is the main regulator of glycogenolysis and is activated by phosphorylation, either by cAMP-dependent protein kinase or by Ca^{2+}-activated phosphorylase kinase [105]. Intracellular calcium acts as a stimulus for cardiac glucose uptake. Accordingly, it has been demonstrated that high-fat low-carbohydrate (HFLC) dietary preparations can significantly reduce myocardial ^{18}F-FDG uptake in oncological patients[102-104],while calcium channel blockers (CCB) may help to reduce myocardial ^{18}F-FDG uptake in a murine model [246]. However, randomized trials evaluating the impact of these interventions on reducing ^{18}F-FDG uptake are lacking.

Also the optimal time point to perform PET acquisition after ^{18}F-FDG injection remains poorly known. Preliminary studies evaluating ^{18}F-FDG-PET/CT as a method for coronary plaque inflammation imaging have performed PET acquisition three hours after ^{18}F-^{18}F-FDG injection [99, 100, 247]. On the other hand, studies evaluating the impact of dietary regimen on the quality of ^{18}F-FDG uptake suppression, have performed PET acquisition one hour after ^{18}F-FDG injection [102, 104]. No data are available regarding the impact of the dietary regimen on ^{18}F-FDG uptake at different time intervals.

The present prospective randomized study evaluated the impacts of different interventions—including complementary FFA loading and CCB—on unwanted myocardial ^{18}F-FDG uptake. We also sought to determine whether measuring insulin, glucose, or circulating FFA level could predict the amplitude of ^{18}F-FDG-uptake suppression. Finally, to clarify the most appropriate time-point for imaging coronary plaque inflammation, we evaluated the impact of different interventions on the myocardial ^{18}F-FDG signal at different time-points.

MATERIALS AND METHODS

Study Population and Intervention Assignment

Thirty-six healthy volunteers were recruited among the paramedical staff of the hospital and were paid for their participation. They were instructed to eat a HFLC meal based on a list of appropriate and inappropriate food items (established by the dietetic department), and then to fast (water permitted) for 12±1 hours. A pre-imaging interview was systematically conducted to precisely check the composition of the meal ingested the evening before.

The volunteers were then randomly assigned, by drawing lots, to one of the following four pre-^{18}F-FDG-PET/CT intervention plans (nine volunteers in each group). ***Group 1*** did not receive any additional preparation to evaluate the effect of HFLC diet alone, and served as reference. ***Group 2*** received a 250-mL liquid mixture containing a commercial high-fat solution (KetoCal®)—comprising 43.8 g fat (78% unsaturated), 1.8 g carbohydrate, and 9.15 g protein—at 60 minutes prior to ^{18}F-FDG injection to evaluate the effect of complementary fatty acid loading on ^{18}F-FDG-uptake. ***Group 3*** received 50 mL olive oil (46 g fat, without carbohydrate or protein) at 60 minutes prior to ^{18}F-FDG injection to evaluate the effect of another form of complementary fatty acid loading on ^{18}F-FDG uptake. ***Group 4*** received 120 mg of Verapamil (p.o.) at 60 minutes prior to ^{18}F-FDG injection to evaluate the effect of CCB on ^{18}F-FDG uptake (Fig. 1). The volunteers were instructed to avoid exercise, alcohol, benzodiazepine, and caffeine for at least 24 hours prior to the injection. Pregnancy was an exclusion criterion, and all female volunteers underwent urine pregnancy testing. All volunteers gave their written informed consent, and the study protocol was approved by the ethical committee of our institution.

FIGURE 1. Study protocol.

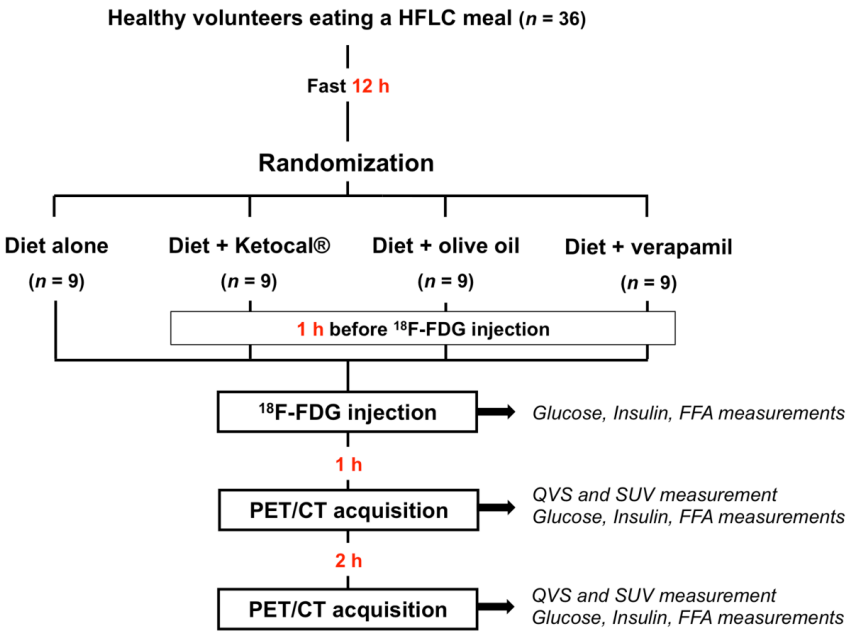

^{18}F-FDG-PET/CT Imaging Protocol

Imaging was performed at 60 and 180 minutes after intravenous administration of 370 MBq^{18}F-FDG to evaluate the impact of the intervention on myocardial uptake at two different time intervals. Images were acquired using a Gemini PET/CT system (Philips Healthcare, The Netherlands). The utilized equipment complied with the EARL accreditation ^{18}F-FDG PET-CT requirements for clinical research [248]. The volunteers breathed normally while CT imaging was performed with a 16-slice multi-detector scanner (adaptive dose in Z-DOM mode; voltage, 120 kV; rotation, 500 ms; pitch, 0.813). PET images (voxel size 4x4x4 mm^3) were obtained in 3D mode from the neck to the liver, with 5 minutes per bed position, and

were iteratively reconstructed (3D line of response time-of-flight algorithm, Philips medical systems) using CT-based attenuation correction, random and scatter corrections. The volunteers were kept in a quiet environment before and between the two imaging time-points. Effective radiation dose from ^{18}F-FDG was estimated at 7.1±0.2 mSv, using ICRP 106 publication (0,019 mSv/MBq conversion factor). Effective radiation dose from CT was 2.1 ± 1.0 mSv per procedure.

Image Analysis

Myocardial ^{18}F-FDG uptake was assessed on 60 and 180 minute images using a qualitative visual scale (QVS) based on the visual uptake categorical scale proposed by Williams and Kolodny [104]. The qualitative visual estimation of ^{18}F-FDG myocardial uptake was graded as follows: 0, homogeneously minimal; 1, mostly minimal or mild uptake; 2, mostly intense or moderate uptake; or 3, homogeneously intense (Fig. 2). QVS grades of 0 and 1 were considered "good suppression", while QVS grades of 2 and 3 were considered "poor suppression". To evaluate the interobserver reliability of the visual grading, images were graded by two independent investigators (F.D. and F.X.H.) who were blinded to the group assignment of each volunteer.

We also quantitatively assessed the myocardial ^{18}F-FDG uptake by measuring the maximum standardized uptake value (SUV_{max}). Based on anatomic boundaries defined by CT, a region of interest (ROI) was drawn around the left ventricle in the axial view at the level of the antero-lateral papillary muscle which was included in the analysis. To obtain a background value for ^{18}F-FDG uptake, six ROIs of 1 cm² each were drawn within the left atrium, and the mean SUV was measured and averaged.

Subsequently, for each volunteer, the target-to-background ratio (TBR) was calculated as the myocardial SUV_{max} divided by atrial blood mean SUV.

FIGURE 2. Qualitative visual scale (QVS) assessing myocardial ^{18}F-FDG uptake.

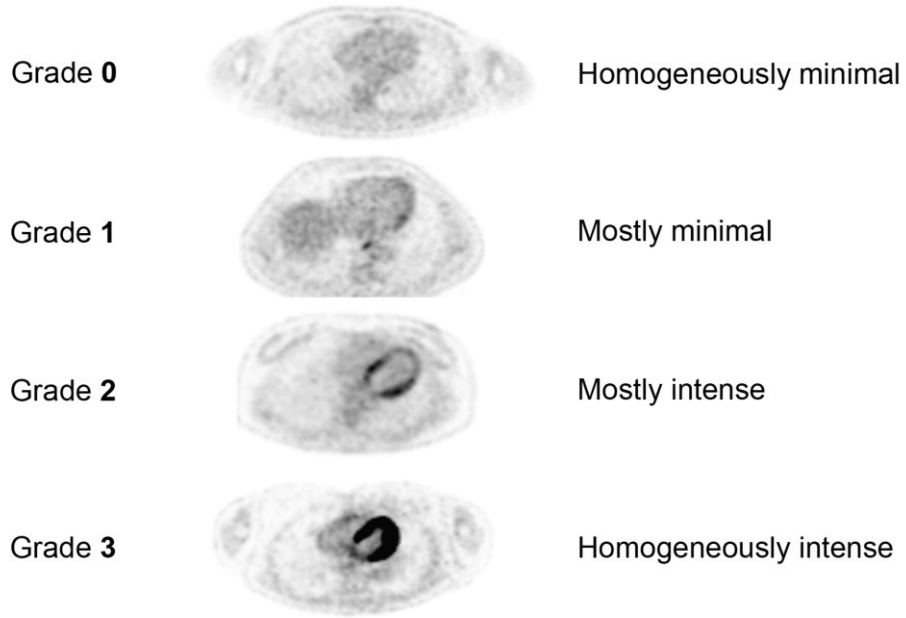

Blood Analysis

Blood samples were collected at ^{18}F-FDG injection, and at both imaging times (60 and 180 minutes after ^{18}F-FDG injection) for measurement of glucose, insulin, and cFFA levels (Fig. 1). Circulating FFA were measured using an enzymatic colorimetric method (Wako® NEFA-HR(2) assay). All measurements were performed in duplicate.

Statistical Analysis

Group comparisons of categorical variables were made using Pearson's chi-squared test. Continuous variables were expressed as mean ± SD. Continuous variables were compared between two groups using the Student's t-test, and were compared among all groups using analysis of variance (Kruskal-Wallis). Individual comparisons between groups were evaluated *post-hoc* using the Mann-Whitney test. We categorized the volunteers into tertiles according to cFFA level, and applied a trend test across ordered groups to assess the relationship between cFFA level and SUV_{max}. We performed a nonlinear regression between the values of SUV_{max} measured at 60 minutes and the cFFA level obtained at the time of injection. Kappa statistics were used to determine the levels of agreement between the visual grading scores of the two readers. For all analyses, differences with $P< 0.05$ were considered significant. Receiver-operating characteristics (ROC) curve analysis was used to identify the best cFFA level cut-off value for predicting myocardial ^{18}F-FDG-uptake suppression. All statistical analyses were performed using SPSS version 15.0 statistical software (Chicago, IL).

RESULTS

There were no significant between-group differences in age, BMI, blood pressure, heart rate, and pre-^{18}F-FDG-injection glucose level (table 1).

Table 1 : Baseline Characteristics of the Volunteers.

	Group 1 Dietalone (n=9)	**Group 2 Ketocal® (n=9)**	**Group 3 Olive oil (n=9)**	**Group 4 Verapamil (n=9)**	***p***
Age (y)	26±4	24±3	26±5	27±8	0.78
Gender (M/F)	6/3	7/2	5/4	7/2	0.71
BMI (kg/m^2)	22±2	24±2	24±4	22±2	0.32
Systolic BP (mmHg)	124±10	128±9	126±15	123±15	0.87
Diastolic BP (mmHg)	75±10	75±10	72±14	78±12	0.86
HR (bpm)	70±14	83±10	84±15	75±8	0.06
Glucose (mg/dL)	87±8	91±8	88±10	90±11	0.72

Values are expressed as mean ± SD or as number. Abbreviations: BMI: body mass index, bpm: beats per minute; BP: blood pressure ; HR : heart rate

Impact of FFA Loading and CCB on Myocardial ^{18}F-FDG Uptake Suppression

QVS grades of 0 or 1, indicating good myocardial uptake suppression, were observed in 8/9 volunteers in group 1, 5/9 volunteers in group 2, 4/9 volunteers in group 3, and 8/9 volunteers in group 4 (Fig. 3a; $P = 0.09$). The mean QVS grade did not significantly differ between groups (Fig. 3b; $P = 0.28$). The quantitative analysis showed that at 60 minutes after ^{18}F-FDG administration, the myocardial SUV_{max} did not significantly differ between groups (group 1, 2.3 ± 0.8; group 2, 4.6 ± 3.3; group 3, 5.5 ± 5.1; and group 4, 3.0 ± 2.7; Fig. 4a, $P = 0.17$). Similar results were obtained at 60 minutes for the TBR values (group 1, 1.50 ± 0.52; group 2, 2.93 ± 2.12; group 3, 3.53 ± 2.89; and group 4, 1.86 ± 1.50; Fig. 4b; $P = 0.14$).

FIGURE 3.

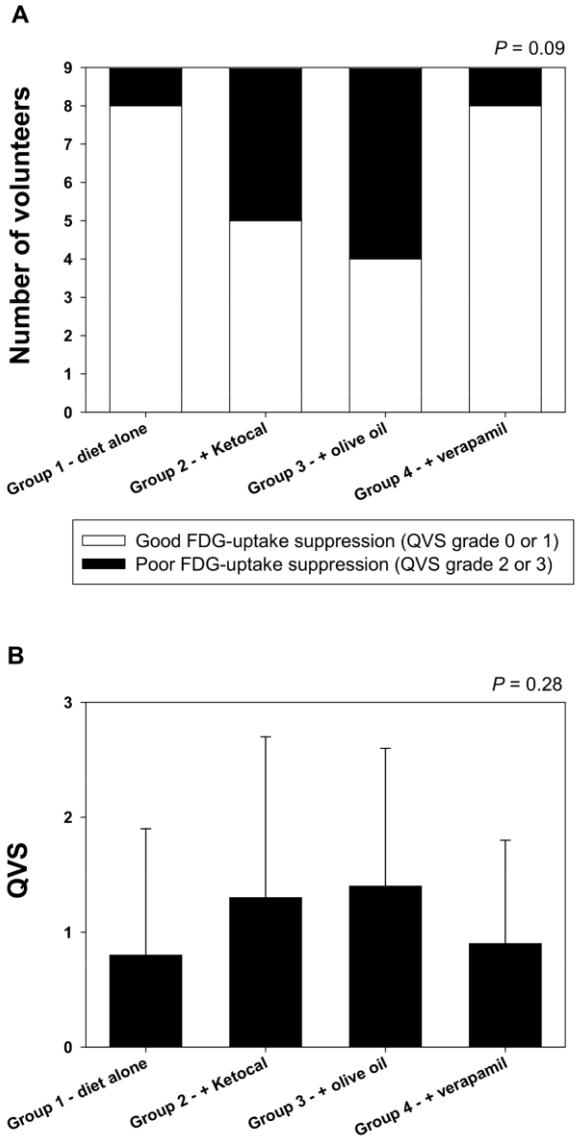

Box plots showing the number of volunteers with good (qualitative visual scale, grade 0 or 1) or poor (qualitative visual scale grade 2 or 3) myocardial ^{18}F-FDG uptake suppression in each group (P = 0.09) (**A**),and the mean qualitative visual scale grade in each group at 60 minutes (P = 0.28) (**B**).

FIGURE 4.

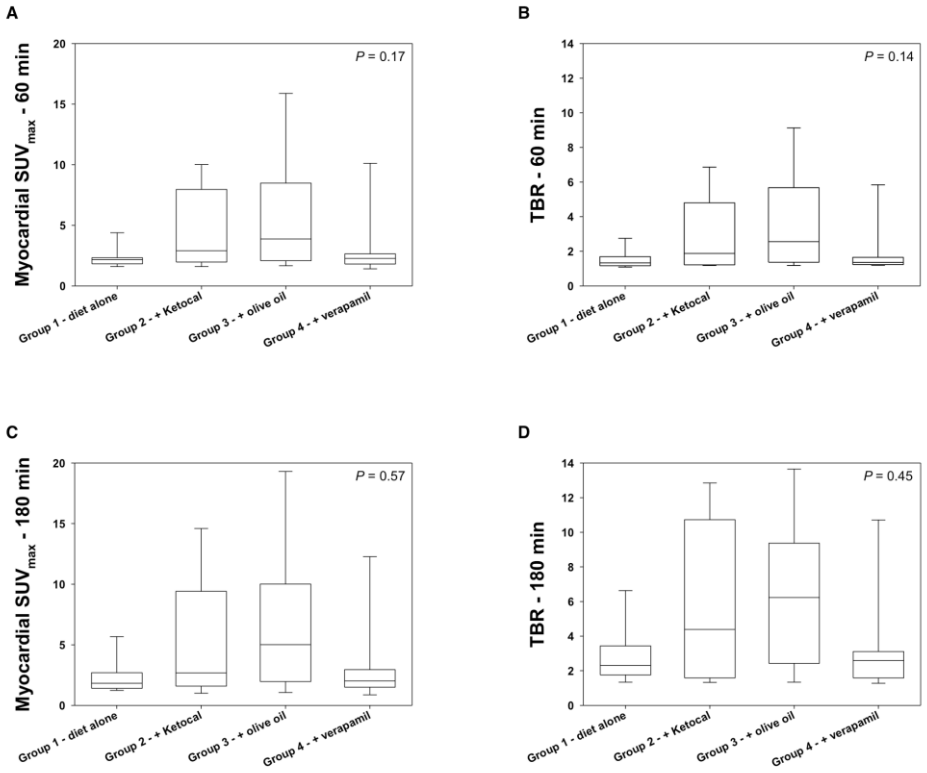

Box plots showing comparisons among study groups of the myocardial SUV_{max} measured 60 minutes after ^{18}F-FDG injection (P = 0.17) (**A**), TBRs measured 60 minutes after ^{18}F-FDG injection (P = 0.14) (**B**), the myocardial SUV_{max} measured 180 minutes after ^{18}F-FDG injection (P = 0.57) (**C**), and TBRs measured 180 minutes after ^{18}F-FDG injection (P = 0.45) (**D**).

Influence of Time-Point Imaging

Imaging was performed at 60 and 180 minutes after ^{18}F-FDG injection and the acquired images were compared. At the 180 minute post-^{18}F-FDG-injection imaging, myocardial SUV_{max} did not significantly differ between groups (group 1, 2.3 ± 1.4; group 2, 5.3 ± 4.9; group 3, 6.8 ± 6.9; and group 4, 3.2 ± 3.5; Fig. 4c; P = 0.57). The myocardial SUV_{max} remained stable within each group between the two time-points. On the other hand, since the left atrial SUV_{max} decreased in the same time, the TBR values increased significantly over time in each group (P = 0.009, 0.015, 0.011, 0.024 for groups 1, 2, 3, and 4, respectively). However, at 180 minutes, the TBR values did not significantly differ between groups (group 1, 2.79 ± 1.64; group 2, 5.63 ± 4.69; group 3, 6.37 ± 4.93; and group 4, 3.21 ± 2.90; Fig. 4d; P = 0.45). Similarly, since the visual analysis accounted for the background activity and because that background activity decreased between the time points, we found that 5 volunteers who had a good myocardial extinction (QVS grade 1) at 60 minutes were reclassified as QVS-2 after 180 minutes.

Blood Analysis

At ^{18}F-FDG injection, the glucose, insulin, and FFA levels were similar among the four study groups (P = 0.78, 0.12, and 0.26, respectively). As expected, the glucose and insulin levels decreased after 60 and 180 minutes, while the FFA level slightly increased over time. Interestingly, volunteers with good (QVS grade 0 or 1) versus poor (QVS grade 2 or 3) myocardial ^{18}F-FDG uptake suppression did not exhibit significantly different glucose (P = 0.97; Fig. 5a) and insulin (P = 0.50, Fig. 5b) levels; however, volunteers with good myocardial ^{18}F-FDG uptake suppression showed

significantly higher FFA level compared with those with poor myocardial ^{18}F-FDG uptake suppression (0.80 ± 0.31 vs. 0.53 ± 0.15 mmol/L, respectively; $P = 0.011$; Fig. 5c).

FIGURE 5.

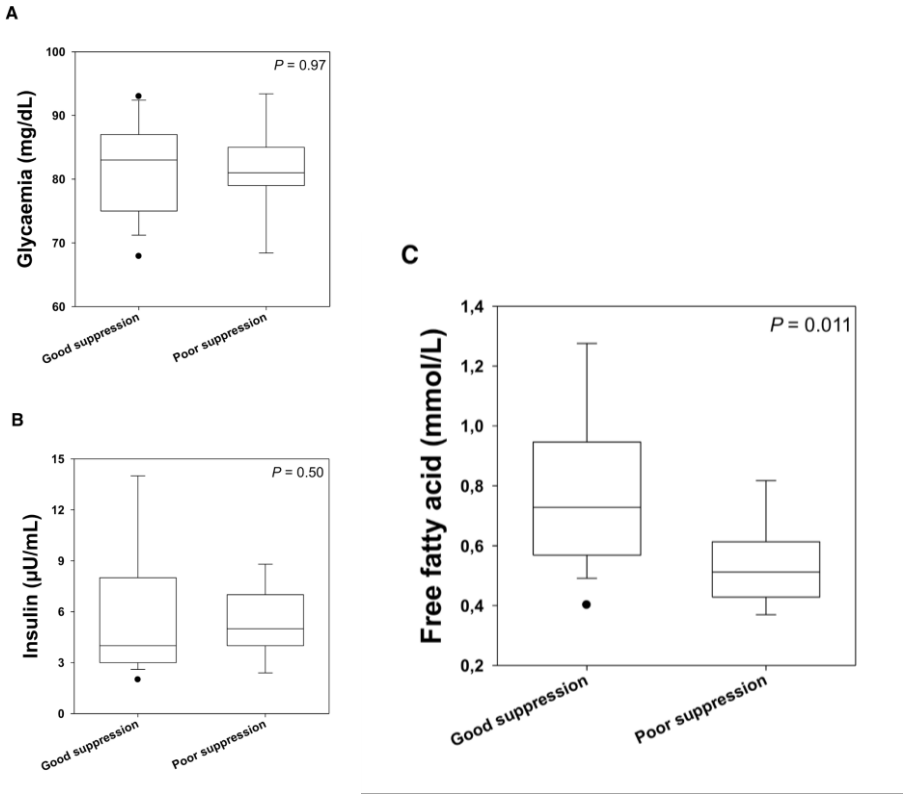

Box plots showing comparisons between volunteers with good versus poor myocardial ^{18}F-FDG uptake suppression (at 60 minutes) with regard to glucose ($P = 0.97$) (**A**), insulin ($P = 0.50$) (**B**), and free fatty acid level ($P = 0.011$) (**C**) measured at the time of ^{18}F-FDG injection.

Correlation with Blood Parameters

We observed a linear trend towards greater suppression in myocardial ^{18}F-FDG uptake measured at 60 minutes after ^{18}F-FDG injection, with the highest cFFA levels obtained at the time of ^{18}F-FDG injection (*P* for trend < 0.001; Fig. 6). When assessed continuously, the cFFA level was significantly related to the suppression of myocardial ^{18}F-FDG uptake (r = 0.61; *P* < 0.001). However, myocardial ^{18}F-FDG uptake suppression was not correlated with glucose (r = 0.10; *P* = 0.54) or insulin level (r = 0.08; *P* = 0.65). ROC analysis demonstrated that a cFFA concentration of >0.65 mmol/L measured at the time of ^{18}F-FDG injection had 68% sensitivity, 82% specificity, and 89% positive predictive value to predict good ^{18}F-FDG uptake suppression (AUC = 0.80; Fig. 7).

FIGURE 6.

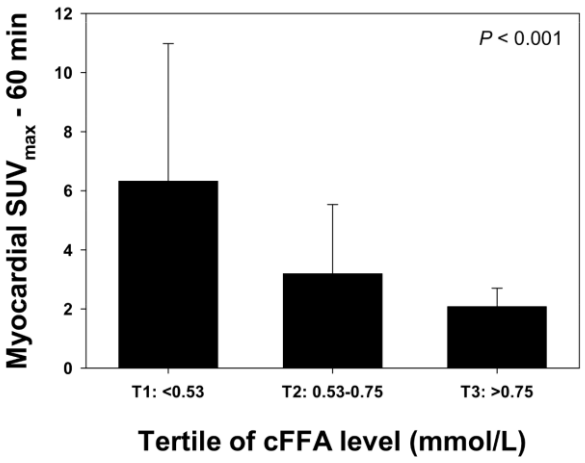

Box plot showing the relationship between myocardial SUV_{max} measured 60 minutes after ^{18}F-FDG injection and tertiles of cFFA level obtained at ^{18}F-FDG injection (*P* for trend < 0.001).

FIGURE 7.

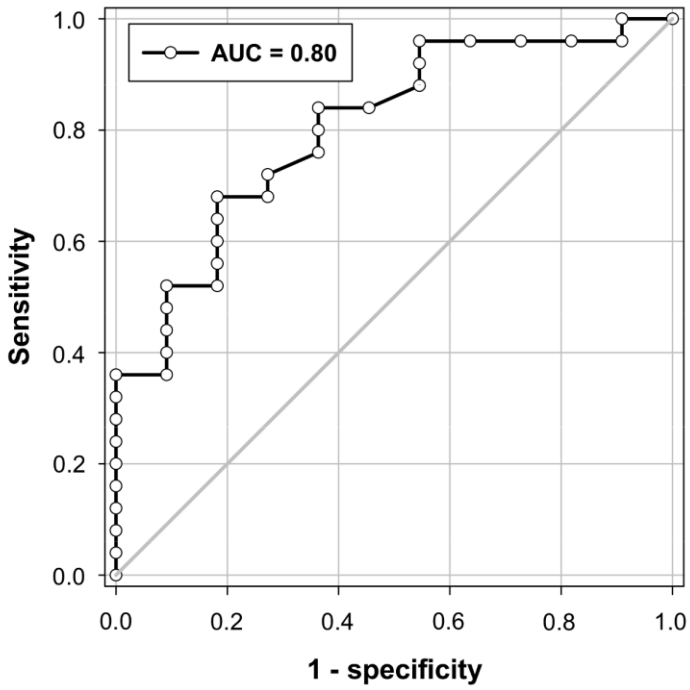

Receiver-operator characteristic (ROC) curve for cFFA concentration measured at the time of ^{18}F-FDG injection for predicting myocardial ^{18}F-FDG uptake suppression (AUC = 0.80).

Interobserver Variability

We found a high Kappa statistic for interobserver variability of the visual assessment of ^{18}F-FDG uptake ($\kappa = 0.8$).

DISCUSSION

This prospective randomized study demonstrates that a HFLC diet administered the evening before ^{18}F-FDG-PET/CT, followed by 12 hours of fasting, is an effective method to obtain good myocardial ^{18}F-FDG uptake suppression. Furthermore, our data showed no additional benefit of administering complementary fatty acid loading or CCB one hour before ^{18}F-FDG injection. One salient finding of this study is the observation that ^{18}F-FDG uptake was inversely correlated with cFFA levels, which could be used to accurately predict the amplitude of myocardial ^{18}F-FDG uptake suppression. This method should allow the avoidance of unnecessary ^{18}F-FDG injection in some patients who are not properly prepared. Finally, our study showed that SUV_{max} values remained stable over time, permitting the imaging of coronary inflammation at either 60 minutes or 180 minutes after ^{18}F-FDG injection.

Although several interesting tracers are being evaluated for vulnerable plaque imaging [125, 151], ^{18}F-FDG-PET/CT is currently the most well-evaluated and available tracer for plaque inflammation imaging. In humans with carotid atherosclerosis, areas of high ^{18}F-FDG uptake co-localize with areas of macrophage accumulation, [96, 249, 250] and can predict subsequent acute ischemic events [251, 252]. Avid ^{18}F-FDG uptake by the myocardium represents the main challenge to overcome before ^{18}F-FDG-PET/CT can be used for imaging coronary plaque inflammation. The present study provides important information regarding how to prepare patients before performing coronary ^{18}F-FDG-PET/CT, and our findings are in agreement with previously published retrospective and non-randomized data [100, 102, 104, 253]. In the fasted state, such as that imposed on our volunteers, the cFFA level is high and the oxidative metabolism is

preferentially dependent on high rates of fatty acid uptake. Furthermore, the volunteers were asked to eat a HFLC meal the evening before imaging, thus inducing an increase in blood triglycerides during postprandial lipemia. Triglycerides are converted by the lipoprotein lipase to FFAs, which then enter fatty acid oxidation pathways. This metabolic pathway explains the very low SUV_{max} of our group 1 volunteers (2.3 ± 0.8), which was significantly lower than the SUV_{max} that we measured in conventionally prepared (6-hour fasting period) 100 consecutive oncologic patients who underwent ^{18}F-FDG-PET/CT at our institution (SUV_{max}: 6.8 ± 4.8; $P = 0.04$; data not shown).

We further found that complementary fatty acid loading (>40 g of fat administered one hour before imaging in groups 2 and 3) provided no additional benefit compared with the fasted volunteers of group 1. There are several potential reasons for this. First, volunteers of all groups had an HFLC meal the evening before imaging, thus inducing an increase in blood triglycerides. Secondly, the time between the additional fatty loading and ^{18}F-FDG injection may have been too brief to further increase the blood triglycerides, as has been previously hypothesized [102]. Regardless of the reason, given the very low SUVmax values obtained in group 1 volunteers, complementary fatty acid loading does not seem necessary to optimize myocardial ^{18}F-FDG signal suppression.

Macrophages contained in atherosclerotic plaques use glucose as fuel, and can also metabolize FFAs. The latter requires oxygen to generate adenosine triphosphate, whereas glucose metabolism does not. Since the plaque interior is relatively anaerobic, glucose is the major substrate for macrophages [254]. Additionally, facilitative transport via the glucose transporter protein (GLUT) system is the pathway predominantly used for

^{18}F-FDG to enter human cells. ^{18}F-FDG uptake in cultured macrophages depends on the degree of macrophage activation [255]. Macrophage activation increases both GLUT-1 and GLUT-3 expressions, while the insulin-sensitive GLUT-4 subtype, which is supposed to be affected by the HFLC diet used in our study, is not detectable. Therefore, macrophage ^{18}F-FDG uptake should not be influenced by the HFLC preparation.

cAMP is involved in myocardial glucose uptake through a Ca^{2+}-dependent mechanism, and CCB reportedly reduce myocardial ^{18}F-FDG-uptake in a murine model [246]. However, our data showed that CCB given one hour before ^{18}F-FDG injection did not improve myocardial-uptake suppression in our volunteers who were asked to fast for 12 hours after an HFLC diet. It remains unknown whether CCB could provide a good ^{18}F-FDG-uptake suppression in conventionally prepared patients (CH-permitted diet followed by 6-hours fasting). Nevertheless, the very low SUV_{max} values that we measured in our group 1 volunteers question the necessity for the use of CCB, which could potentially lead to side effects. Some authors have attempted to raise cFFAs levels by infusing unfractionated heparin in order to stimulate lipoprotein lipase [256]. Again, because of the contraindications and the potential side effects of this medication, we think that a LCHF meal followed by 12 hours of fasting represents a safer alternative for improving myocardial ^{18}F-FDG uptake suppression.

It is recommended that vascular PET studies involve a longer ^{18}F-FDG circulation time than that for oncology PET imaging. This is intended to allow sufficient ^{18}F-FDG accumulation in the arterial wall, and to permit the reduction of blood ^{18}F-FDG levels by decay and excretion [254]. For imaging carotid arteries and aorta, the optimum time-point is between 60 and 180 minutes [257]. The exact optimum time-point for coronary artery

imaging is unknown. This time-point must account for the risk of a partial-volume effect of ^{18}F-FDG activity spilling into the arterial wall from the vessel lumen, as well as from the myocardium. Our data showed that the decreased myocardial ^{18}F-FDG uptake remained stable over time. This suggests that with adequate myocardial ^{18}F-FDG uptake suppression, the detection of coronary plaque inflammation would not be impacted by the myocardial ^{18}F-FDG signal being measured at either 60 or 180 minutes after ^{18}F-FDG injection. The optimal timing for imaging coronary plaque should predominantly depend on the arterial lesion uptake itself. Further studies are needed to determine the optimal timing for imaging coronary plaques in patients.

Although good myocardial ^{18}F-FDG uptake suppression was obtained in the majority of volunteers prepared with a HFLC diet followed by 12 hours of fasting, the myocardial ^{18}F-FDG uptake remained too high in a minority of volunteers. Therefore, it is extremely important to be able to predict the amplitude of suppression, and to thus avoid unnecessary injections of ^{18}F-FDG in inadequately prepared patients. Glucose and insulin levels do not predict myocardial ^{18}F-FDG uptake suppression. One exciting finding of the present work was that myocardial ^{18}F-FDG uptake could be predicted by the total cFFA measured before ^{18}F-FDG injection with an excellent positive predictive value. The measurement could be easily and quickly (about 30 min) obtained in a clinical imaging center and should help to refine the quality of vulnerable coronary plaque detection in patients. Finally, beyond this potential clinical application, our data support the use of our group-1 regimen and the measurement of total cFFA for detecting cardiac involvement of sarcoidosis which is a definite indication for ^{18}F-FDG-PET imaging.

The main limitation of the present work is the relatively small number of volunteers included in the study. However, the study was randomized, and the SUV_{max} values obtained in group 1 volunteers were very low compared to those that we usually obtain in patients referred for oncological disease. Given the very low SUV_{max} values obtained in group 1 volunteers, the number of volunteers in the 3 other groups should have been very high for identifying difference from group 1. Consequently, we decided to end the study after 9 volunteers because we felt it unethical to continue enrolling volunteers. Normal volunteers have been recruited to perform this study. That can be seen as another limitation. Nevertheless, our results are in accordance with those obtained in older patients by other groups [102, 104]. Furthermore, it has been previously shown that the myocardial glucose utilization does not increase with age [258]. Finally, we did not look at regional variability in tracer uptake. Thus, whether any of the interventions increases or decreases regional variability in ^{18}F-FDG uptake remains undetermined, as well as the impact of a potential regional uptake on the visualization of coronary plaque inflammation.

CONCLUSION

A HFLC diet administered the evening before ^{18}F-FDG-PET/CT, followed by fasting for 12 hours, is a simple and effective method to obtain good myocardial ^{18}F-FDG uptake suppression in a large majority of subjects. No additional benefit was conferred by complementary fatty acid loading or CCB administered one hour before ^{18}F-FDG injection. Myocardial ^{18}F-FDG uptake is inversely correlated with cFFA levels, which could be used to accurately predict the amplitude of myocardial ^{18}F-FDG uptake suppression. This method could allow avoidance of unnecessary ^{18}F-FDG injection in patients who are not properly prepared. Finally, when adequately suppressed, the myocardial ^{18}F-FDG signal remains low and stable over time, allowing opportunities for coronary inflammation imaging over a broad time range.

DATA NOT PUBLISHED

Myocardial uptake evolution within each group between the two time-points.

Myocardial SUV_{max} remain stable. The TBR values increasing significantly over time in each group (P = 0.009, 0.015, 0.011, 0.024 for groups 1, 2, 3, and 4, respectively) due to the diminution of the left atrium SUV_{mean}.Delayed imaging at 180 minutes resulted in superior contrast between blood-pool and myocardial FDG activity compared to imaging at earlier time-points induce by the washout of the blood pool activity.

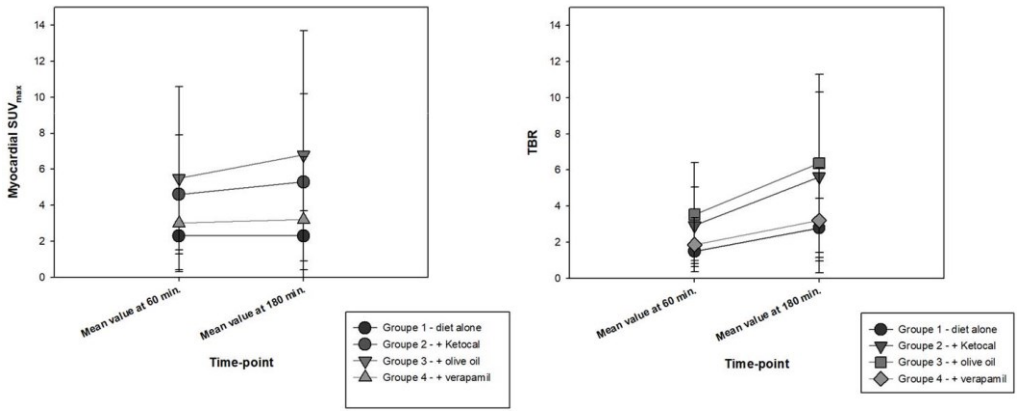

FFA evolution within time in the whole volunteers and separated by groups.

FFA slightly increased over the time in the whole population. The increase is particularly marked in groups 2 and 3 (ketocal and olive oil). The increase in fatty acids in these two groups may be more pronounced later, which may suggest that administering this fatty acid load 1 hour before injection is too short.

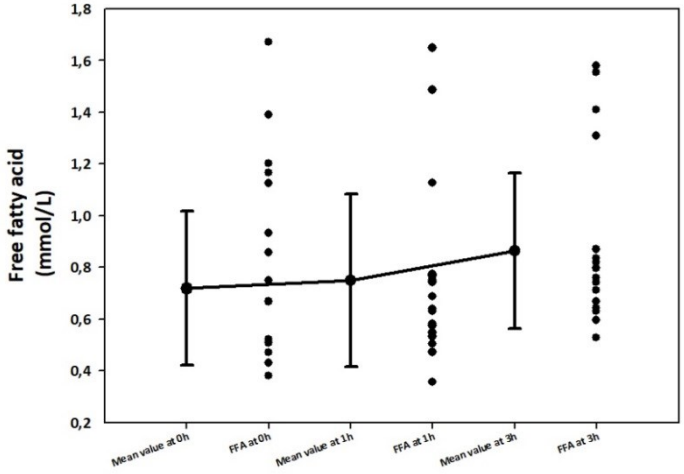
Free fatty acid (mmol/L)
1,8
1,6
1,4
1,2
1,0
0,8
0,6
0,4
0,2
Mean value at 0h
FFA at 0h
Mean value at 1h
FFA at 1h
Mean value at 3h
FFA at 3h

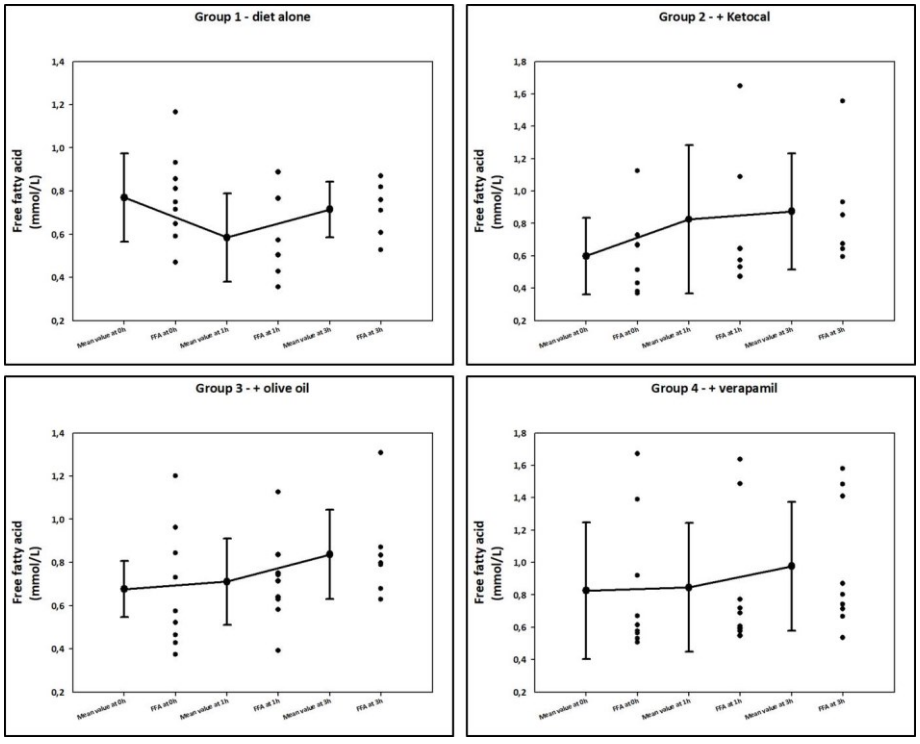
Group 1 - diet alone
Group 2 - + Ketocal
Group 3 - + olive oil
Group 4 - + verapamil
Free fatty acid (mmol/L)

VII. SUMMARY AND FUTURE PESPECTIVE

CVD is a global health concern and vulnerable plaque is a major actor in its most severe clinical manifestations. Inflammation and neovascularization are two major features of vulnerable plaque. The early identification and treatment of vulnerable plaque before the occurrence of a clinical event remains a “holy grail” in the management of CVD. The research described in this thesis highlights the practical challenges in trying to define the optimal imaging strategy.

The first part of this thesis explores the temporal association between inflammation and neovascularization within carotid plaque assessed by FDG-PET/CT and CEUS in a population of symptomatic and asymptomatic patients scheduled for carotid endarterectomy. Data obtained by imaging were validated using histological assessment of endarterectomy specimens. Thereby, we demonstrated, in the largest series with histological validation available at this time, that inflammation and neovascularization are not systematically associated in the carotid plaques of patients, which suggests a temporal separation of these processes. This association is subject to conflicting data in literature, highlighting the challenge of non-invasive imaging strategies.

CEUS has major benefits over other imaging modalities, as it is widely available, low-cost, quick to perform, and does not use an ionizing radiation source. Nevertheless, we have also shown the difficulties of applying this technique in advanced disease. FDG-PET/CT is a clinically available technique but is limited by the availability of the technology, the cost, its

time-consuming nature, and the involvement of ionizing radiation. Despite these limitations, to date, it is the most common non-invasive method used to detect metabolically active vulnerable atherosclerotic plaques.

In the second part of this thesis, we conducted a prospective randomized study to evaluate the impact of different interventions aiming to suppress myocardial glucose uptake evaluated by uptake of ^{18}F-FDG. The goal of myocardial FDG suppression is to improve the quality of cardiac and coronary FDG-PET/CT images and allow visualization of coronary plaque inflammation, but also to improve the quality of non-coronary cardiac FDG-PET/CT images (e.g. for sarcoidosis, infectious disease, or myocardial ischemia). We demonstrated that a high-fat low-carbohydrate diet followed by 12-hour fasting is a simple, easily applicable, and effective method of obtaining a good suppression of myocardial FDG uptake. The addition of a complementary oral fatty acid or a calcium channel blocker one hour before FDG injection does not provide additional benefit.
Determination of free fatty acid levels could be a useful method for predicting the amplitude of myocardial FDG uptake suppression that may allow avoidance of unnecessary FDG injections in patients without proper preparation. We also showed that the decrease in myocardial FDG uptake remained stable over time.

<u>According to this work, we identified some future directions</u>:
One future research direction will be to compare these two techniques in a broader population of patients with varying degrees of carotid stenosis and comorbidities to better understand the link between inflammation and neovascularization.

Inflammation also seems more pronounced when neurological symptoms are present, whereas neovascularization does not seem to be. Those data conflict with a previous study (S*taub et al*.) [159], possibly due to differences in patient population; our series included a population with more advanced disease.

Another step for the future is to evaluate the potential of these two techniques to predict cardiovascular events during long-term prospective follow-up.

As described in the introduction, the macrophage population is composed of various phenotypes. We demonstrate the correlation between high FDG uptake and presence of macrophages without any phenotype distinction. Identifying correlation between imaging and macrophages phenotypes represents a field of investigation in continuity with our work.

The future development of neovascularization analysis with automatic software-based quantification seems to be crucial, requiring histological validation in a large population.

In addition, the high-fat low-carbohydrate diet should be compared with a standard preparation in a large population including, among others, patients with CVD. The impact of a patient's characteristics and cardiovascular risk factors on suppression of myocardial FDG uptake should be investigated. Acute cardiovascular event modify the myocardial metabolism, the impact on the quality of the preparation should be evaluated. Detection of coronary vulnerable plaque may be the next step.

Regarding the free fatty acid levels and the cut-off value, our results must be confirmed; it would also be interesting to assess this level at a timepoint even earlier before FDG injection.

Cumulative evidence has demonstrated that imaging of atherosclerosis may also be useful for stratifying cardiovascular risk and for detecting high-risk patients who are likely to suffer a cardiovascular event. The current treatment strategy in such cases remains systemic medication; local treatment of vulnerable plaques is currently under investigation.

Strategies oriented towards detecting patients at high risk of atherothrombotic events could evaluate plaques in more accessible arteries or propose a single "all arteries" examination to assess a global atherosclerosis burden and marker of vulnerability. This appears to be a more cost-effective clinical solution applicable for population screening. More evidence, in large prospective multicenter trials, is warranted to establish the prognostic value of the various plaque characteristics and imaging modalities to predict clinical events such as acute cardiac events or stroke.

Another approach is the development of new nuclear molecular imaging tracers (PET or SPECT). However, the exposure to ionizing radiation remains a major limitation for its use in screening asymptomatic individuals or as a valuable follow-up imaging method. MRI imaging does not use an ionizing radiation source and could constitute an interesting alternative; this is under evaluation.

Invasive imaging modalities remain important to provide more details on vulnerable plaque for research purposes. A future hybrid intravascular

imaging methods are expected to shed light on the mechanisms regulating atherosclerosis and plaque evolution. Another important research pathway is the evaluation of therapeutic effects of agents specially developed to reduce plaque vulnerability. Future invasive approaches aimed at stabilizing vulnerable plaques before the occurrence of atherothrombotic events should be a promising addition to the present practice of treating symptomatic atherosclerotic obstructions.

VIII. REFERENCES

1. Writing Group, M., et al., *Executive Summary: Heart Disease and Stroke Statistics--2016 Update: A Report From the American Heart Association.* Circulation, 2016. **133**(4): p. 447-54.
2. Madjid, M., et al., *Finding vulnerable atherosclerotic plaques: is it worth the effort?* Arterioscler Thromb Vasc Biol, 2004. **24**(10): p. 1775-82.
3. Bentzon, J.F., et al., *Mechanisms of plaque formation and rupture.* Circ Res, 2014. **114**(12): p. 1852-66.
4. Anderson, K.M., et al., *An updated coronary risk profile. A statement for health professionals.* Circulation, 1991. **83**(1): p. 356-62.
5. Conroy, R.M., et al., *Estimation of ten-year risk of fatal cardiovascular disease in Europe: the SCORE project.* Eur Heart J, 2003. **24**(11): p. 987-1003.
6. Bourantas, C.V., et al., *Early detection and invasive passivation of future culprit lesions: a future potential or an unrealistic pursuit of chimeras?* Am Heart J, 2013. **165**(6): p. 869-881 e4.
7. Ross, R., *Atherosclerosis--an inflammatory disease.* N Engl J Med, 1999. **340**(2): p. 115-26.
8. Libby, P., *Inflammation in atherosclerosis.* Nature, 2002. **420**(6917): p. 868-74.
9. Libby, P., P.M. Ridker, and A. Maseri, *Inflammation and atherosclerosis.* Circulation, 2002. **105**(9): p. 1135-43.
10. Hansson, G.K., *Inflammation, atherosclerosis, and coronary artery disease.* N Engl J Med, 2005. **352**(16): p. 1685-95.
11. Falk, E., *Pathogenesis of atherosclerosis.* J Am Coll Cardiol, 2006. **47**(8 Suppl): p. C7-12.
12. Clinton, S.K., et al., *Macrophage colony-stimulating factor gene expression in vascular cells and in experimental and human atherosclerosis.* Am J Pathol, 1992. **140**(2): p. 301-16.
13. Virmani, R., et al., *Coronary artery atherosclerosis revisited in Korean war combat casualties.* Arch Pathol Lab Med, 1987. **111**(10): p. 972-6.
14. Libby, P., et al., *Inflammation in atherosclerosis: from pathophysiology to practice.* J Am Coll Cardiol, 2009. **54**(23): p. 2129-38.

15. Halvorsen, B., et al., *Atherosclerotic plaque stability--what determines the fate of a plaque?* Prog Cardiovasc Dis, 2008. **51**(3): p. 183-94.
16. Wolfs, I.M., M.M. Donners, and M.P. de Winther, *Differentiation factors and cytokines in the atherosclerotic plaque micro-environment as a trigger for macrophage polarisation.* Thromb Haemost, 2011. **106**(5): p. 763-71.
17. Butcher, M.J. and E.V. Galkina, *Phenotypic and functional heterogeneity of macrophages and dendritic cell subsets in the healthy and atherosclerosis-prone aorta.* Front Physiol, 2012. **3**: p. 44.
18. Bouhlel, M.A., et al., *PPARgamma activation primes human monocytes into alternative M2 macrophages with anti-inflammatory properties.* Cell Metab, 2007. **6**(2): p. 137-43.
19. Chinetti-Gbaguidi, G., et al., *Human atherosclerotic plaque alternative macrophages display low cholesterol handling but high phagocytosis because of distinct activities of the PPARgamma and LXRalpha pathways.* Circ Res, 2011. **108**(8): p. 985-95.
20. Duewell, P., et al., *NLRP3 inflammasomes are required for atherogenesis and activated by cholesterol crystals.* Nature, 2010. **464**(7293): p. 1357-61.
21. Stoger, J.L., et al., *Distribution of macrophage polarization markers in human atherosclerosis.* Atherosclerosis, 2012. **225**(2): p. 461-8.
22. Bories, G., et al., *Liver X receptor activation stimulates iron export in human alternative macrophages.* Circ Res, 2013. **113**(11): p. 1196-205.
23. Mosser, D.M. and J.P. Edwards, *Exploring the full spectrum of macrophage activation.* Nat Rev Immunol, 2008. **8**(12): p. 958-69.
24. Zizzo, G., et al., *Efficient clearance of early apoptotic cells by human macrophages requires M2c polarization and MerTK induction.* J Immunol, 2012. **189**(7): p. 3508-20.
25. Lusis, A.J., *Atherosclerosis.* Nature, 2000. **407**(6801): p. 233-41.
26. Langheinrich, A.C., et al., *Vasa vasorum and atherosclerosis - Quid novi?* Thromb Haemost, 2007. **97**(6): p. 873-9.
27. Virmani, R., et al., *Atherosclerotic plaque progression and vulnerability to rupture: angiogenesis as a source of intraplaque hemorrhage.* Arterioscler Thromb Vasc Biol, 2005. **25**(10): p. 2054-61.
28. Virmani, R., et al., *Pathology of the vulnerable plaque.* J Am Coll Cardiol, 2006. **47**(8 Suppl): p. C13-8.

29. Falk, E., P.K. Shah, and V. Fuster, *Coronary plaque disruption.* Circulation, 1995. **92**(3): p. 657-71.
30. Davies, M.J., *Stability and instability: two faces of coronary atherosclerosis. The Paul Dudley White Lecture 1995.* Circulation, 1996. **94**(8): p. 2013-20.
31. Narula, J., et al., *Arithmetic of vulnerable plaques for noninvasive imaging.* Nat Clin Pract Cardiovasc Med, 2008. **5 Suppl 2**: p. S2-10.
32. Brott, T.G., et al., *2011 ASA/ACCF/AHA/AANN/AANS/ACR/ASNR/CNS/SAIP/SCAI/SIR/SNIS/SVM/SVS guideline on the management of patients with extracranial carotid and vertebral artery disease: executive summary: a report of the American College of Cardiology Foundation/American Heart Association Task Force on Practice Guidelines, and the American Stroke Association, American Association of Neuroscience Nurses, American Association of Neurological Surgeons, American College of Radiology, American Society of Neuroradiology, Congress of Neurological Surgeons, Society of Atherosclerosis Imaging and Prevention, Society for Cardiovascular Angiography and Interventions, Society of Interventional Radiology, Society of NeuroInterventional Surgery, Society for Vascular Medicine, and Society for Vascular Surgery.* J Am Coll Cardiol, 2011. **57**(8): p. 1002-44.
33. Fisher, M., et al., *Carotid plaque pathology: thrombosis, ulceration, and stroke pathogenesis.* Stroke, 2005. **36**(2): p. 253-7.
34. Kramer, M.C., et al., *Relationship of thrombus healing to underlying plaque morphology in sudden coronary death.* J Am Coll Cardiol, 2010. **55**(2): p. 122-32.
35. Muller, J.E. and G.H. Tofler, *Triggering and hourly variation of onset of arterial thrombosis.* Ann Epidemiol, 1992. **2**(4): p. 393-405.
36. Naghavi, M., et al., *From vulnerable plaque to vulnerable patient: a call for new definitions and risk assessment strategies: Part I.* Circulation, 2003. **108**(14): p. 1664-72.
37. Naghavi, M., et al., *From vulnerable plaque to vulnerable patient: a call for new definitions and risk assessment strategies: Part II.* Circulation, 2003. **108**(15): p. 1772-8.
38. Schaar, J.A., et al., *Terminology for high-risk and vulnerable coronary artery plaques. Report of a meeting on the vulnerable plaque, June 17 and 18, 2003, Santorini, Greece.* Eur Heart J, 2004. **25**(12): p. 1077-82.

39. Siebler, M., et al., *Cerebral microembolism in symptomatic and asymptomatic high-grade internal carotid artery stenosis.* Neurology, 1994. **44**(4): p. 615-8.
40. Freilinger, T.M., et al., *Prevalence of nonstenosing, complicated atherosclerotic plaques in cryptogenic stroke.* JACC Cardiovasc Imaging, 2012. **5**(4): p. 397-405.
41. Bayer-Karpinska, A., A. Schindler, and T. Saam, *Detection of Vulnerable Plaque in Patients with Cryptogenic Stroke.* Neuroimaging Clin N Am, 2016. **26**(1): p. 97-110.
42. Virmani, R., et al., *Lessons From Sudden Coronary Death : A Comprehensive Morphological Classification Scheme for Atherosclerotic Lesions.* Arteriosclerosis, Thrombosis, and Vascular Biology, 2000. **20**(5): p. 1262-1275.
43. Burke, A.P., et al., *Coronary risk factors and plaque morphology in men with coronary disease who died suddenly.* N Engl J Med, 1997. **336**(18): p. 1276-82.
44. Glagov, S., et al., *Compensatory enlargement of human atherosclerotic coronary arteries.* N Engl J Med, 1987. **316**(22): p. 1371-5.
45. Redgrave, J.N., et al., *Histological assessment of 526 symptomatic carotid plaques in relation to the nature and timing of ischemic symptoms: the Oxford plaque study.* Circulation, 2006. **113**(19): p. 2320-8.
46. Spagnoli, L.G., et al., *Extracranial thrombotically active carotid plaque as a risk factor for ischemic stroke.* JAMA, 2004. **292**(15): p. 1845-52.
47. Galis, Z.S., et al., *Increased expression of matrix metalloproteinases and matrix degrading activity in vulnerable regions of human atherosclerotic plaques.* J Clin Invest, 1994. **94**(6): p. 2493-503.
48. Redgrave, J.N., et al., *Critical cap thickness and rupture in symptomatic carotid plaques: the oxford plaque study.* Stroke, 2008. **39**(6): p. 1722-9.
49. Virmani, R., et al., *Histopathology of carotid atherosclerotic disease.* Neurosurgery, 2006. **59**(5 Suppl 3): p. S219-27; discussion S3-13.
50. Wasserman BA, W.R., Trout III HH and Virmani R, *Response to Letter by Karapanayiotides et al.* Stroke, 2006. **8**(37): p. 1647.
51. Wasserman, B.A., et al., *Low-grade carotid stenosis: looking beyond the lumen with MRI.* Stroke, 2005. **36**(11): p. 2504-13.

52. Davies, M.J., et al., *Risk of thrombosis in human atherosclerotic plaques: role of extracellular lipid, macrophage, and smooth muscle cell content.* Br Heart J, 1993. **69**(5): p. 377-81.
53. Fernandez-Ortiz, A., et al., *Characterization of the relative thrombogenicity of atherosclerotic plaque components: implications for consequences of plaque rupture.* J Am Coll Cardiol, 1994. **23**(7): p. 1562-9.
54. Tedgui, A. and Z. Mallat, *Apoptosis as a determinant of atherothrombosis.* Thromb Haemost, 2001. **86**(1): p. 420-6.
55. Libby, P., *Molecular bases of the acute coronary syndromes.* Circulation, 1995. **91**(11): p. 2844-50.
56. Gossl, M., et al., *Impact of coronary vasa vasorum functional structure on coronary vessel wall perfusion distribution.* Am J Physiol Heart Circ Physiol, 2003. **285**(5): p. H2019-26.
57. Williams, J.K. and D.D. Heistad, *Structure and function of vasa vasorum.* Trends Cardiovasc Med, 1996. **6**(2): p. 53-7.
58. Jeziorska, M. and D.E. Woolley, *Neovascularization in early atherosclerotic lesions of human carotid arteries: its potential contribution to plaque development.* Hum Pathol, 1999. **30**(8): p. 919-25.
59. Sluimer, J.C., et al., *Thin-walled microvessels in human coronary atherosclerotic plaques show incomplete endothelial junctions relevance of compromised structural integrity for intraplaque microvascular leakage.* J Am Coll Cardiol, 2009. **53**(17): p. 1517-27.
60. Kumamoto, M., Y. Nakashima, and K. Sueishi, *Intimal neovascularization in human coronary atherosclerosis: its origin and pathophysiological significance.* Hum Pathol, 1995. **26**(4): p. 450-6.
61. Mofidi, R., et al., *Association between plaque instability, angiogenesis and symptomatic carotid occlusive disease.* Br J Surg, 2001. **88**(7): p. 945-50.
62. Semenza, G.L., *Expression of hypoxia-inducible factor 1: mechanisms and consequences.* Biochem Pharmacol, 2000. **59**(1): p. 47-53.
63. North, S., M. Moenner, and A. Bikfalvi, *Recent developments in the regulation of the angiogenic switch by cellular stress factors in tumors.* Cancer Lett, 2005. **218**(1): p. 1-14.

64. Sluimer, J.C. and M.J. Daemen, *Novel concepts in atherogenesis: angiogenesis and hypoxia in atherosclerosis.* J Pathol, 2009. **218**(1): p. 7-29.
65. Kolodgie, F.D., et al., *Intraplaque hemorrhage and progression of coronary atheroma.* N Engl J Med, 2003. **349**(24): p. 2316-25.
66. Mulligan-Kehoe, M.J. and M. Simons, *Vasa vasorum in normal and diseased arteries.* Circulation, 2014. **129**(24): p. 2557-66.
67. Moreno, P.R., et al., *Neovascularization in human atherosclerosis.* Circulation, 2006. **113**(18): p. 2245-52.
68. Pedro R. Moreno, K.-R.P., William N. O'Connor, Annapoorna S. Kini, Marc Sirol, Samin K. Sharma, Valentin Fuster., *Increased Inflammation and Neovascularization in Diabetes Atherosclerosis is no Longer Present in Fibrocalcific Plaques: A Marker of Stabilization ?* J Am Coll Cardiol, 2005. **45**: p. A402.
69. Corti, R., et al., *Lipid lowering by simvastatin induces regression of human atherosclerotic lesions: two years' follow-up by high-resolution noninvasive magnetic resonance imaging.* Circulation, 2002. **106**(23): p. 2884-7.
70. Mann, J. and M.J. Davies, *Mechanisms of progression in native coronary artery disease: role of healed plaque disruption.* Heart, 1999. **82**(3): p. 265-8.
71. Stone, G.W., et al., *A prospective natural-history study of coronary atherosclerosis.* N Engl J Med, 2011. **364**(3): p. 226-35.
72. Barlis, P., et al., *Assessment of culprit and remote coronary narrowings using optical coherence tomography with long-term outcomes.* Am J Cardiol, 2008. **102**(4): p. 391-5.
73. Kubo, T., et al., *The dynamic nature of coronary artery lesion morphology assessed by serial virtual histology intravascular ultrasound tissue characterization.* J Am Coll Cardiol, 2010. **55**(15): p. 1590-7.
74. Tian, J., et al., *Distinct morphological features of ruptured culprit plaque for acute coronary events compared to those with silent rupture and thin-cap fibroatheroma: a combined optical coherence tomography and intravascular ultrasound study.* J Am Coll Cardiol, 2014. **63**(21): p. 2209-16.
75. Wang, Z., et al., *Angioscopic study of silent plaque disruption in nonischemic related coronary artery in patients with stable ischemic heart disease.* Int Heart J, 2010. **51**(6): p. 383-7.

76. Burke, A.P., et al., *Healed plaque ruptures and sudden coronary death: evidence that subclinical rupture has a role in plaque progression.* Circulation, 2001. **103**(7): p. 934-40.
77. Arbab-Zadeh, A., et al., *Acute coronary events.* Circulation, 2012. **125**(9): p. 1147-56.
78. Hackett, D., G. Davies, and A. Maseri, *Pre-existing coronary stenoses in patients with first myocardial infarction are not necessarily severe.* Eur Heart J, 1988. **9**(12): p. 1317-23.
79. Ambrose, J.A., et al., *Angiographic progression of coronary artery disease and the development of myocardial infarction.* J Am Coll Cardiol, 1988. **12**(1): p. 56-62.
80. Fujii, K., et al., *Intravascular ultrasound profile analysis of ruptured coronary plaques.* Am J Cardiol, 2006. **98**(4): p. 429-35.
81. Mann, J.M. and M.J. Davies, *Assessment of the severity of coronary artery disease at postmortem examination. Are the measurements clinically valid?* Br Heart J, 1995. **74**(5): p. 528-30.
82. *Endarterectomy for asymptomatic carotid artery stenosis. Executive Committee for the Asymptomatic Carotid Atherosclerosis Study.* JAMA, 1995. **273**(18): p. 1421-8.
83. *Risk of stroke in the distribution of an asymptomatic carotid artery. The European Carotid Surgery Trialists Collaborative Group.* Lancet, 1995. **345**(8944): p. 209-12.
84. Longstreth, W.T., Jr., et al., *Asymptomatic internal carotid artery stenosis defined by ultrasound and the risk of subsequent stroke in the elderly. The Cardiovascular Health Study.* Stroke, 1998. **29**(11): p. 2371-6.
85. Boden, W.E., et al., *The evolving pattern of symptomatic coronary artery disease in the United States and Canada: baseline characteristics of the Clinical Outcomes Utilizing Revascularization and Aggressive DruG Evaluation (COURAGE) trial.* Am J Cardiol, 2007. **99**(2): p. 208-12.
86. Sedlis, S.P., et al., *Effect of PCI on Long-Term Survival in Patients with Stable Ischemic Heart Disease.* N Engl J Med, 2015. **373**(20): p. 1937-46.
87. Schwartz, L., et al., *Baseline coronary angiographic findings in the Bypass Angioplasty Revascularization Investigation 2 Diabetes trial (BARI 2D).* Am J Cardiol, 2009. **103**(5): p. 632-8.
88. Barnett, H.J., et al., *Benefit of carotid endarterectomy in patients with symptomatic moderate or severe stenosis. North American*

Symptomatic Carotid Endarterectomy Trial Collaborators. N Engl J Med, 1998. **339**(20): p. 1415-25.
89. Halliday, A., et al., *Prevention of disabling and fatal strokes by successful carotid endarterectomy in patients without recent neurological symptoms: randomised controlled trial.* Lancet, 2004. **363**(9420): p. 1491-502.
90. Farb, A., et al., *Coronary plaque erosion without rupture into a lipid core. A frequent cause of coronary thrombosis in sudden coronary death.* Circulation, 1996. **93**(7): p. 1354-63.
91. Frink, R.J., *Chronic ulcerated plaques: new insights into the pathogenesis of acute coronary disease.* J Invasive Cardiol, 1994. **6**(5): p. 173-85.
92. Tarkin, J.M., F.R. Joshi, and J.H. Rudd, *PET imaging of inflammation in atherosclerosis.* Nat Rev Cardiol, 2014. **11**(8): p. 443-57.
93. Lederman, R.J., et al., *Detection of atherosclerosis using a novel positron-sensitive probe and 18-fluorodeoxyglucose (FDG).* Nucl Med Commun, 2001. **22**(7): p. 747-53.
94. Babior, B.M., *The respiratory burst of phagocytes.* J Clin Invest, 1984. **73**(3): p. 599-601.
95. Rudd, J.H.F., *Imaging Atherosclerotic Plaque Inflammation With [18F]-Fluorodeoxyglucose Positron Emission Tomography.* Circulation, 2002. **105**(23): p. 2708-2711.
96. Tawakol, A., et al., *In vivo 18F-fluorodeoxyglucose positron emission tomography imaging provides a noninvasive measure of carotid plaque inflammation in patients.* J Am Coll Cardiol, 2006. **48**(9): p. 1818-24.
97. Menezes, L.J., et al., *Investigating vulnerable atheroma using combined (18)F-FDG PET/CT angiography of carotid plaque with immunohistochemical validation.* J Nucl Med, 2011. **52**(11): p. 1698-703.
98. Wells, R.G. and T.D. Ruddy, *The dream of imaging coronary artery inflammation with FDG PET/CT imaging.* J Nucl Cardiol, 2016.
99. Rogers, I.S., et al., *Feasibility of FDG imaging of the coronary arteries: comparison between acute coronary syndrome and stable angina.* JACC Cardiovasc Imaging, 2010. **3**(4): p. 388-97.
100. Cheng, V.Y., et al., *Coronary arterial 18F-FDG uptake by fusion of PET and coronary CT angiography at sites of percutaneous stenting for acute myocardial infarction and stable coronary artery disease.* J Nucl Med, 2012. **53**(4): p. 575-83.

101. Joshi, N.V., et al., *18F-fluoride positron emission tomography for identification of ruptured and high-risk coronary atherosclerotic plaques: a prospective clinical trial.* Lancet, 2014. **383**(9918): p. 705-13.
102. Cheng, V.Y., et al., *Impact of carbohydrate restriction with and without fatty acid loading on myocardial 18F-FDG uptake during PET: A randomized controlled trial.* J Nucl Cardiol, 2010. **17**(2): p. 286-91.
103. Wykrzykowska, J., et al., *Imaging of inflamed and vulnerable plaque in coronary arteries with 18F-FDG PET/CT in patients with suppression of myocardial uptake using a low-carbohydrate, high-fat preparation.* J Nucl Med, 2009. **50**(4): p. 563-8.
104. Williams, G. and G.M. Kolodny, *Suppression of myocardial 18F-FDG uptake by preparing patients with a high-fat, low-carbohydrate diet.* AJR Am J Roentgenol, 2008. **190**(2): p. W151-6.
105. Depre, C., J.L.J. Vanoverschelde, and H. Taegtmeyer, *Glucose for the Heart.* Circulation, 1999. **99**(4): p. 578-588.
106. Goldberg, I.J., C.M. Trent, and P.C. Schulze, *Lipid metabolism and toxicity in the heart.* Cell Metab, 2012. **15**(6): p. 805-12.
107. Hue, L. and H. Taegtmeyer, *The Randle cycle revisited: a new head for an old hat.* Am J Physiol Endocrinol Metab, 2009. **297**(3): p. E578-91.
108. Stanley, W.C., F.A. Recchia, and G.D. Lopaschuk, *Myocardial substrate metabolism in the normal and failing heart.* Physiol Rev, 2005. **85**(3): p. 1093-129.
109. Szablewski, L., *Glucose transporters in healthy heart and in cardiac disease.* Int J Cardiol, 2017. **230**: p. 70-75.
110. Gandhi, G.R., et al., *Gallic acid attenuates high-fat diet fed-streptozotocin-induced insulin resistance via partial agonism of PPARgamma in experimental type 2 diabetic rats and enhances glucose uptake through translocation and activation of GLUT4 in PI3K/p-Akt signaling pathway.* Eur J Pharmacol, 2014. **745**: p. 201-16.
111. Hardie, D.G. and D. Carling, *The AMP-activated protein kinase--fuel gauge of the mammalian cell?* Eur J Biochem, 1997. **246**(2): p. 259-73.
112. Lopaschuk, G.D., et al., *Myocardial fatty acid metabolism in health and disease.* Physiol Rev, 2010. **90**(1): p. 207-58.

113. Zhuang, H. and I. Codreanu, *Growing applications of FDG PET-CT imaging in non-oncologic conditions.* J Biomed Res, 2015. **29**(3): p. 189-202.
114. Arun, S., et al., *Comparison of Tc-99m tetrofosmin myocardial perfusion scintigraphy and exercise F18-FDG imaging in detection of myocardial ischemia in patients with coronary artery disease.* J Nucl Cardiol, 2015. **22**(1): p. 98-110.
115. Gould, K.L. and H. Taegtmeyer, *Myocardial ischemia, fluorodeoxyglucose, and severity of coronary artery stenosis: the complexities of metabolic remodeling in hibernating myocardium.* Circulation, 2004. **109**(12): p. e167-70; author reply e167-70.
116. Nakamura, I., et al., *Detection of early stage atherosclerotic plaques using PET and CT fusion imaging targeting P-selectin in low density lipoprotein receptor-deficient mice.* Biochem Biophys Res Commun, 2013. **433**(1): p. 47-51.
117. Li, X., et al., *Targeting P-selectin by gallium-68-labeled fucoidan positron emission tomography for noninvasive characterization of vulnerable plaques: correlation with in vivo 17.6T MRI.* Arterioscler Thromb Vasc Biol, 2014. **34**(8): p. 1661-7.
118. Liu, Y., et al., *PET imaging of chemokine receptors in vascular injury-accelerated atherosclerosis.* J Nucl Med, 2013. **54**(7): p. 1135-41.
119. Luehmann, H.P., et al., *PET/CT imaging of chemokine receptor CCR5 in vascular injury model using targeted nanoparticle.* J Nucl Med, 2014. **55**(4): p. 629-34.
120. Tahara, N., et al., *2-deoxy-2-[18F]fluoro-D-mannose positron emission tomography imaging in atherosclerosis.* Nat Med, 2014. **20**(2): p. 215-9.
121. Rominger, A., et al., *In vivo imaging of macrophage activity in the coronary arteries using 68Ga-DOTATATE PET/CT: correlation with coronary calcium burden and risk factors.* J Nucl Med, 2010. **51**(2): p. 193-7.
122. Li, X., et al., *68Ga-DOTATATE PET/CT for the detection of inflammation of large arteries: correlation with18F-FDG, calcium burden and risk factors.* EJNMMI Res, 2012. **2**(1): p. 52.
123. Mojtahedi, A., et al., *Assessment of vulnerable atherosclerotic and fibrotic plaques in coronary arteries using (68)Ga-DOTATATE PET/CT.* Am J Nucl Med Mol Imaging, 2015. **5**(1): p. 65-71.

124. Pugliese, F., et al., *Imaging of vascular inflammation with [11C]-PK11195 and positron emission tomography/computed tomography angiography.* J Am Coll Cardiol, 2010. **56**(8): p. 653-61.
125. Gaemperli, O., et al., *Imaging intraplaque inflammation in carotid atherosclerosis with 11C-PK11195 positron emission tomography/computed tomography.* Eur Heart J, 2012. **33**(15): p. 1902-10.
126. Bucerius, J., et al., *Feasibility of 18F-fluoromethylcholine PET/CT for imaging of vessel wall alterations in humans--first results.* Eur J Nucl Med Mol Imaging, 2008. **35**(4): p. 815-20.
127. Kato, K., et al., *Evaluation and comparison of 11C-choline uptake and calcification in aortic and common carotid arterial walls with combined PET/CT.* Eur J Nucl Med Mol Imaging, 2009. **36**(10): p. 1622-8.
128. Nahrendorf, M., et al., *Nanoparticle PET-CT imaging of macrophages in inflammatory atherosclerosis.* Circulation, 2008. **117**(3): p. 379-87.
129. Paeng, J.C., et al., *Feasibility and kinetic characteristics of (68)Ga-NOTA-RGD PET for in vivo atherosclerosis imaging.* Ann Nucl Med, 2013. **27**(9): p. 847-54.
130. Su, H., et al., *Atherosclerotic plaque uptake of a novel integrin tracer (1)(8)F-Flotegatide in a mouse model of atherosclerosis.* J Nucl Cardiol, 2014. **21**(3): p. 553-62.
131. Beer, A.J., et al., *PET/CT imaging of integrin alphavbeta3 expression in human carotid atherosclerosis.* JACC Cardiovasc Imaging, 2014. **7**(2): p. 178-87.
132. Golestani, R., et al., *Feasibility of vascular endothelial growth factor imaging in human atherosclerotic plaque using (89)Zr-bevacizumab positron emission tomography.* Mol Imaging, 2013. **12**(4): p. 235-43.
133. Mateo, J., et al., *Noninvasive assessment of hypoxia in rabbit advanced atherosclerosis using (1)(8)F-fluoromisonidazole positron emission tomographic imaging.* Circ Cardiovasc Imaging, 2014. **7**(2): p. 312-20.
134. Dweck, M.R., et al., *Coronary arterial 18F-sodium fluoride uptake: a novel marker of plaque biology.* J Am Coll Cardiol, 2012. **59**(17): p. 1539-48.
135. Broisat, A., et al., *99mTc-cAbVCAM1-5 imaging is a sensitive and reproducible tool for the detection of inflamed atherosclerotic lesions in mice.* J Nucl Med, 2014. **55**(10): p. 1678-84.

136. Glaudemans, A.W., et al., *In vivo and in vitro evidence that (9)(9)mTc-HYNIC-interleukin-2 is able to detect T lymphocytes in vulnerable atherosclerotic plaques of the carotid artery.* Eur J Nucl Med Mol Imaging, 2014. **41**(9): p. 1710-9.
137. Winkel, L.C., et al., *Folate receptor-targeted single-photon emission computed tomography/computed tomography to detect activated macrophages in atherosclerosis: can it distinguish vulnerable from stable atherosclerotic plaques?* Mol Imaging, 2014. **13**.
138. Jager, N.A., et al., *Folate receptor-beta imaging using 99mTc-folate to explore distribution of polarized macrophage populations in human atherosclerotic plaque.* J Nucl Med, 2014. **55**(12): p. 1945-51.
139. Li, D., et al., *Molecular imaging of atherosclerotic plaques targeted to oxidized LDL receptor LOX-1 by SPECT/CT and magnetic resonance.* Circ Cardiovasc Imaging, 2010. **3**(4): p. 464-72.
140. Tavakoli, S., et al., *Matrix metalloproteinase activation predicts amelioration of remodeling after dietary modification in injured arteries.* Arterioscler Thromb Vasc Biol, 2011. **31**(1): p. 102-9.
141. Razavian, M., et al., *Atherosclerosis plaque heterogeneity and response to therapy detected by in vivo molecular imaging of matrix metalloproteinase activation.* J Nucl Med, 2011. **52**(11): p. 1795-802.
142. Razavian, M., et al., *Integrin-targeted imaging of inflammation in vascular remodeling.* Arterioscler Thromb Vasc Biol, 2011. **31**(12): p. 2820-6.
143. Vancraeynest, D., et al., *alphaVbeta3 integrin-targeted microSPECT/CT imaging of inflamed atherosclerotic plaques in mice.* EJNMMI Res, 2016. **6**(1): p. 29.
144. Annovazzi, A., et al., *99mTc-interleukin-2 scintigraphy for the in vivo imaging of vulnerable atherosclerotic plaques.* Eur J Nucl Med Mol Imaging, 2006. **33**(2): p. 117-26.
145. Elmaleh, D.R., et al., *Rapid noninvasive detection of experimental atherosclerotic lesions with novel 99mTc-labeled diadenosine tetraphosphates.* Proc Natl Acad Sci U S A, 1998. **95**(2): p. 691-5.
146. Tepe, G., et al., *Tc-99m-labeled endothelin derivative for imaging of experimentally induced atherosclerosis.* Atherosclerosis, 2001. **157**(2): p. 383-92.
147. Schafers, M., et al., *Scintigraphic imaging of matrix metalloproteinase activity in the arterial wall in vivo.* Circulation, 2004. **109**(21): p. 2554-9.

148. Fujimoto, S., et al., *Molecular imaging of matrix metalloproteinase in atherosclerotic lesions: resolution with dietary modification and statin therapy.* J Am Coll Cardiol, 2008. **52**(23): p. 1847-57.
149. Kolodgie, F.D., et al., *Targeting of apoptotic macrophages and experimental atheroma with radiolabeled annexin V: a technique with potential for noninvasive imaging of vulnerable plaque.* Circulation, 2003. **108**(25): p. 3134-9.
150. Derlin, T., et al., *Correlation of inflammation assessed by 18F-FDG PET, active mineral deposition assessed by 18F-fluoride PET, and vascular calcification in atherosclerotic plaque: a dual-tracer PET/CT study.* J Nucl Med, 2011. **52**(7): p. 1020-7.
151. Joshi, N.V., et al., *18F-fluoride positron emission tomography for identification of ruptured and high-risk coronary atherosclerotic plaques: a prospective clinical trial.* The Lancet, 2014. **383**(9918): p. 705-713.
152. Claudon, M., et al., *Guidelines and good clinical practice recommendations for contrast enhanced ultrasound (CEUS) - update 2008.* Ultraschall Med, 2008. **29**(1): p. 28-44.
153. Peltier, M., et al., *Assessment of the physiologic significance of coronary disease with dipyridamole real-time myocardial contrast echocardiography. Comparison with technetium-99m sestamibi single-photon emission computed tomography and quantitative coronary angiography.* J Am Coll Cardiol, 2004. **43**(2): p. 257-64.
154. Feinstein, S.B., *Contrast ultrasound imaging of the carotid artery vasa vasorum and atherosclerotic plaque neovascularization.* J Am Coll Cardiol, 2006. **48**(2): p. 236-43.
155. ten Kate, G.L., et al., *Usefulness of contrast-enhanced ultrasound for detection of carotid plaque ulceration in patients with symptomatic carotid atherosclerosis.* Am J Cardiol, 2013. **112**(2): p. 292-8.
156. van den Oord, S.C., et al., *Effect of carotid plaque screening using contrast-enhanced ultrasound on cardiovascular risk stratification.* Am J Cardiol, 2013. **111**(5): p. 754-9.
157. Shah, F., et al., *Contrast-enhanced ultrasound imaging of atherosclerotic carotid plaque neovascularization: a new surrogate marker of atherosclerosis?* Vasc Med, 2007. **12**(4): p. 291-7.
158. Coli, S., et al., *Contrast-enhanced ultrasound imaging of intraplaque neovascularization in carotid arteries: correlation with histology and plaque echogenicity.* J Am Coll Cardiol, 2008. **52**(3): p. 223-30.
159. Staub, D., et al., *Vasa vasorum and plaque neovascularization on contrast-enhanced carotid ultrasound imaging correlates with*

cardiovascular disease and past cardiovascular events. Stroke, 2010. **41**(1): p. 41-7.
160. Giannoni, M.F., et al., *Contrast carotid ultrasound for the detection of unstable plaques with neoangiogenesis: a pilot study.* Eur J Vasc Endovasc Surg, 2009. **37**(6): p. 722-7.
161. McCarthy, M.J., et al., *Angiogenesis and the atherosclerotic carotid plaque: an association between symptomatology and plaque morphology.* J Vasc Surg, 1999. **30**(2): p. 261-8.
162. Xiong, L., et al., *Correlation of carotid plaque neovascularization detected by using contrast-enhanced US with clinical symptoms.* Radiology, 2009. **251**(2): p. 583-9.
163. Claudon, M., et al., *Guidelines and good clinical practice recommendations for Contrast Enhanced Ultrasound (CEUS) in the liver - update 2012: A WFUMB-EFSUMB initiative in cooperation with representatives of AFSUMB, AIUM, ASUM, FLAUS and ICUS.* Ultrasound Med Biol, 2013. **39**(2): p. 187-210.
164. Vavuranakis, M., et al., *Quantitative analysis of carotid plaque vasa vasorum by CEUS and correlation with histology after endarterectomy.* Vasa, 2013. **42**(3): p. 184-95.
165. Saba, L. and G. Mallarini, *Carotid plaque enhancement and symptom correlations: an evaluation by using multidetector row CT angiography.* AJNR Am J Neuroradiol, 2011. **32**(10): p. 1919-25.
166. Ajduk, M., et al., *Multidetector-row computed tomography in evaluation of atherosclerotic carotid plaques complicated with intraplaque hemorrhage.* Ann Vasc Surg, 2009. **23**(2): p. 186-93.
167. Fischer, C., et al., *Coronary CT angiography versus intravascular ultrasound for estimation of coronary stenosis and atherosclerotic plaque burden: a meta-analysis.* J Cardiovasc Comput Tomogr, 2013. **7**(4): p. 256-66.
168. Weigold, W.G., et al., *Standardized medical terminology for cardiac computed tomography: a report of the Society of Cardiovascular Computed Tomography.* J Cardiovasc Comput Tomogr, 2011. **5**(3): p. 136-44.
169. Voros, S., et al., *Prospective validation of standardized, 3-dimensional, quantitative coronary computed tomographic plaque measurements using radiofrequency backscatter intravascular ultrasound as reference standard in intermediate coronary arterial lesions: results from the ATLANTA (assessment of tissue characteristics, lesion morphology, and hemodynamics by angiography with fractional flow reserve, intravascular ultrasound*

and virtual histology, and noninvasive computed tomography in atherosclerotic plaques) I study. JACC Cardiovasc Interv, 2011. **4**(2): p. 198-208.
170. Kroner, E.S., et al., *Positive remodeling on coronary computed tomography as a marker for plaque vulnerability on virtual histology intravascular ultrasound.* Am J Cardiol, 2011. **107**(12): p. 1725-9.
171. Sato, A., et al., *In vivo evaluation of fibrous cap thickness by optical coherence tomography for positive remodeling and low-attenuation plaques assessed by computed tomography angiography.* Int J Cardiol, 2015. **182**: p. 419-25.
172. Motoyama, S., et al., *Plaque Characterization by Coronary Computed Tomography Angiography and the Likelihood of Acute Coronary Events in Mid-Term Follow-Up.* J Am Coll Cardiol, 2015. **66**(4): p. 337-46.
173. Seifarth, H., et al., *Histopathological correlates of the napkin-ring sign plaque in coronary CT angiography.* Atherosclerosis, 2012. **224**(1): p. 90-6.
174. Wintermark, M., et al., *High-resolution CT imaging of carotid artery atherosclerotic plaques.* AJNR Am J Neuroradiol, 2008. **29**(5): p. 875-82.
175. Das, M., et al., *Carotid plaque analysis: comparison of dual-source computed tomography (CT) findings and histopathological correlation.* Eur J Vasc Endovasc Surg, 2009. **38**(1): p. 14-9.
176. Walker, L.J., et al., *Computed tomography angiography for the evaluation of carotid atherosclerotic plaque: correlation with histopathology of endarterectomy specimens.* Stroke, 2002. **33**(4): p. 977-81.
177. Ajduk, M., et al., *Comparison of multidetector-row computed tomography and duplex Doppler ultrasonography in detecting atherosclerotic carotid plaques complicated with intraplaque hemorrhage.* Coll Antropol, 2013. **37**(1): p. 213-9.
178. Miralles, M., et al., *Quantification and characterization of carotid calcium with multi-detector CT-angiography.* Eur J Vasc Endovasc Surg, 2006. **32**(5): p. 561-7.
179. Hyafil, F., et al., *Noninvasive detection of macrophages using a nanoparticulate contrast agent for computed tomography.* Nat Med, 2007. **13**(5): p. 636-41.
180. Hyafil, F., et al., *Quantification of inflammation within rabbit atherosclerotic plaques using the macrophage-specific CT contrast*

agent N1177: a comparison with 18F-FDG PET/CT and histology. J Nucl Med, 2009. **50**(6): p. 959-65.
181. Cormode, D.P., et al., *Atherosclerotic plaque composition: analysis with multicolor CT and targeted gold nanoparticles.* Radiology, 2010. **256**(3): p. 774-82.
182. Ouimet, T., et al., *Molecular and cellular targets of the MRI contrast agent P947 for atherosclerosis imaging.* Mol Pharm, 2012. **9**(4): p. 850-61.
183. Kramer, C.M. and J. Narula, *Atherosclerotic plaque imaging: the last frontier for cardiac magnetic resonance.* JACC Cardiovasc Imaging, 2009. **2**(7): p. 916-8.
184. Fayad, Z.A., et al., *Noninvasive in vivo human coronary artery lumen and wall imaging using black-blood magnetic resonance imaging.* Circulation, 2000. **102**(5): p. 506-10.
185. Gharib, A.M., et al., *The feasibility of 350 mum spatial resolution coronary magnetic resonance angiography at 3 T in humans.* Invest Radiol, 2012. **47**(6): p. 339-45.
186. Yim, Y.J., et al., *High signal intensity halo around the carotid artery on maximum intensity projection images of time-of-flight MR angiography: a new sign for intraplaque hemorrhage.* J Magn Reson Imaging, 2008. **27**(6): p. 1341-6.
187. Gaens, M.E., et al., *Dynamic contrast-enhanced MR imaging of carotid atherosclerotic plaque: model selection, reproducibility, and validation.* Radiology, 2013. **266**(1): p. 271-9.
188. Calcagno, C., et al., *The complementary roles of dynamic contrast-enhanced MRI and 18F-fluorodeoxyglucose PET/CT for imaging of carotid atherosclerosis.* Eur J Nucl Med Mol Imaging, 2013. **40**(12): p. 1884-93.
189. den Hartog, A.G., et al., *Current status of clinical magnetic resonance imaging for plaque characterisation in patients with carotid artery stenosis.* Eur J Vasc Endovasc Surg, 2013. **45**(1): p. 7-21.
190. Kerwin, W.S., et al., *MR imaging of adventitial vasa vasorum in carotid atherosclerosis.* Magn Reson Med, 2008. **59**(3): p. 507-14.
191. Millon, A., et al., *Clinical and histological significance of gadolinium enhancement in carotid atherosclerotic plaque.* Stroke, 2012. **43**(11): p. 3023-8.
192. Taqueti, V.R., et al., *Increased microvascularization and vessel permeability associate with active inflammation in human atheromata.* Circ Cardiovasc Imaging, 2014. **7**(6): p. 920-9.

193. Qiao, Y., et al., *Carotid plaque neovascularization and hemorrhage detected by MR imaging are associated with recent cerebrovascular ischemic events.* AJNR Am J Neuroradiol, 2012. **33**(4): p. 755-60.
194. Chan, J.M., et al., *Imaging of the vulnerable carotid plaque: biological targeting of inflammation in atherosclerosis using iron oxide particles and MRI.* Eur J Vasc Endovasc Surg, 2014. **47**(5): p. 462-9.
195. Winter, P.M., et al., *Molecular imaging of angiogenesis in early-stage atherosclerosis with alpha(v)beta3-integrin-targeted nanoparticles.* Circulation, 2003. **108**(18): p. 2270-4.
196. Garcia-Garcia, H.M., et al., *IVUS-based imaging modalities for tissue characterization: similarities and differences.* Int J Cardiovasc Imaging, 2011. **27**(2): p. 215-24.
197. Di Mario, C., et al., *Detection and characterization of vascular lesions by intravascular ultrasound: an in vitro study correlated with histology.* J Am Soc Echocardiogr, 1992. **5**(2): p. 135-46.
198. Kostamaa, H., et al., *Calcified plaque cross-sectional area in human arteries: correlation between intravascular ultrasound and undecalcified histology.* Am Heart J, 1999. **137**(3): p. 482-8.
199. Garcia-Garcia, H.M., et al., *Tissue characterisation using intravascular radiofrequency data analysis: recommendations for acquisition, analysis, interpretation and reporting.* EuroIntervention, 2009. **5**(2): p. 177-89.
200. Nair, A., et al., *Coronary plaque classification with intravascular ultrasound radiofrequency data analysis.* Circulation, 2002. **106**(17): p. 2200-6.
201. Nair, A., et al., *Automated coronary plaque characterisation with intravascular ultrasound backscatter: ex vivo validation.* EuroIntervention, 2007. **3**(1): p. 113-20.
202. Nasu, K., et al., *Accuracy of in vivo coronary plaque morphology assessment: a validation study of in vivo virtual histology compared with in vitro histopathology.* J Am Coll Cardiol, 2006. **47**(12): p. 2405-12.
203. Rodriguez-Granillo, G.A., et al., *In vivo intravascular ultrasound-derived thin-cap fibroatheroma detection using ultrasound radiofrequency data analysis.* J Am Coll Cardiol, 2005. **46**(11): p. 2038-42.
204. Pundziute, G., et al., *Evaluation of plaque characteristics in acute coronary syndromes: non-invasive assessment with multi-slice computed tomography and invasive evaluation with intravascular*

ultrasound radiofrequency data analysis. Eur Heart J, 2008. **29**(19): p. 2373-81.
205. Brown, A.J., et al., *Direct Comparison of Virtual-Histology Intravascular Ultrasound and Optical Coherence Tomography Imaging for Identification of Thin-Cap Fibroatheroma.* Circ Cardiovasc Imaging, 2015. **8**(10): p. e003487.
206. Calvert, P.A., et al., *Association between IVUS findings and adverse outcomes in patients with coronary artery disease: the VIVA (VH-IVUS in Vulnerable Atherosclerosis) Study.* JACC Cardiovasc Imaging, 2011. **4**(8): p. 894-901.
207. Cheng, J.M., et al., *In vivo detection of high-risk coronary plaques by radiofrequency intravascular ultrasound and cardiovascular outcome: results of the ATHEROREMO-IVUS study.* Eur Heart J, 2014. **35**(10): p. 639-47.
208. Guedes, A., et al., *Long-term safety of intravascular ultrasound in nontransplant, nonintervened, atherosclerotic coronary arteries.* J Am Coll Cardiol, 2005. **45**(4): p. 559-64.
209. Honda, Y. and P.J. Fitzgerald, *Frontiers in intravascular imaging technologies.* Circulation, 2008. **117**(15): p. 2024-37.
210. Ozaki, Y., et al., *Comparison of contrast media and low-molecular-weight dextran for frequency-domain optical coherence tomography.* Circ J, 2012. **76**(4): p. 922-7.
211. Jang, I.K., et al., *Visualization of coronary atherosclerotic plaques in patients using optical coherence tomography: comparison with intravascular ultrasound.* J Am Coll Cardiol, 2002. **39**(4): p. 604-9.
212. Tearney, G.J., et al., *Quantification of macrophage content in atherosclerotic plaques by optical coherence tomography.* Circulation, 2003. **107**(1): p. 113-9.
213. Tian, J., et al., *Significance of intraplaque neovascularisation for vulnerability: optical coherence tomography study.* Heart, 2012. **98**(20): p. 1504-9.
214. Tearney, G.J., et al., *Consensus standards for acquisition, measurement, and reporting of intravascular optical coherence tomography studies: a report from the International Working Group for Intravascular Optical Coherence Tomography Standardization and Validation.* J Am Coll Cardiol, 2012. **59**(12): p. 1058-72.
215. Kume, T., et al., *Measurement of the thickness of the fibrous cap by optical coherence tomography.* Am Heart J, 2006. **152**(4): p. 755 e1-4.

216. Phipps, J.E., et al., *Macrophages and intravascular OCT bright spots: a quantitative study.* JACC Cardiovasc Imaging, 2015. **8**(1): p. 63-72.
217. Manfrini, O., et al., *Sources of error and interpretation of plaque morphology by optical coherence tomography.* Am J Cardiol, 2006. **98**(2): p. 156-9.
218. Uemura, S., et al., *Thin-cap fibroatheroma and microchannel findings in optical coherence tomography correlate with subsequent progression of coronary atheromatous plaques.* Eur Heart J, 2012. **33**(1): p. 78-85.
219. Kilic, I.D., et al., *Near-infrared spectroscopy-intravascular ultrasound: scientific basis and clinical applications.* Eur Heart J Cardiovasc Imaging, 2015. **16**(12): p. 1299-306.
220. Gardner, C.M., et al., *Detection of lipid core coronary plaques in autopsy specimens with a novel catheter-based near-infrared spectroscopy system.* JACC Cardiovasc Imaging, 2008. **1**(5): p. 638-48.
221. Kang, S.J., et al., *Combined IVUS and NIRS detection of fibroatheromas: histopathological validation in human coronary arteries.* JACC Cardiovasc Imaging, 2015. **8**(2): p. 184-94.
222. Inaba, S., et al., *Intravascular Ultrasound and Near-Infrared Spectroscopic Characterization of Thin-Cap Fibroatheroma.* Am J Cardiol, 2017. **119**(3): p. 372-378.
223. Puri, R., et al., *Near-Infrared Spectroscopy Enhances Intravascular Ultrasound Assessment of Vulnerable Coronary Plaque: A Combined Pathological and In Vivo Study.* Arterioscler Thromb Vasc Biol, 2015. **35**(11): p. 2423-31.
224. Madder, R.D., et al., *Detection by near-infrared spectroscopy of large lipid cores at culprit sites in patients with non-ST-segment elevation myocardial infarction and unstable angina.* Catheter Cardiovasc Interv, 2015. **86**(6): p. 1014-21.
225. Hoogi, A., et al., *Carotid plaque vulnerability: quantification of neovascularization on contrast-enhanced ultrasound with histopathologic correlation.* AJR Am J Roentgenol, 2011. **196**(2): p. 431-6.
226. Li, C., et al., *Quantification of carotid plaque neovascularization using contrast-enhanced ultrasound with histopathologic validation.* Ultrasound Med Biol, 2014. **40**(8): p. 1827-33.
227. Staub, D., et al., *Correlation of carotid artery atherosclerotic lesion echogenicity and severity at standard US with intraplaque*

neovascularization detected at contrast-enhanced US. Radiology, 2011. **258**(2): p. 618-26.
228. Tavakoli, S., A. Vashist, and M.M. Sadeghi, *Molecular imaging of plaque vulnerability.* J Nucl Cardiol, 2014. **21**(6): p. 1112-28; quiz 1129.
229. Vancraeynest, D., et al., *Imaging the vulnerable plaque.* J Am Coll Cardiol, 2011. **57**(20): p. 1961-79.
230. Rudd, J.H., et al., *(18)Fluorodeoxyglucose positron emission tomography imaging of atherosclerotic plaque inflammation is highly reproducible: implications for atherosclerosis therapy trials.* J Am Coll Cardiol, 2007. **50**(9): p. 892-6.
231. Hellings, W.E., et al., *Composition of carotid atherosclerotic plaque is associated with cardiovascular outcome: a prognostic study.* Circulation, 2010. **121**(17): p. 1941-50.
232. Hulten, L.M. and M. Levin, *The role of hypoxia in atherosclerosis.* Curr Opin Lipidol, 2009. **20**(5): p. 409-14.
233. Moreno, P.R., et al., *Plaque neovascularization is increased in ruptured atherosclerotic lesions of human aorta: implications for plaque vulnerability.* Circulation, 2004. **110**(14): p. 2032-8.
234. Martinet, W., H. De Loof, and G.R. De Meyer, *mTOR inhibition: a promising strategy for stabilization of atherosclerotic plaques.* Atherosclerosis, 2014. **233**(2): p. 601-7.
235. Herrmann, J., et al., *Angiogenesis in atherogenesis.* Arterioscler Thromb Vasc Biol, 2006. **26**(9): p. 1948-57.
236. Sadat, U., et al., *Inflammation and neovascularization intertwined in atherosclerosis: imaging of structural and molecular imaging targets.* Circulation, 2014. **130**(9): p. 786-94.
237. Truijman, M.T., et al., *Combined 18F-FDG PET-CT and DCE-MRI to assess inflammation and microvascularization in atherosclerotic plaques.* Stroke, 2013. **44**(12): p. 3568-70.
238. Pedersen, S.F., et al., *Microvessel density but not neoangiogenesis is associated with 18F-FDG uptake in human atherosclerotic carotid plaques.* Mol Imaging Biol, 2012. **14**(3): p. 384-92.
239. Wendorff, C., et al., *Carotid Plaque Morphology Is Significantly Associated With Sex, Age, and History of Neurological Symptoms.* Stroke, 2015. **46**(11): p. 3213-9.
240. Toutouzas, K., et al., *Vulnerable plaque imaging: updates on new pathobiological mechanisms.* Eur Heart J, 2015. **36**(45): p. 3147-54.

241. Marnane, M., et al., *Plaque inflammation and unstable morphology are associated with early stroke recurrence in symptomatic carotid stenosis.* Stroke, 2014. **45**(3): p. 801-6.
242. Figueroa, A.L., et al., *Distribution of inflammation within carotid atherosclerotic plaques with high-risk morphological features: a comparison between positron emission tomography activity, plaque morphology, and histopathology.* Circ Cardiovasc Imaging, 2012. **5**(1): p. 69-77.
243. Tawakol, A., et al., *Relation between resting amygdalar activity and cardiovascular events: a longitudinal and cohort study.* Lancet, 2017. **389**(10071): p. 834-845.
244. Go, A.S., et al., *Heart disease and stroke statistics--2013 update: a report from the American Heart Association.* Circulation, 2013. **127**(1): p. e6-e245.
245. Ogawa, M., et al., *(18)F-FDG accumulation in atherosclerotic plaques: immunohistochemical and PET imaging study.* J Nucl Med, 2004. **45**(7): p. 1245-50.
246. Gaeta, C., et al., *Reduced myocardial 18F-FDG uptake after calcium channel blocker administration. Initial observation for a potential new method to improve plaque detection.* Eur J Nucl Med Mol Imaging, 2011. **38**(11): p. 2018-24.
247. Nitta, Y., et al., *Pioglitazone decreases coronary artery inflammation in impaired glucose tolerance and diabetes mellitus: evaluation by FDG-PET/CT imaging.* JACC Cardiovasc Imaging, 2013. **6**(11): p. 1172-82.
248. Boellaard R., H.I., Ettinger S., et al., *EARL FDG-PET/CT accreditation program: Feasibility overview and results of first 55 successfully accredited sites.* Journal of Nuclear Medicine, 2013. **54**(suppl. 2): p. 2052.
249. Tahara, N., et al., *The prevalence of inflammation in carotid atherosclerosis: analysis with fluorodeoxyglucose-positron emission tomography.* Eur Heart J, 2007. **28**(18): p. 2243-8.
250. Folco, E.J., et al., *Hypoxia but not inflammation augments glucose uptake in human macrophages: Implications for imaging atherosclerosis with 18fluorine-labeled 2-deoxy-D-glucose positron emission tomography.* J Am Coll Cardiol, 2011. **58**(6): p. 603-14.
251. Rominger, A., et al., *18F-FDG PET/CT identifies patients at risk for future vascular events in an otherwise asymptomatic cohort with neoplastic disease.* J Nucl Med, 2009. **50**(10): p. 1611-20.

252. Figueroa, A.L., et al., *Measurement of arterial activity on routine FDG PET/CT images improves prediction of risk of future CV events.* JACC Cardiovasc Imaging, 2013. **6**(12): p. 1250-9.
253. Coulden, R., et al., *Suppression of myocardial 18F-FDG uptake with a preparatory "Atkins-style" low-carbohydrate diet.* Eur Radiol, 2012. **22**(10): p. 2221-8.
254. Rudd, J.H., et al., *Imaging atherosclerotic plaque inflammation by fluorodeoxyglucose with positron emission tomography: ready for prime time?* J Am Coll Cardiol, 2010. **55**(23): p. 2527-35.
255. Deichen, J.T., et al., *Uptake of [18F]fluorodeoxyglucose in human monocyte-macrophages in vitro.* Eur J Nucl Med Mol Imaging, 2003. **30**(2): p. 267-73.
256. Ishimaru, S., et al., *Focal uptake on 18F-fluoro-2-deoxyglucose positron emission tomography images indicates cardiac involvement of sarcoidosis.* Eur Heart J, 2005. **26**(15): p. 1538-43.
257. Menezes, L.J., et al., *Vascular inflammation imaging with 18F-FDG PET/CT: when to image?* J Nucl Med, 2009. **50**(6): p. 854-7.
258. Kates, A.M., et al., *Impact of aging on substrate metabolism by the human heart.*J Am Coll Cardiol, 2003. **41**(2): p. 293-9.